Study on Structure and Vacuum Membrane Distillation Performance of PVDF Composite Membranes: Influence of Molecular Weight and Blending

Zuolong Chen

A thesis submitted to the

Faculty of Graduate and Postdoctoral Studies in partial fulfillment of the requirements for the

Master of Applied Science in Chemical Engineering

Department of Chemical and Biological Engineering

Faculty of Engineering

University of Ottawa

Abstract

In this study, membranes were made from three polyvinylidene fluoride (PVDF) polymers individually and the blend systems of high (H) and low (L) molecular weight PVDF by phase inversion process. After investigating membrane casting solutions' viscous and thermodynamic properties, the membranes so fabricated were characterized by scanning electron microscopy, gas permeation tests, porosity measurement, contact angle (CA) and liquid entry pressure of water (LEPw) measurement, and further subjected to vacuum membrane distillation (VMD) in a scenario that was applicable for cooling processes, where the feed water temperature was maintained at 27^{o}C. It was found that PVDF solutions' viscosities and thermodynamic instabilities were determined by the types of PVDF employed in single polymer systems and the mixing ratios of two PVDF polymers in blend systems. Thus the membrane properties and performances were influenced by the aforesaid factors as well. In single polymer systems, it was found that the membrane surface roughness and porosity increased with an increase in molecular weight. Among all the membranes casted in this study, the water vapor flux of VMD was found to be the highest at the intermediate range of H:L ratio, i.e., 4:6, at which the thickness of the sponge-like layer showed a minimum, the finger-like macro-voids formed a more orderly single-layer structure, and the LEPw showed a minimum. A conclusion can be made that blend systems of high molecular weight PVDF polymers and low molecular weight PVDF polymers could be used to optimize membrane performance in vacuum membrane distillation.

Key words: Polyvinylidene fluoride, low and high molecular weight, blended membrane, membrane characterization, vacuum membrane distillation

Résumé

Dans cette étude, les membranes étaient faites individuellement de trois polymères de polyfluorure de vinylidène (PFVD) et les systèmes mélangés des poids moléculaires PFVD hauts (H) et bas (B) par un processus d'inversion de phase. Après investir les propriétés visqueuses et thermodynamiques des solutions de coulage, les membranes fabriquées étaient caractérisées par; microscopie électronique à balayage, tests de perméation de gaz, mesure de porosité, mesure de l'angle de contact (AC) et de la pression d'entrée liquide de l'eau (PELe), et ensuite soumise à distillation membrane sous vide (DMSV) dans un scénario qui était applicable pour un processus refroidissant, où la température d'alimentation d'eau était maintenue à 27^{o}C. C`était trouvé que les viscosités et instabilités thermodynamiques des solutions PFVD étaient déterminés par le type de PFVD employé dans les systèmes de polymère simple et les ratios de mélange des deux polymères PFVD dans les systèmes mélangés. Ainsi les propriétés et performances des membranes étaient aussi influencées par les facteurs mentionnés. Dans les systèmes de polymère simple, ça a était trouvé que la rudesse et porosité de membrane augmenté avec l'augmentation de poids moléculaire. Parmi toutes les membranes coulées dans cette étude, le flux de vapeur d'eau de DMSV était plus haut que le niveau intermédiaire du ratio de H:B, i.e., 4 :6 , à laquelle l'épaisseur du couche spongieuse a montré un minimum, les macros vides en forme de doigts ont formaient une structure à couche simple avec plus d'ordre, et le PELe a montré un minimum. Une conclusion peut être faite que les systèmes mélangés des polymères PFVD dont le poids moléculaire est haut et des polymères PFVD dont le poids moléculaires est bas, peuvent être utilisé pour optimiser la performance des membranes dans le processus de distillation membrane sous vide.

Mots clés : Polyfluorure de vinylidène, haut et bas poids moléculaires, membrane mélangé, caractérisation de membrane, distillation de membrane sous vide

Acknowledgement

I would like to express my sincerest and heartfelt appreciation to those wonderful souls who helped me accomplish this study.

I would first like to recognize Dr. Christopher Q. Lan, my supervisor, for his valued guidance, support, background knowledge and patience. My deepest gratitude is also extended to Dr.Takeshi Matsuura, my co-supervisor, and Dr. Dipak Rana for their patient guidance, precious help and background knowledge in the completion of this study.

I would like to extend my gratitude to the all of the staff in the Department of Chemical and Biological Engineering in the Faculty of Engineering, University of Ottawa.

Thanks are also given to the Carleton SEM lab and Dr. Jianqun Wang, for their help with SEM test.

I would like to thank the Arkema Inc. (Philadelphia, PA, USA) for the gift of polyvinylidene fluoride (Kynar®) polymers and the National Research Council, Ottawa, Canada for generously offering the backing material.

Table of Contents

List of Figures

List of Tables

Legend

J Membrane mass flux (g/m^2·s)

C_m Membrane coefficient (m/s)

ΔP The pressure difference between the feed and permeate surfaces of the membrane (Pa)

T_m Temperature of membrane feed / permeate surface ($^\circ C$)

R Gas constant($J/mol \cdot K$),

τ Membrane tortuosity.

θc Contact angle ($^\circ$)

γ_{SG} The solid-vapor interfacial energy (J)

γ_{SL} The solid-liquid interfacial energy (J)

γ_{LG} The liquid-vapor interfacial energy (J)

γ_l Surface tension of the liquid

B Gas permeance in gas permeation test ($mol/m^2 s \cdot Pa$)

M Molecular weight of the gas (kg/mol)

T Absolute temperature (K)

r_p Membrane pore size (m)

μ Viscosity of the gas in gas permeation test ($Pa \cdot s$)

ε Membrane porosity

L_p Effective pore length (m)

P_m Mean pressure within the membrane pore set to the average of the feed and permeate gas pressures. (Pa)

W_W and W_D are the weight of the wet and dry membrane (g), respectively;

A Membrane area (cm^2)

h Membrane thickness (cm)

ρ Density of the testing liquid (g/cm^3).

Chapter 1. Introduction

Since the 1960s, membrane distillation has been intensively studied and utilized in some areas. Meanwhile, a variety of approaches have been employed to optimize membranes and membrane distillation configurations to enhance the performances of membrane distillation. A wide range of polymers and additives were investigated in these studies, in which polyvinylidene fluoride (PVDF) has been established as one of the best polymers. This could be attributed to its excellent mechanical strength, thermal stability, chemical resistance, and high hydrophobicity (1). Among the numerous parameters that can affect the properties and performance of distillation membranes, it was demonstrated with membrane prepared with polyethersulfone (PES), another popular polymer for distillation membrane fabrication, that the polymer's molecular weight has significant influence on membrane properties and distillation performances (2). It was found that this theory can be used to optimize membrane in a simple and useful way. However, relevant data is scarce on PVDF membranes, because not much work is done to investigate the effects of molecular weight and the mixing ratio in blended PVDF systems on membrane properties and performances. Hence the study of the effect of PVDF molecular weight on PVDF membrane properties and membrane distillation performance can be meaningful and significant.

The objective of this study was to systematically investigate the impacts of the molecular weights of three PVDF polymers(i.e., Kynar® 740, Kynar® MG 15 and Kynar® HSV 900) and therefore different viscous and thermodynamic properties on the pore size, porosity, surface properties, morphology, and vacuum membrane distillation performance of membranes casted by using phase inversion technology. The effects of the ratio of two

polymers (i.e., Kynar® HSV 900 andKynar®740) on membrane properties and performance were also investigated.

The membranes so fabricated will be used in a personal cooling system which employs vacuum membrane distillation technology to achieve personal cooling purpose. A schematic of the personal cooling system is shown below (3):

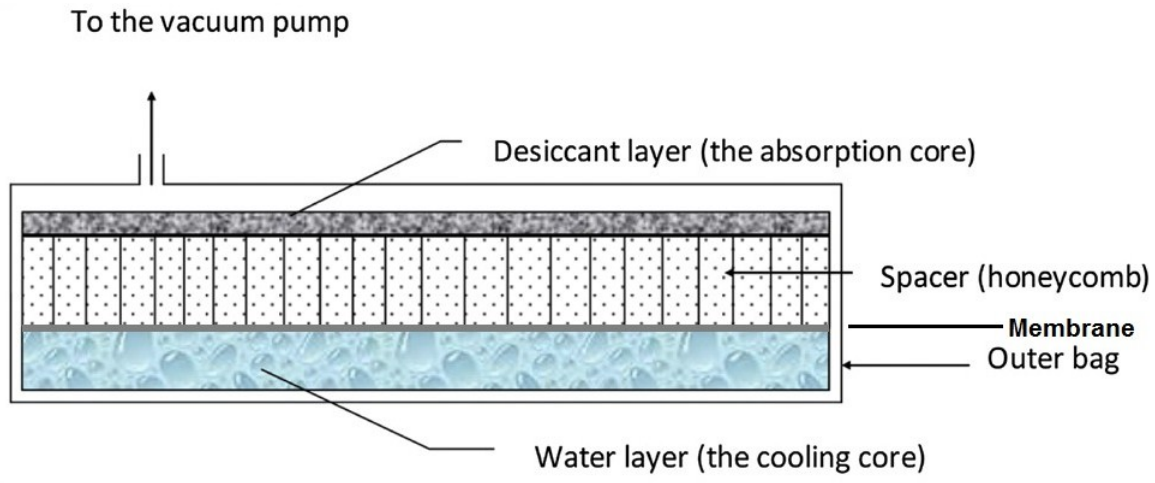

Figure 1-1 A schematic of the personal cooling system

The membrane here in the cooling systems acts as a physical barrier which prevents water liquid from penetrating the membrane while let the water vapor go through. Thus the distillation of water can be used to lower the surface temperature of the water layer side and maintain a relatively low temperature for human bodies. It was found that the cooling system should have the efficiency of 250 W to work well in this application.

This system is mainly used in natural conditions, in which the temperature varies from 20˚C to 45˚C. As a matter of fact, the VMD performance of membranes in this study were tested at the temperature of 27˚C.

This temperature is also suitable for food industries in which VMD technology is also employed.

Chapter 2 is the literature review that talks about the background knowledge of membrane technology and membrane distillation process. Besides, Chapter 3 and Chapter 4 are about the papers written based on this study, i.e Study on the Structure and vacuum membrane distillation performance of PVDF composite membranes: Influence of molecular weight, Study on the Structure and vacuum membrane distillation performance of PVDF composite membranes: Influence of blending ratio of two PVDF polymers of different molecular weights.

Three polyvinylidene fluoride (PVDF) polymers were used in this study: Kynar®740, Kynar® MG 15 and Kynar® HSV 900.

In Chapter 3, three PVDF materials were individually studied, covering the membrane casting solution properties, membrane properties and performances. The result illustrated that as the membrane casting solutions' thermodynamic and viscous properties were changed by the PVDF polymers added, the membranes casted from these solutions showed significant differences in both membrane properties and vacuum membrane distillation performance. More specifically, the Kynar® MG 15 membrane, which was casted from the Kynar® MG 15 PVDF of the intermediate molecular weight, showed the maximum VMD flux and the minimum LEPw value among all three PVDF membranes. And the cross-sectional SEM images illustrated significant difference between the three PVDF membranes in both finger-like layers and sponge-like layers. It was also found that the membrane porosity increased with an increase in molecular weight.

In Chapter 4, Kynar® 740 and Kynar® HSV 900 polymers were mixed at different mixing ratios. Similar to Chapter 3, a set of solution and membrane properties were examined. Then VMD performance was tested too. A conclusion was reached that the mixing ratio of two polyvinylidene fluorides could significantly affect some solution and membrane properties, as well as vacuum membrane distillation performances. More specifically, the VMD flux showed a maximum at the H:L ratio of 4:6, at which the average flux reached 528 $g/h \cdot m^2$. This could be explained by the maximum

pore size and the finest finger-like channel observed in membranes casted from H:L=4:6 casting solutions. It should be mentioned that a commercial PTFE membrane tested under the same testing condition showed a flux of 379.4 g/m^2. Besides, the porosity data revealed that H:L=4:6 membranes also had relatively higher porosity.

Chapter 5 is the conclusion part of this thesis. It was found that in both cases, the interplay of kinetic effects and polymer solutions' thermodynamic instabilities, along with the interplay of two pore formation theories resulted in the difference in membrane formation, membrane morphology, membrane pore size and other properties. Thus membrane performance determined by these factors was also affected. These effects can be attributed to the difference in PVDF molecular weights (Chapter 3) or the difference in mixing ratios of two PVDF polymers (Chapter 4). It is believed that PVDF molecular weight and the mixing ratio of two PVDF polymers have complicated influences on membrane properties and performance.

It was found that the molecular weight of PVDF polymer and the mixing ratio of two PVDF polymers of different molecular weights can significantly affect some membrane properties and VMD performance while maintaining some other membrane features (i.e. hydrophobicity).

By blending PVDF of different molecular weights membranes of better for membrane distillation performance can be obtained than PVDF of individual molecular weight. This study offers a simple and economical way to optimize membranes for membrane distillation processes, thus offering a new method to obtain a wide range of membrane casting solutions' properties and membrane features. The result in this study has already been used in other researches in our research group.

Reference:

1. Liu F, Hashim NA, Liu Y, Abed MRM, Li K. Progress in the production and modification of PVDF membranes. J Membr Sci. 2011;375(1-2):1-27.
2. Zhou C, Hou Z, Lu X, Liu Z, Bian X, Shi L, et al. Effect of polyethersulfone molecular weight on structure and performance of ultrafiltration membranes. Industrial and Engineering Chemistry Research. 2010;49(20):9988-97.
3. Yang Y. Man-portable personal cooling garment based on vacuum desiccant cooling. - Applied Thermal Engineering. 2012:- 18.

Chapter 2. Literature Review

2.1 Introduction

2.1.1 A general introduction of membrane technology

The first commercially applicable membrane was fabricated using phase inversion method in 1960 (1). Since then, numerous new innovations in this field have been made, and nowadays membrane technology is widely utilized in the modern society. Deemed as a versatile technology, copious types of membranes were invented for various usages including reverse osmosis, nano-filtration, ultra-filtration, micro-filtration, gas separation electrolysis, dialysis, electrodialysis, gas separation, vapor permeation, pervaporation, membrane distillation, and membrane contactors (2). These technologies have been extensively used in wastewater treatment, seawater desalination, ultrafiltration in food industry and many other fields.

Normally, membranes can be made with different configurations, including flat-sheet and tubular (hollow-fiber) geometry. A significant advantage of hollow-fiber membranes is that it has the highest membrane packing density per module volume, while due to the difficulties of making hollow-fiber membranes and other reasons, flat sheet membranes are commonly used in large-scale reverse osmosis separation processes (3).

Membranes can also be categorized as porous and non-porous membranes. For porous membranes, based on their pore size, they could be divided into four main types: reverse osmosis (RO, pore size 0.0001 to 0.001 μm), nano-filtration (NF, pore size: 0.001 to 0.01 μm), ultra-filtration (UF, pore size 0.01 to 0.1 μm) and micro-filtration (MF, pore size 0.1 to 5 μm) (4). A few factors can affect the pore size and porosity of porous membranes, including the polymer type, the additives in polymer solution, the solvent and the polymer concentration in the casting solution (5). Pore size and porosity of porous membranes can significantly influence membrane performances. For microfiltration and ultrafiltration

membranes, pore size and porosity can determine the efficiency of filtration (6). Thus certain pore size and porosity are required for certain filtration efficiencies and other filtration requirements. Another important factor is the morphology of porous membrane, from which it can be observed that there are usually two layers in polymeric porous membranes: the upper layer is a channel-like layer that usually has macrovoids or finger-like structures, while the lower layer is a sponge-like layer. The formation of both structures varies from the membrane preparing methods and materials.

In the past few decades, researchers have spent a large amount of time and energy on controlling those properties for better membrane filtration performance, which also highlights the importance of the studies of polymeric porous membranes. In order to fabricate various kinds of porous membranes for different uses, a few methods were invented and employed in modern membrane industry, such as sintering, track etching and phase separation processes. Nowadays, controlled phase separation process is most commonly used in porous membrane fabrications (6).The morphology of the membranes fabricated in these ways, along with membrane pore sizes and porosities could be largely determined by aforesaid methods. For example, the structure of membrane could be significantly affected by the rate of phase inversion process, which could be determined by two parameters: the thermodynamic stability of polymer solutions and the diffusion rate of coagulant into polymer solution (7). Detailed discussions about these two parameters will be given later in this literature review.

In terms of the polymeric materials, a larger amount of polymers have been studied as well for membranes that are used in separation processes, especially when a membrane separates gas and liquid phase. In order to prevent the penetration of liquid into membrane pores, hydrophobic materials are employed for fabrication of such membranes (8). A copious amount of such polymeric materials have been developed, including polyamide, polyimide, polyethylene (PE), polypropylene (PP), polytetrafluoroethylene (PTFE), polyvinylidene

fluoride (PVDF), polyvinylchloride (PVC) and other materials. Owing to its high mechanical strength, outstanding chemical resistance and high hydrophobicity, PVDF has been used in ultrafiltration and microfiltration membranes for a long time (9). In which membrane distillation is included.

Besides all the parameters that have been mentioned, some other parameters that can affect membrane properties are worth discussing too: membrane fabricating conditions (fabricating environment temperature, humidity, forming methods, bath composition and temperature), polymer solution properties (viscosity (10), temperature, and cloud point) as well as polymer molecular weight. All these factors will be discussed in this review later.

2.1.2 **Membrane Distillation**

With the growing demand of obtaining fresh water from seawater and polluted water, membrane distillation has been extensively studied in recent decades. Interestingly enough, thanks to the rapid developments in this area, the utilization of this technology has been extended to other areas as well, i.e. food industry (11), cooling systems and radioactive waste treatments (12). Membrane distillation is a thermally-driven separation process, in which only vapour molecules are able to pass through a porous hydrophobic membrane that acts as a physical barrel (13).

The feed is usually heated and due to the hydrophobic property of the membrane that prevents penetration of the aqueous liquid, a vapor-liquid interface is formed at each pore entrance and the vapour is driven by the vapour pressure difference between pore inlet and outlet, which forces the vapour to permeate through the open membrane pores.

Compared with conventional distillation methods, this promising process is cleaner, more environmentally friendly and economical. It does not need large vapour space for evaporation. Also, instead of heating water to the boiling point in atmospheric pressure with a massive

amount of energy, membrane distillation process does not demand too much energy because of its high efficiency (14). As a result of its low operating temperature, it is also favoured by food industry (better flavour) (15) and medical industry (not sterilizing biological fluids). Membrane distillation has some other advantages too. For example, reverse osmosis is a pressure driven process which needs to be operated in high pressure. While in membrane distillation process, the operating pressure is relatively low. Consequently, lower unit cost and better safety can be benefitted from the lower operating pressure. Because of this, a large number of less expensive materials could be used to make membranes for membrane distillation. Due to the relatively large pore size of the membranes used in MD and the much less operating pressure, fouling problems would not be as severe as they are in RO and other membrane separation processes. In terms of the energy sources, membrane distillation could be easily achieved by using several energy sources in different areas, for example, solar energy and hydro energy (16). Generally speaking, based on the arrangements of their distillate channels and/or the methods in which those channels are operated, membrane distillation can be categorized into several types: 1). Direct contact MD (DCMD), in which the hot solution (feed) is directly in contact with the membrane surface, is the simplest membrane distillation configuration. And it has already been widely used in many fields (17); 2). Air gap MD (AGMD), in which stagnant air is employed between the membrane and the condensation surface, reduces heat loss by conduction but increases mass transfer resistance. (18); 3). Sweeping gas MD (SGMD), in which inert gas is used to sweep the vapour at the permeate membrane side to reduce heat loss, is suitable for removing volatile compounds from aqueous solutions and 4). Vacuum MD (VMD), in which vacuum is applied on the permeate side. VMD has been proved to be a promising distillation method with a large amount of advantages (19). Similar to other membrane distillation configurations, vapor is also driven by the vapour pressure difference that is caused in VMD by applying vacuum on

the permeate side. This process does not consume a large amount of heat, since the heat loss by conduction is prevented by the nearly zero thermal conductivity of vacuum. The VMD configuration is shown in Figure 2-1 (13).

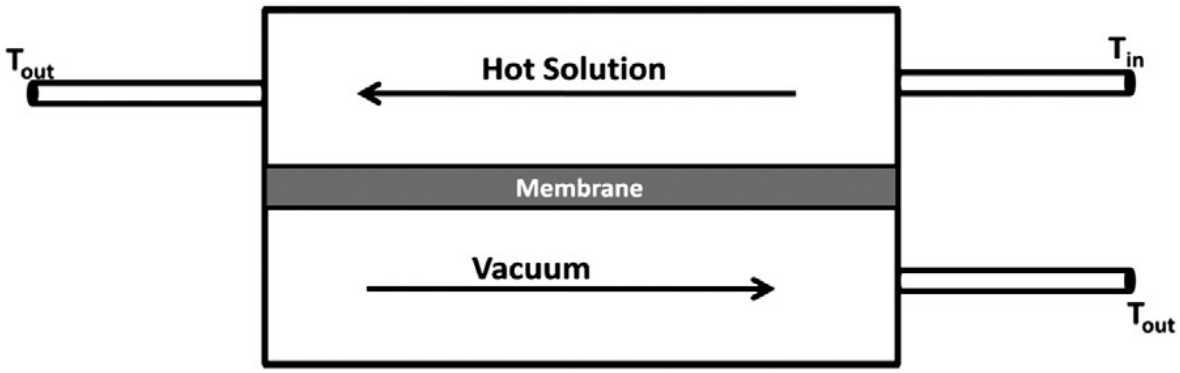

Figure 2-1Vacuum Membrane Distillation (13)

By employing vacuum on the permeate side, the vapour pressure of the feed side does not need to be very high. Hence the temperature of the feed liquid can be relatively low. In some cases, the temperature of feed liquid could be lowered to room temperature (23°C). In this way, the energy that is necessary to heat the feed is almost zero. Another advantage of using vacuum membrane distillation is that as the vapour is sucked and taken away by the vacuum, the condensation occurs outside the membrane module. Hence, there is no condensed liquid on the permeate surface that may lower the efficiency.

2.2 Membrane Formation

2.2.1 Membrane Formation methods

There are many methods to prepare porous polymeric films. Generally speaking, sintering, stretching, track etching and phase separation processes are the most commonly used ones. The membranes prepared by these methods vary greatly in terms of membrane properties and performances. Most industrial membranes are prepared by phase separation process (6), which can be categorized into the following few cases (20, 21):

- **Thermally induced phase separation** (TIPS).

  This process is a thermally driven process to eliminate the solvent in polymer solution to form the polymeric membrane films. In this process, the solvent could be removed by extraction, evaporation or freeze drying methods.

- **Air-casting of a polymer solution** (22)

  The polymer is dissolved in a mixture of a volatile solvent and a less volatile nonsolvent. When the amount of solvent decreased in evaporation process, the solubility of polymer will decrease, and thus phase separation can take place.

- **Precipitation from the vapour phase**

  Phase separation of the polymer solution is introduced by the penetration of nonsolvent vapour in the solution.

- **Immersion precipitation**

  Immersion precipitation is one of the most popular methods to prepare polymeric membrane. In this process, a polymer solution is cast as a thin film on a supporting material, and then the solution is immersed in a nonsolvent bath. Solvent/nonsolvent exchange takes place in the polymer solution, thus precipitation happens.

2.2.1.1 *Immersion precipitation*

Immersion precipitation is the most commonly used method in membrane preparation and the membranes prepared by this method are widely used in membrane distillation, especially for PVDF membrane (9).

Figure 2-2 shows the schematic of membrane formation process in immersion precipitation. This is a ternary system that basically consists of three components: Nonsolvent, solvent and polymer. Other components could be added into this system for different purposes, while in this section, the most basic model is used for discussion.

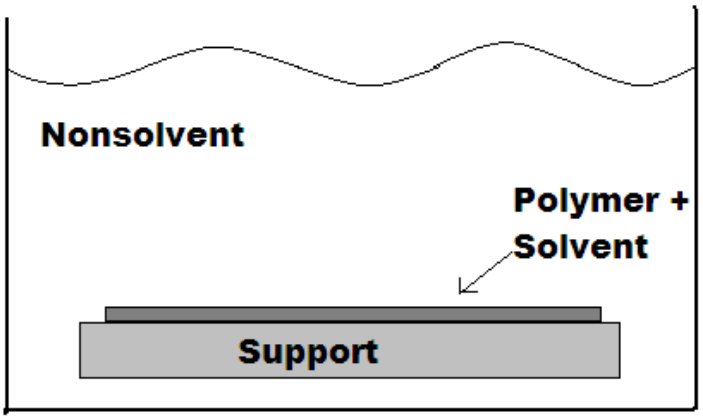

Figure 2-2 Membrane formation process in immersion precipitation.

Three types of phase transitions occur in this process, and these three transitions are also the most important factors that can determine the membrane properties, morphology and membrane performance. More specifically, these three phase transitions are: liquid-liquid demixing (the key role in this process), vitrification and solid-liquid demixing such as gelation (crystallization of the polymer).

2.2.1.2 *Liquid-liquid demixing*

The ternary liquid-liquid demixing could be analysed by employing ternary diagram and Flory-Huggins theory.

A ternary diagram is a triangle diagram in which the three corners of the diagram represent the three components in polymer solutions: polymer, nonsolvent and solvent. Basically, the diagram could be separated into two parts: homogeneous region and liquid-liquid demixing gap. The liquid-liquid demixing gap can be reached when sufficient amount of nonsolvent exists in the polymer solution or insufficient solvent is employed. Figure 2-3 gives an example of a typical ternary diagram for liquid-liquid demixing analysis (6). When nonsolvent is added to a polymer solution, the solution composition moves from the solvent/polymer axis to the arrow direction in the triangular diagram (Figure 2-3). Upon

reaching the bimodal line, the liquid-liquid demixing will take place. The binodal line is also referred to as the "cloud point curve." Inside the liquid-liquid demixing gap, there is a subdivided region of spinodal demixing, the boundary of this demixing gap is named as spinodal line. In order to understand the ternary diagram and liquid-liquid demixing process, Flory–Huggins solution theory is very useful (23, 24). When analysing the polymer solution mixing process, this theory offers a mathematical model of the thermodynamics of polymer solutions using Gibbs free energy change for mixing a polymer with a solvent.

$$\Delta G_m = RT[n_1 \ln \emptyset_1 + n_2 \ln \emptyset_2 + n_1 \emptyset_2 x_{12}] \quad (1)$$

In this equation, $n_1$and n_2 are the number of moles of solvent and polymer, respectively. Similar to the moles of solvent and polymer, $\emptyset_1$ and $\emptyset_2$ are the volume fractions of solvent and polymer respectively. *R* is the gas constant and *T* is the absolute temperature.x_{12} is a parameter introduced to take the energy of interdispersing polymer and solvent molecules into consideration. Also, sometimes in order to make the assumption more accurate, other parameters can be taken into consideration too.

Many people have discussed the effect of these parameters on liquid-liquid demixing gap and membrane properties casted by these polymer solutions, a brief summary will be given here to show the parameters that influence the demixing process and demixing gap (6, 25-27):

- A polymer-nonsolvent interaction parameter determines the area of the liquid-liquid demixing gap. High polymer-nonsolvent interaction parameters locate the intersection of the demixing gap with the polymer-nonsolvent axis at a high polymer concentration.
- Low polymer-solvent affinity can increase the magnitude of the demixing gap.
- High solvent-nonsolvent interaction parameter, which means low affinity between solvent and nonslovent, brings big differences in solvent/nonsolvent ratio in the equilibrium phases.

Besides, other parameters can affect χ too, e.g. some papers mentioned that the ratio of the homopolymer chain lengths could determine the value of χ as well (28).

From the demixing point of view, the membrane formation process could be studied based on the interaction parameters of solvent, nonsolvent and polymer, thus this theory is widely used in membrane formation studies. It should be pointed out that this theory is more justified for concentrated solutions than for dilute polymer solutions (29).

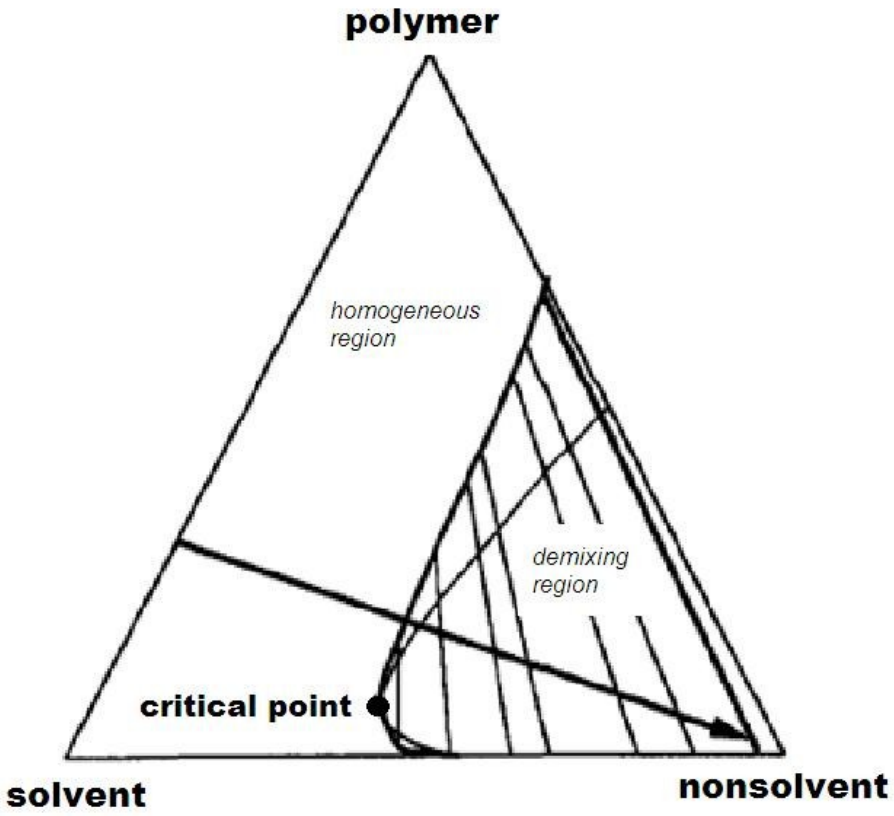

Figure 2-3 Liquid-liquid demixing gap. (6)

2.2.1.3 ***Liquid-liquid demixing and vitrification***

Liquid-liquid demixing is not the only transition in membrane formation process. Other transitions could take place and be demonstrated on the ternary diagram as well. For example,

the formation of a glass from a polymer solution could be considered as a gel transition, and it is also called as vitrification.

The boundary of glass transition, if plotted as a straight line, divides the diagram into several parts of the liquid-liquid demixing gap, i.e. the glass state is divided into a homogenous stable glassy state and a metastable glassy state. As for the liquid-liquid demixing gap, it is not affected by the glass transition when the composition is below glass transition line. While it can be influenced when the composition is above the glass transition line. From the phase diagram, it is obvious that when the composition is located at high polymer concentration area and close to polymer-nonsolvent axis, the polymer rich phase will vitrify. While the vitrification is not the end of the phase separation process, the process will still take place in a slow speed (30).

In the diagram, the composition of the interface can reach different parts through different paths, for example, Radovanovic (31, 32) mentioned that due to the net outflow of solvent, sometimes the composition of the interface can reach a homogenous glassy state without entering the liquid-liquid demixing gap. While in other conditions, the composition will reach the liquid-liquid demixing gap at first, then as the exchange between solvent and nonsolvent continues, the polymer rich phase will keep moving towards the polymer-nonsolvent axis, as the polymer concentration in polymer rich phase is relatively high, this phase will eventually pass the glass transition. As an important transition during membrane formation process, vitrification phenomenon has been widely studied for a few decades, the ternary phase diagram of some common ternary polymer systems have already been studied and published in membrane fabrication field. For example, as a commonly used polymer solution, the polyphenylene oxide/trichloroethane (TCE)/ethanol system was studied by Burghardt (33), and other researchers can easily make assumptions and models for this particular demixing process. It should be mentioned that there are quite a few factors that can influence the

vitrification process (glass transition), for example, the increased viscosity of polymer solution can lower down the glass transition boundary significantly (34). More details will be given later in this review.

2.2.1.4 *Crystallization of polymers*

The crystallization happens in phase transition process as well. This phenomenon can bring significant influences to membrane formation process and determine many membrane properties such as membrane morphology and other structures. Similar to the liquid-liquid demixing gap and vitrification area, crystallization (liquid-solid demixing) could be indicated on the phase diagram too. Many factors can determine the crystallization of polymers, among which the polymer concentration of the solution and the molecular weight of polymer are some of the key factors (35). More specifically, kinetic aspects can strongly influence the crystallization: at high concentrations, the interpenetration of crystals can give rise to stiff brittle crystalline gels. The existence of the crystalline gels could affect the membrane morphology, and is influenced by other parameters. For instance, the formation of gels could be promoted by stirring the solution, increasing the polymer concentration and increasing the molecular weight of the polymer (36, 37). In this case, it could be seen that the molecular weight plays an important role in membrane formation process.

In phase diagrams that have liquid-liquid demixing gap and solid-liquid demixing gap, usually the liquid-liquid demixing gap is located at higher nonsolvent concentrations than the solid-liquid demixing gap, and many studies have observed this phenomenon (38). Based on this fact, it could be assumed that at higher nonsolvent concentrations, liquid-liquid demixing transition is more likely to take place than solid-liquid demixing, and also the composition of polymer solution can move from the crystallization gap to liquid-liquid demixing gap when the concentration of nonsolvent increases.

The crystallization of polymer sometimes is favored in some certain areas, for example, highly porous membranes that are suitable for drug delivery could be obtained by solid-liquid demixing induced fibre morphologies (39).

2.2.2 **Demixing speed**

Distinguished by the demixing speed, two kinds of demixing processes can result in two different types of membrane morphology.

Instantaneous liquid-liquid demixing is a demixing in which the membrane is formed immediately.

Delayed liquid-liquid demixing is a demixing in which the membrane formation process takes some time to finish.

Figure 2-4 shows the composition path of these two types of liquid-liquid demixing process at the very beginning of immersion in a nonsolvent bath (< 1s) (40). In figure 2-4, *b* represents the bottom composition of the membrane film while *t* represents the top composition. It is indicated that the bottom composition did not change in the liquid-liquid demixing process. In figure 2-4a, the path crossed the liquid-liquid demixing boundary, which means that liquid-liquid demixing starts immediately after immersion. While in figure 2-4b, the path did not cross the boundary at the first one second of immersion process, which means that the liquid-liquid demixing did not take place soon after the immersion. But in this case, the liquid-liquid demixing will eventually happen after a while, compositions beneath the top layer will cross the boundary then. Because of this, the morphologies of membranes casted from these two polymer solutions will be completely different.

Generally, a membrane formed as a result of instantaneous demixing would have a relatively porous top layers, and this type of membranes is usually used for

microfiltration/ultrafiltration. And the delayed liquid-liquid demixing can form a relatively dense top layer (40).

Other influences and the mechanisms of these two types of demixing process will be discussed in the next session.

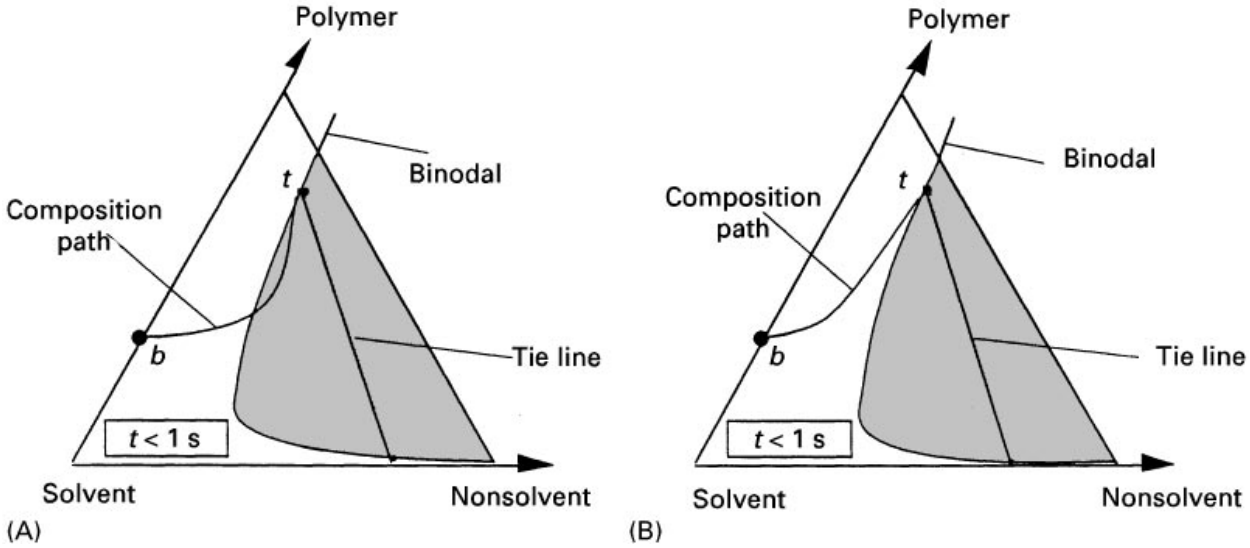

Figure 2-4 Two demixings. (40)

2.2.3 **Two dominating factors**

During the membrane formation process, thermodynamic effect and kinetic effect are the two dominating factors correlated with each other in the phase inversion process to determine the membrane formation (10). The thermodynamic effect is influenced by solution's thermodynamic property, while the kinetic effect is mainly determined by the rheological property of polymer solution. Generally speaking, the overall diffusion can be influenced by the solution viscosity, which is the main factor that determines the rheological property of polymer solution. The overall diffusion is inhibited by the increase of the solution viscosity and favoured with the decrease of the solution viscosity. Consequently, the viscosity can affect the exchange between solvent and non-solvent during the phase inversion process. In

terms of macrovoid structures, those two factors play important roles in the formation of macrovoid structures as well. More specifically, it is reported that the initial pores of macrovoid structures is possibly initiated by non-homogeneous demixing on the cast solution surface, which is favored by dynamic fluctuation caused by rapid exchange between solvent and non-solvent; while the growth of the pores is affected by rheological property of the solution. From the thermodynamic view point, enhanced thermodynamic instability, which could be observed as the shift of the cloud point to the P-S axis on the ternary phase diagram, promotes the instantaneous demixing in the phase separation process, resulting in thinning of the top skin layer, and formation of more finger –like structure and less sponge-like structure (7, 41). From the kinetic view point, on the other hand, the increase in viscosity brings higher diffusion resistance, which decreases the solvent/nonsolvent exchange rate in the phase inversion process. Consequently, this process could promote the delayed demixing and result in the thickening of the top skin layer, as well as the formation of less finger-like structure and more sponge-like structure (42). The finger-like and sponge-like structures are common structures in membrane morphology. The effect of these structures on membrane performances has been talked about a lot in some papers (41).

2.2.4 **Two pore formation mechanisms**

The dense surface layer of membrane is considered to be the selective layer that determines the selectivity of membrane. The pore size is the key factor on this layer that controls a membrane's permeability. There are two types of pore formation mechanisms that need more detailed discussions: Aggregate pores and network pores (43, 44).

Aggregate pores are larger than network pores and they could exit at the same time on membrane surface layer. The aggregate pores are considered to originate from the interstitial space between polymer aggregates; while the network pores are formed as the space between

polymer chain segments in each polymer aggregate. Many parameters will determine which type of pore is favoured during the phase inversion process, and the pore size and pore size distribution are significantly influenced by the factors such as casting solution concentration and viscosity, additive in the casting solution, conditions under which the phase separation takes places, solvent/nonsolvent exchange rate, the casting solution temperature and the casting atmosphere, and the composition and the temperature of the gelation media. For example, it is reported that the increase in the polymer concentration can decrease the distance between the polymer aggregates and decrease the aggregate size too. Some papers have covered this topic and studied the mechanisms of the formation of these two types of pores (45).

2.3 Factors that can affect membrane properties and performances in membrane fabrication process

2.3.1 Effect of the solvent used in membrane casting solutions

Different solvents used in membrane casting solutions can determine the membrane properties and performances significantly. As solvents, the most important thing is that when the solvent is used to dissolve a particular polymer, the polymer and solvent must be completely miscible with each other to generate a homogeneous state. In polymeric membrane fabrication field, the most commonly used organic solvents are N,N-dimethylacetamide (DMAC), dimethylformamide (DMF), 1-methyl-2-pyrrolidinone (NMP) and triethyl phosphate (TEP). Their solvent powers to a particular polymer are quite different as well. For instance, for PVDF polymer, DMAC shows the strongest solvent power while TEP shows a relatively low solvent power (46). It is quite obvious that when a solvent with strong solvent power demands a larger amount of nonsolvent to induce phase inversion. Thus when a solvent that has weak solvent power is used, a small amount of nonsolvent will be

needed to induce the phase inversion process, resulting in the appearance of an earlier liquid-liquid phase separation. In this case, macrovoids will be less likely to be formed and the development of sponge like structure is favoured. Also, the affinity between solvent and nonsolvent makes a difference as well: the weaker affinity may favor the formation of a sponge-like membrane structure. Another property of solvent that can influence the membrane formation process is the exchange rate between solvent and nonsolvent in the immersion-precipitation process, lower exchange rate may favour the formation of shorter finger-like structures with sponge structures while higher exchange rate may result in longer finger-like (macrovoid) structures with less sponge-like structures.

The thickness of membranes is also largely determined by the solvent used in polymer solutions. For example, literatures show that in some cases, when N-Methyl-2-pyrrolidone (NMP) is used as a solvent, the shrinkage of membrane structure caused by the outflow of solvent from the original polymer casting solution is limited due to the early formation of membrane skin layer (46). While the outflow of a large amount of solvent before the completion of phase inversion process may bring greater shrinkage of membrane. The early formation of skin layer can also result in irregular macrovoids, as the outflow of the solvent is prevented by the skin layer while the nonsolvent continues to enter. Thus NMP solvent should not be considered as a good solvent for PVDF polymer casting solution.

2.3.1.1 ***Polymer solution additives***

Polymeric membranes are casted from polymer solutions that usually consist of three compositions: solvent, non-solvent and polymer. Sometimes other additives are added into the polymer solutions to modify some membrane properties for different purposes. For instance, due to the addition of other materials, membrane surface properties, membrane pore size, membrane porosity, membrane morphology, membrane absorption performance and

other properties can be significantly changed (47). More specifically, additives in membrane casting solutions can be categorized into several types: polymeric additives (including high molecular weight polymers and low molecular weight polymers (48)), solvent additives, non-solvent additives, organic and inorganic acid and inorganic salt. Generally speaking, the effects of different additives are summarized as follows:

2.3.1.2 *Polymeric additives*

The addition of high molecular weight polymers results in dramatic changes in polymer solution properties and the structure of membranes. The porosity of membranes is usually increased, the pores are well interconnected and macrovoid structure is also more likely to be formed (48). Regarding membrane performance, it is reported that the addition of polyvinylpyrrolidone (PVP) can also bring significant increase in membrane permeability (49). Some explanations were given in literatures too. By adding new polymers into the casting solution, a new quaternary system is formed as a polymer a/polymer b/solvent/ non-solvent quaternary system, thus the interplay of two polymers on membrane formation process should not be neglected. More precisely, in terms of the demixing of the two polymers, Cabasso (50) mentioned that the micro phase demixing between the two polymers could prevent the formation of the dense top layer, which can decrease the resistance for liquid to go through membranes and enhance membrane performances. Also, phase separation of polymer solution could be enhanced by the addition of high molecular weight additives such as PVP. It is reported that by adding 5 wt. % PVP into 15 wt. % PS solution, the demixing speed of solvent and non-solvent during membrane formation process was accelerated due to the enhanced thermodynamic instability. PVP can also increase the nucleation and membrane structure growth rate, since PVP is a hydrophilic polymer, so the PVP in polymer solutions can promote water inflow in membrane formation process, resulting in a faster growth rate. Another explanation is about the leaching of PVP into the

water bath. It is worth mentioning that some researchers found the PVP leaching can result in a decrease in the polymer concentration, and the promotion of nucleation and membrane structure growth rate (51). The leaching of PVP can also benefit the formation of a porous membrane top layer. In this way, PVP is acting as a demixing enhancer that accelerates the phase separation in the polymer solution. The leaching efficiency could also be determined by PVP content. Figure 2-5 shows the relationship between PVP content and PVP retention factor (51). It should be pointed out that the higher retention factor leads to the lower leaching efficiency. In other words, as retention factor decreases, PVP leaches more easily into the water bath and form a porous membrane structure. In summary, because of the addition of PVP, the macrovoid (finger-like structure) could be favored to be formed. While by keeping adding more PVP into membrane casting solutions, the delayed demixing would then prevail the instantaneous demixing. This fact is attributed to the increased rheological hindrance (10). Because of high molecular weight polymers' non-solvent and high viscosity traits, high molecular weight polymers can bring huge influence to the interplay of thermodynamic effect and kinetic effect in membrane formation process. But rather than simply enhancing the thermodynamic effect, it actually acts as a complicated role depending on its content in polymer solutions and its molecular weight. In terms of the effect of polymer molecular weight on membrane structure and properties, a brief summary will be given below.

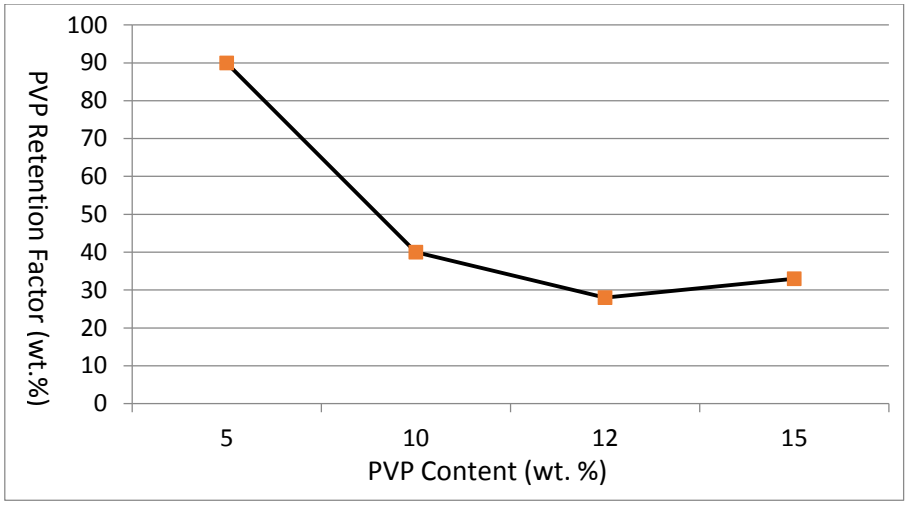

Figure 2-5 Effect of PVP content on PVP retention factor. (51)

With regards to low molecular weight additives, even though it is always deemed as a second polymer, but it could also be used to improve the morphology and performance of membranes. Due to its low viscosity, it may act as high molecular weight additives that can affect the phase inversion process in membrane formation and thus affects membrane morphology. But other literatures also mentioned that the addition of a low molecular weight additive can also result in the swelling of polymers or the formation of supermolecular aggregates (52, 53).

2.3.1.3 ***Inorganic salt***

Inorganic salts such as lithium chloride (LiCl), lithium nitrate ($LiNO_3$) and lithium perchlorate ($LiClO_4$) can also bring dramatic effect on membrane properties and morphologies. It is reported in literatures that the addition of LiCl can result in larger cavities that extended the membrane thickness by 50% (54). And with the increase of the amount of LiCl added, the cavities get larger (55). A more open structure of the membrane could be formed due to the addition of LiCl by increasing the rate of PVDF precipitation during the

immersion step. And the increased rate of PVDF precipitation is caused by the higher tendency of the solvent to mix with non-solvent (water). It is also mentioned that better membrane performance (gas permeation) (55) could be achieved and the viscosity of polymer solutions could be changed by the addition of LiCl as well. In terms of membrane properties, it is reported that membrane porosity and pore size were increased by the addition of LiCl while the LEP was decreased.

Other inorganic salts can change membrane properties and performances as well. The addition of $LiClO_4$ to polymer solution was also reported to have effect on membrane properties. The gelation of the polymer solution could be easily achieved with the presence of 2 wt% $LiClO_4$ (46). Also, some papers reported that sodium carbonate can improve the pore size distribution of the membrane as well (56). The formation of the skin layer and the gelation process are also significantly affected by the addition of other inorganic salts, such as potassium carbonate and sodium bicarbonate, resulting in the change of the skin layer thickness and pore size distribution of membranes.

2.3.2 **Casting Conditions**

2.3.2.1 ***Temperature***

Coagulation bath temperature can also affect the membrane properties. It is reported that the bath temperature can influence the membrane coagulation rate (57).As the solvent outflux and water influx speed could be accelerated by the higher coagulation bath temperature (58). It is also found that at higher temperature, liquid-liquid demixing could suppress crystallization process. More specifically, at the temperature of 50°C or higher, the liquid-liquid demixing would be favored, thus a cellular morphology in the substrate and finger-like structure are more likely to be formed. While at lower temperature, crystallization takes place first by suppressing the liquid-liquid demixing. Besides, the pore size of membrane was reported to be reduced when the annealing temperature reached 100°C (59).

2.3.2.2 *Effect of post-treatment*

The post-treatment in membrane fabrication process can significantly affect the membrane properties and performances too. The additives in gelation bath and the gelation bath temperature are the factors that have been studied.

It is reported by Radovanovic et al. (32) that the change of solvent concentration in the gelation bath can bring complex effects on membrane formation process. Small amount of solvent as additives in the gelation bath could promote instantaneous liquid-liquid demixing while large amount of solvent additives could delay the formation of membrane. Thus the skin layer of membrane can be affected.

Great shrinkage of the wet polymeric membranes often takes place during the drying process and the shrinkage can bring about the reduction of membrane porosity and/or pore size. One of the main reasons to have post-treatment is to reduce the shrinkage by employing the organic non-solvent exchange method (32).

2.4 **Membrane mass transfer**

Membrane mass transfer has been studied extensively in the membrane distillation field. The methods to calculate the membrane transfer may vary from for membrane distillation configurations. In this section, the mass transfer studies for the most basic membrane distillation configuration- direct contact membrane distillation and vacuum membrane distillation will be covered.

2.4.1 **Direct Contact Membrane Distillation.**

The very basic membrane equation for the pressure driven mass transfer is

$$J = C_m \Delta P \qquad (2)$$

Where J is the membrane mass flux, C_m is the membrane coefficient and $\Delta P$is the pressure difference between the feed and permeate surfaces of the membrane (13).

In the case of membrane distillation, the vapor pressure difference is used for the pressure difference. Further, applying the Antoine equation for water(60), the pressure difference can be replaced by temperature difference across the membrane surfaces when the separation process is for pure water or very dilute aqueous solution, the equation becomes(17, 61):

$$J = C_m \frac{dP}{dT}(T_{f,m} - T_{p,m}) \qquad (3)$$

Where $T_{f,m}$ and $T_{p,m}$ mean the temperature of membrane feed and permeate surface.

The membrane transport can also be expressed as the resistance to the vapour flow. Martinez and Rodriguez-Maroto (13, 62) used this approach and listed the membrane coefficients (reciprocal of the membrane resistances) for many membranes of different pore sizes. It was found that membrane coefficient is mainly determined by polymer type, pore size and temperature. In some studies, the membrane coefficient varies from $3.8*10^{-7}$ kg/m^2 Pa s to $21.5*10^{-7}$ kg/m^2 Pa s (63-66).

Many factors will have effects on the membrane coefficient, such as water activity, pore size distribution, membrane fouling resistance, temperature and membrane structures (67-69).

2.4.2 **Vacuum Membrane Distillation**

In vacuum membrane distillation process, due to the removal of air trapped in membrane pores, the molecular diffusion can be neglected when calculating membrane mass transfer flux. Thus, it was suggested that the Knudsen mechanism and Poiseuille flow are used in this case (70-72).

It is widely acknowledged that (73) Knudsen type flow is predominant when the ratio of the pore radius to the mean free path r_p/λ is less than 0.05. In this case, the molecule–pore wall collisions dominate the vapor-transport mechanism and the molar flow rate (mol/s) of component i can be calculated by (73):

$$F_i^k = \frac{2\pi}{3}\frac{1}{RT}\left(\frac{8RT}{\pi M_i}\right)^{\left(\frac{1}{2}\right)}\frac{r_k^3}{\tau\delta}\,(P_{i,m} - P_{i,p}) \qquad (4)$$

In this equation, r_k is the pore radius where Knudsen flow mechanism if applicable; M_i is the molecular weight of vapor; R is the gas constant; $P_{i,m}$ and $P_{i,p}$ are the partial pressures at the upstream and the downstream of the membrane surface, respectively. δ is the membrane thickness; and τ is thepore tortuosity. It should be noted that $P_{i,m}$ and $P_{i,p}$ correspond to $P_{f,m}$ and $P_{p,m}$ in equation (4).

While when r_p/λ is larger than 50, the molecule-molecule collisions will dominate and viscous flow will take place, in this case, Poiseuille flow model should be employed, and the equation used here is as below:

$$F_i^k = \frac{\pi r_v^4}{8\eta_i}\frac{P}{RT}\frac{1}{\tau\delta}(P_{i,m} - P_{i,p}) \qquad (5)$$

In this formula, r_v is the pore radius where the Poiseuille flow mechanism is applicable, η_i is the viscosity of species, and P is the average pressure in the pore.

When r_p/λ is between 0.05 and 50, both molecule-molecule and molecule-wall interactions should be taken into consideration. Thus, another equation should be introduced to calculate the flow rate (74):

$$F_i^k = \frac{\pi}{\tau\delta RT}[\frac{2}{3}\left(\frac{8RT}{\pi M_i}\right)^{\left(\frac{1}{2}\right)} r_t^3 + \frac{r_v^4}{8\eta_i}p](P_{i,m} - P_{i,p}) \qquad (6)$$

where r_t is the pore radius where the above equation for the transition region is applicable.

2.5 Membrane characterization

2.5.1 **Membrane surface properties**

Membrane surface properties can significantly affect membrane performances in many aspects. For example, surface modification can reduce fouling that is considered as one of the most serious drawbacks of the membranes for water treatment such as RO, NF, UF and MF. Accordingly, the modified surface should be characterized (75, 76). Indeed, remarkable progresses have been made recently for the membrane characterization. One of the important methods is to characterize the membrane by its hydrophobicity/hydrophilicity character, surface free energy and work of adhesion.

2.5.1.1 ***Membrane hydrophobicity/ hydrophilicity***

Liquid contact angle is usually used to describe the membrane hydrophobicity/ hydrophilicity property. The contact angle is defined as the angle that is formed when a liquid/vapor interface meets a solid surface. It can be usually described as Young's equation at a thermodynamic equilibrium between the three phases: the liquid phase, the solid phase and the gas/vapor phase:

$$0 = \gamma_{SG} - \gamma_{SL} - \gamma_{SG} \cos \theta c \qquad (7)$$

In this equation, θc is the contact angle, γ_{SG} is the solid-vapor interfacial energy, $\gamma_{SL}$is the solid-liquid interfacial energy and $\gamma_{LG}$is the liquid-vapor interfacial energy. Thus, the contact angle is related with surface energy and the properties of the solid, the liquid as well as the gas/vapor in this system.

When measured by using hydrophilic liquid (i.e. water), the increase in contact angle means the increase in hydrophobicity and the decrease in the wettability of membrane surface.

Porous and hydrophobic membranes should be used in vacuum membrane distillation

(VMD), which is an evaporative process that physically separates the aqueous liquid feed from the gaseous permeate kept under vacuum (77). In order to fulfill this requirement, polymers that have low values of the surface energy (high hydrophobicity) are used to make membrane casting solutions. These polymers include polytetrafluoroethylene (PTFE), polypropylene (PP), polyvinylidene fluoride (PVDF) and others (78). In this way, the feed liquid cannot penetrate into the pores easily while the evaporated vapor can. This also ensures that membranes for VMD have enough pores for vapour to go through. In terms of PVDF membranes, it was reported in previous publications that membranes made from PVDF (where the molecular weight of this PVDF material was not mentioned) exhibited the water contact angle of approximately 86–88° (78).

2.5.1.2 *Membrane Surface Free Energy and Work of Adhesion*

Membrane surface free energy is a very important membrane property, for it determines the liquid wettability, adhesion and repellency (79, 80). In order to calculate surface free energy, the Lifshitz-van der Waals and polar, Lewis acid-base interactions are used as the following Young equation:

$$(1+\cos\theta)\gamma_L = 2(\gamma_S^{LW}\gamma_L^{LW})^{\frac{1}{2}} + 2(\gamma_S^{+}\gamma_L^{-})^{\frac{1}{2}} + 2(\gamma_s^{-}\gamma_L^{+})^{\frac{1}{2}} \qquad (8)$$

Where γ is the surface free energy, the subscripts *S* and *L* indicate the solid/vapor and liquid/vapor boundary respectively. LW, +, - mean the apolar or Lifshitz-van der Waals component, Lewis acid component and Lewis base component of the surface free energy (81). The three components of the surface free energy of solid (which means membrane), γ_S^{LW}, γ_S^{+} and`γ_s^{-}) are obtained by measuring the contact angles of three liquids, usually water, ethylene glycol and diiodomethane From these surface energy components, the total surface energy of membrane can be calculated as:

$$\gamma_s = \gamma_s^{LW} + \gamma_S^{AB} = \gamma_s^{LW} + 2(\gamma_S^{+}\gamma_S^{-})^{\frac{1}{2}} \qquad (9)$$

Adhesion is defined as the process of attachment of a substance to the surface of another substance (82). In a typical solid-liquid-gas/vapor system, the contact angle is used to quantify adhesiveness, and the smaller contact angle results in stronger adhesion. The work of adhesion is calculated by using the Young-Dupre equation that describes the interactive force between the liquid and solid phases (83). Higher work of adhesion value results in a high degree of wetting between the used liquid and solid surface.

$$\gamma(1 + \cos\theta_C) = \Delta W \qquad (10)$$

The work of adhesion - as well as the liquid contact angle and surface free energy- is supposed to be an intrinsic property of the polymer chemistry but in reality it is also affected by surface roughness.

2.5.2 **Surface Roughness**

The surface roughness could be defined as the deviation of the actual membrane surface topography from an ideal atomically smooth surface (84). As one of membrane properties it plays an important role to decide the membrane performance, as it can affect the transmembrane transport and fouling potential. Especially for RO and NF membranes, surface roughness is one of the key factors that can determine membrane fouling (85). Other researches also showed that for ultrafiltration membranes, the surface roughness can be potentially correlated with the membrane pore size distribution and other membrane properties as well (86). The average roughness is the mean value of the surface height relative the centre plane. It is determined by including the volumes of the surface above and below the plane. An equation could be used to calculate the surface roughness (R_{AVG}) (87):

$$R_{AVG} = \sum_{n=1}^{N} \frac{|Z_n - \overline{Z}|}{N} \qquad (11)$$

N is the number of point in the sample area, Zn is the height of the sample point and $\overline{Z}$ is that of the plane.

Usually, roughness parameters can be calculated from the AFM image with an AFM software program.

2.5.3 **Liquid Entry Pressure**

Porous hydrophobic membranes do not permit passage of water until a critical transmembrane pressure difference is exceeded. Liquid entry pressure (LEP) is the pressure difference at which the liquid penetrates into the largest pores of the hydrophobic membrane, which is abbreviated as LEP (88). This critical pressure difference is correlated to the interfacial tension, the contact angle of the liquid on the surface (surface free energy and liquid-phobicity), temperature as well as the size and shape of membrane pores (63, 89). This property is very important in membrane distillation process, since the pores of the MD membrane should be filled only by vapour. Thus a high LEP in membrane distillation process is favoured in this field. One of the advantages of employing LEP measurement to evaluate membrane performance in membrane distillation is that the LEP only takes the pores that connect both ends of the membrane into consideration, as the liquid cannot go through the plugged pores. Consequently only active pores are included in this measurement and inactive pores are excluded.

The pressure difference at the liquid-vapor interface could be expressed by using the Laplace-Young equation (90).

It could be concluded from the equation that a membrane with high hydrophobicity, small pore size, and high surface tension for the feed solution usually shows a high LEP (91). This kind of membrane is favoured in membrane distillation process, while there is a dilemma that small pore size may bring low membrane distillation flux. However, liquid is more likely and easily to penetrate membranes in vacuum membrane distillation than other membrane

distillation configurations, thus membranes that have small pore sizes are favoured in this particular configuration (74, 92).

2.5.4 **Membrane Pore Size and Porosity**

There are three types of pores in polymeric membranes (93):

2.5.4.1 ***Pore Types***

Cylindrical

Cylinder shaped pores are the pores that go through the whole membrane, which means that this type of pores connects both sides of the membrane and allows feed to permeate through the porous membrane. This type of pores is the most commonly assumed pores in membrane distillations. These pores usually have lower surface areas as compared to other types of pores.

Sponge

Sponge pores exist as randomly shaped cavities, channels, throughout the whole membrane. These pores have relatively larger surface area that can more likely to trap particles. Unlike the cylindrical pores, sponge pores are usually far less uniform.

Blind Pores

Blind pores are pores that do not go through the membrane and connect both sides of the membrane. Thus there is no permeation through these pores.

2.5.4.2 ***Porosity, Pore size and pore size distribution measurement***

Membrane porosity is a measure of the void spaces in a porous membrane and is expressed as the fraction of the void volume over the total volume. Higher membrane porosity means that the membrane has more void fractions. Thus it can result in larger evaporation surface area, higher permeate flux and lower conductive heat loss (13).

The optimum membrane porosity of membranes in membrane distillation systems is reported to range between from 30% to 85% (94). By taking other membrane properties into consideration, effective porosity is used to make the measurement more accurate. The effective porosity ε_e is defined as the ratio of the porosity (ε) and the effective pore length (L_p) (95):

$$\varepsilon_e = \varepsilon / L_P \qquad (12)$$

Membrane pore size is a key factor in membrane distillation. The increase in membrane pore size will result in the increase in membrane distillation flux, while when the pore size is too large the liquid will penetrate into the membrane and it will stop acting as a physical barrier. Thus the membrane distillation cannot take place anymore. Hence when choosing the membrane for membrane distillation, two factors should be considered in terms of the membrane pore size: 1) The pores should be large enough to ensure a relatively high flux; 2) the pores must be small enough to prevent liquid from penetrating through the membrane under the membrane distillation operating conditions. Consequently, the optimum pore size should be determined based on the operating conditions. Generally speaking, the pore sizes of membranes used in membrane distillation processes should be in the range from 100nm to 1μm (94, 96).

Molar flux through a pore is mainly related to some membrane characteristic parameters: membrane's average pore size, membrane porosity, membrane tortuosity and membrane thickness. An equation is given below to show the correlation:

$$N \propto \frac{r^{\alpha}\varepsilon}{\delta\tau} \qquad (13)$$

r^{α} is the average pore size for Knudsen diffusion or the average squared pore size for viscous flux, ε is membrane porosity, τ is membrane tortuosity and δ is membrane thickness. It can be concluded from the equation that in order to maximize membrane distillation flux, pore

size and membrane porosity should be increased while membrane tortuosity and thickness should be decreased. It is reported that in some membrane distillation systems, porosity could be the dominating factor (97). As membranes do not usually have uniform pore sizes, membrane pore size distribution should be taken into consideration as well. Khayet (61) reported that when mean pore size is used to calculate vapour transfer coefficient instead of pore size distribution, the result may not be accurate. As a result, all the aforesaid parameters should be considered when analysing membrane distillation models.

There are quite a few factors that can affect these membrane characteristics. For example, it is reported that increasing polymer's molecular weight would bring a larger pore size in the skin layer of membrane, lower membrane porosity, higher strength and permeability and lower rejection. The average pore size at the surface layer of asymmetric polymeric membranes is increased by a decrease in polymer concentration (98). Because of the slowed exchange between solvent and nonsolvent in the phase separation process, increased polymer solution viscosity can also decrease membrane pore sizes. It is also reported that membranes prepared with higher amounts of non-solvent additives in the polymer solutions have relatively larger pore sizes (92).

With regards to membrane pore size and pore size distribution measurement, various methods have been proposed (4):

1) Microscopic method
2) Bubble pressure and gas transport method
3) Mercury porosimetry
4) Liquid-vapor equilibrium method (BJH)
5) Gas-liquid equilibrium method (permporometry)
6) Liquid-solid equilibrium method (thermoporometry)

Gas permeability method is a frequently used technique to measure the pore size of membranes samples. This method can only measure the average pore size by measuring the flow rate of a gas through a porous membrane while the pore size distribution cannot be measured (99). Figure 2-6 shows the schematic of the measurement of gas permeation method:

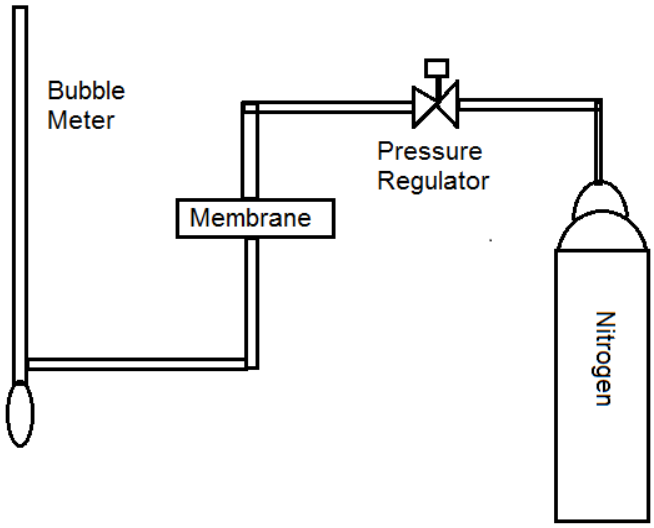

Figure 2-6 Gas permeation test setup.

The pressure regulator is used to control the pressure, and usually nitrogen is used. A bubble flow meter is used to measure the gas flow rate.

The pore size is obtained by the method described by Khayet et al (100). According to the method, the permeance is given as (101):

$$B = \frac{4}{3}\left(\frac{2}{\pi MRT}\right)^{0.5}\frac{rp^{\varepsilon}}{L_p} + \frac{P_m}{8\mu RT}\frac{r_P^2\varepsilon}{L_p} = I_0 + S_0P_m \qquad (14)$$

where B is the gas permeance (mol/m^{2}sPa), M is the molecular weight of the gas (kg/mol), R is the gas constant (J/mol•K), T is the absolute temperature (K), r_p is the pore size (m), μ is the viscosity of the gas (Pa s), ε is the membrane porosity, L_p is the effective pore length (m),

and P_m is the mean pressure within the membrane pore (Pa), which is set equal to the average of the feed and permeate gas pressures. From the linear plot of B versus P_m, slope S_o and intercept I_o are obtained. The pore size, r_p, is calculated by

$$r_p = \frac{16}{3}\left(\frac{S_0}{I_0}\right)\left(\frac{8RT}{\pi M}\right)^{0.5}\mu \qquad (15)$$

This method has been widely used by many researchers. But the accuracy is one of the main problems of using this method (4, 102, 103).

2.5.5 **Investigations of membrane pore size and porosity by near field microscopy.**

Microscopy has been widely employed to investigate membrane properties in membrane researches. Usually three types of microscopy are mainly used: scan electronic microscope (SEM), tapping mode atomic force microscopy (TM – AFM) and transmission electron microscopy (TEM).

Banerjee et al (104) determined and tested a method to detect sheet uniformity by using a SEM microscope.

Using a SEM microscope, paper samples were mounted at 90°C and photographed at a 25x or 100x magnifications. A 3-D topography was created by having an electron beam traverse the surface of the vacuum contained sample in the raster pattern. The impinged surface points in turn emit secondary electrons and these are collected by an in column detector. However it should be noted that due to the spatial arrangement, the angle between the electron beam and locations on the sample surface will vary slightly. The result was an image, where lighter areas represented fiber mass, and darker areas related to more void space.

The accuracy of this method was tested by comparing the effect of the addition of debonders on membranes. Debonders can be used to decrease the roughness of a membrane side. It was found that, using this SEM method, the roughness of the top half increased, but the roughness

decreased for the bottom half, showing the accuracy of SEM in detecting membrane roughness.

Another trial was done through the addition a c-PAM (a retention aid). c-PAM promotes fibre flocculation which reduces uniformity. SEM detection in this manner was able to sense the increase in SEM roughness index upon c-PAM addition.

Widiatmoko et al. (105) designed a method based on the principle that SEM images are composed of greybit scale with integer scale of 0 – 255. Depressions or dips are represented as dark areas, and peaks and heights as lighter areas. Given a top view SEM image of a porous membrane, Widiatmoko et al. stated that it was possible to obtain pore size information from dark pixels.

A program was created, where an SEM image file is read, and a threshold integer value is set. Pixels within the SEM image darker than this threshold were defined as a pore, while pixels lighter than this threshold value were considered peaks. When one pore was found the program marked all adjacent dark pixels as a pore in order to determine the pore area.

However, the most difficult part is determining the threshold value. Should the threshold value be too low, pores may be omitted, and should the threshold value be too high, adjacent pores might be detected as a singular large pore.

The solution proposed was to determine the threshold value by using the cumulative frequency of pixel values (the number of all pixels darker than a value divided by the number of all pixels). Widiatmoko et al. found that after examination of SEM images, suitable threshold values exist lower than the limit of 20% of the darkest pixels. The proposed method offers a simple way to calculate pore size distribution of SEM images. However it is noted that the performance is limited to solid porous materials, or materials containing holes. In materials with no properly defined pores, this method proves to be inadequate. In addition,

the information within the analyzed images in this study was reduced to one-bit. This greatly removes the majority of information contained in the image. This method may require refining.

Khayet et al (92), used tapping mode atomic force microscopy (TM – AFM) to obtain mean pore size and pore size distribution, pore density, surface porosity and roughness parameters and then compared these values to those determined from a gas permeation test. More specifically, laboratory prepared PVDF membranes and two commercial PVDF membranes were structurally characterized by a tapping mode atomic force microscope (TM-AFM) on a Nanoscope III equipped with 1553D scanner from Digital Instruments, Santa Barbara, CA, USA. Small pieces approximately 0.5 × 0.5 cm in area were cut from the membrane. This sample was then fixed over a magnetic holder. To obtain the pore size, cross-sectional line profiles were chosen to traverse micron scan surface areas of the TM-AFM images (106). The diameters of the low valleys (pores) were measured by a pair of cursors along the reference line, where the horizontal distance between each pair of cursors was the diameter of the pore.

When compared with mean pore sizes obtained from gas permeation tests, it was found that TM-AFM methods obtained mean pore values that were 1.2 to 2.1 times higher than values determined from the gas permeation test. In addition, it was found that the TM-AFM determined mean pore sizes were also larger for commercial membranes GVHP and HVHP.

When values obtained using TM-AFM were used in calculations to determine VMD water vapor flux, it was found that predictions obtained from the mean pore size values obtained by TM-AFM were closer to experimentally measured values. While the values obtained by gas permeation testing, were closer to the predictions.

It is suggested by Phattaranawik et al. (107), that the low precision of TM-AFM method, may be due to pore contraction during the metal coating procedure needed to prepare the membrane for TM-AFM viewing. Results regarding TM-AFM analysis to determine mean pore size are inconclusive. While water vapor flux using TM-AFM obtained values were closer to experimental measurements, gas permeation obtained values were closer to predictions.

2.5.6 **Membrane Tortuosity and Thickness**

Membrane tortuosity is used in cylindrical shape membrane model. The term tortuosity is a property of curve being tortuous and commonly used to describe diffusion in porous media (108). It can be calculated by expressing the length of the curve (L) to the distance between the ends of the curve (C):

$$\tau = \frac{L}{C} \qquad (16)$$

High tortuosity value can result in the increase in mass transfer resistance, thus brings low permeate flux. Macki-Meares(109) suggested a most ideal correlation to maximize the permeate flux in membrane distillation:

$$\tau = \frac{(2-\varepsilon)^2}{\varepsilon} \qquad (17)$$

There are two membrane thicknesses. One is the total membrane thickness and the other is the thickness of the skin layer of the membrane. Membrane thickness is also a very important membrane property. The effect of total membrane thickness on membrane performance cannot be neglected. In membrane distillation systems, membrane thickness can significantly influence the permeate flux. The increased membrane thickness will result in lower permeate flux and less heat loss due to the increased mass transfer resistance. While the membranes

used in membrane distillation systems should also be thick enough to fulfill the strength requirement for membranes. It was reported that the optimum membrane thickness for membrane distillation systems should range from 30μm to 60μm (110).

2.6 **Membrane Distillation Operation Parameters**

The operational conditions can significantly influence the MD efficiency, especially for vacuum membrane distillation. Some of the parameters that affect the membrane performance are as follows: feed temperature, vacuum degree, feed concentration, feed recirculation rate and membrane type.

The feed temperature is one of the key factors that can determine the permeate flux. It is reported that when the temperature difference between the hot and the cold fluid is constant, the permeate flux is mainly determined by the hot fluid temperature due to high vapor pressure on the feed side. Many researches have shown that increased temperature could result in higher vapour flux due to the improved diffusion coefficient (111, 112). As a result of the increased diffusivity, the mass transfer coefficient is also enhanced by the increased feed temperature (113, 114).

As the vapour pressure decreases when the feed concentration increases, the permeate flux can also decrease due to the decreased vapour pressure. Thus increased feed concentration can lead to lower permeate flux (68). On the other hand, as the feed evaporates when membrane distillation takes place, the feed concentration would increase. As a result the permeate flux is reduced by the prolonged operation time (115). Some other literatures also reported that the increase in acid concentration may cause the lessened permeate flux (116).

For vacuum membrane distillation, the vacuum level is another key factor that can influence the permeate flux and VMD performance. Increase in permeate flux is observed by enhancing

the vacuum level, since the water vapor pressure on the permeate side is significantly lowered, thus the enlarged transmembrane pressure difference can bring about higher permeate flux. Figure 2-7 shows the correlation between the vacuum level and the permeate flux at two temperatures (112). The sensitivity of the flux is also reported to be reduced as the vacuum level increases (117).

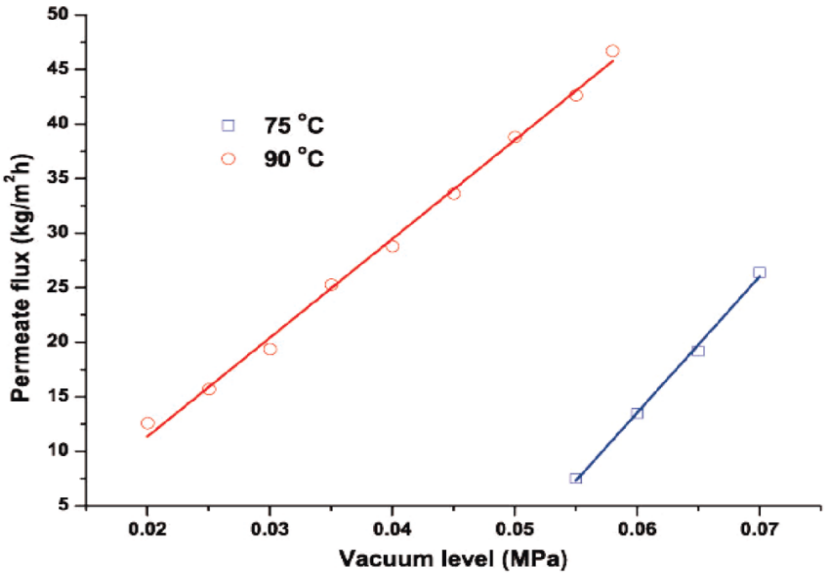

Figure 2-7 The correlation between vacuum level and permeate flux at certain temperatures.(112)

A membrane that has high porosity and large pore size is favoured in membrane distillation configurations. Also, the membrane thickness and tortuosity should be carefully chosen when determining which membrane should be used in certain membrane distillation systems. Such discussions have been done in previous parts in this literature review.

References

1. Sidney LS, Sourirajan, inventor; Univ C, assignee. **High flow porous membranes for separating water from saline solutions**. United States 1964 .

2. Pinnau, I., Freeman, B.D. **Membrane formation and modification**. American Chemical Society; 1999.

3. Baker RW. **Membrane separation systems - recent developments and future directions**. William Andrew Publishing/Noyes; 1991.

4. Nakao S. Determination of pore size and pore size distribution. 3. filtration membranes. J Membr Sci. 1994;96(1-2):131-65.

5. Chae Park H, Po Kim Y, Yong Kim H, Soo Kang Y. Membrane formation by water vapor induced phase inversion. J Membr Sci. 1999;156(2):169-78.

6. Van De Witte P, Dijkstra PJ, Van Den Berg JWA, Feijen J. Phase separation processes in polymer solutions in relation to membrane formation. J Membr Sci. 1996;117(1-2):1-31.

7. Bakeri G, Matsuura T, Ismail AF. The effect of phase inversion promoters on the structure and performance of polyetherimide hollow fiber membrane using in gas-liquid contacting process. J Membr Sci. 2011;383(1-2):159-69.

8. Jia Z, Chang Q, Qin J, Sun H. Preparation of nanoparticles with a continuous gas-liquid membrane contactor: Absorption process. J Membr Sci. 2010;352(1-2):50-4.

9. Liu F, Hashim NA, Liu Y, Abed MRM, Li K. Progress in the production and modification of PVDF membranes. J Membr Sci. 2011;375(1-2):1-27.

10. Han M-, Nam S-. Thermodynamic and rheological variation in polysulfone solution by PVP and its effect in the preparation of phase inversion membrane. J Membr Sci. 2002;202(1-2):55-61.

11. Alves VD, Coelhoso IM. Orange juice concentration by osmotic evaporation and membrane distillation: A comparative study. J Food Eng. 2006;74(1):125-33.

12. Zakrzewska-Trznadel G, Harasimowicz M, Chmielewski AG. Concentration of radioactive components in liquid low-level radioactive waste by membrane distillation. J Membr Sci. 1999;163(2):257-64.

13. Alkhudhiri A, Darwish N, Hilal N. Membrane distillation: A comprehensive review. Desalination. 2012;287:2-18.

14. Winter D, Koschikowski J, Wieghaus M. Desalination using membrane distillation: Experimental studies on full scale spiral wound modules. J Membr Sci. 2011;375(1-2):104-12.

15. Calabrò V, Jiao BL, Drioli E. Theoretical and experimental study on membrane distillation in the concentration of orange juice. Industrial and Engineering Chemistry Research. 1994;33(7):1803-8.

16. Blanco Gálvez J, García-Rodríguez L, Martín-Mateos I. Seawater desalination by an innovative solar-powered membrane distillation system: The MEDESOL project. Desalination. 2009;246(1-3):567-76.

17. Hsu ST, Cheng KT, Chiou JS. Seawater desalination by direct contact membrane distillation. Desalination. 2002;143(3):279-87.

18. Banat FA, Simandl J. Desalination by membrane distillation: A parametric study. Sep Sci Technol. 1998;33(2):201-26.

19. Lawson KW, Lloyd DR. Membrane distillation. J Membr Sci. 1997;124(1):1-25.

20. Strathmann, H., Production of microporous media by phase inversion. In: D. R. Lloyd (Ed.), Materials Science of Synthetic Membranes, ACS Symposium Series No. 269, American Chemical Society, Washington, DC, p. 165-195 (1985).

21. Strathmann H, Kock K. The formation mechanism of phase inversion membranes. Desalination. 1977;21(3):241-55.

22. Zeman L, Fraser T. Formation of air-cast cellulose acetate membranes. part I. study of macrovoid formation. J Membr Sci. 1993;84(1-2):93-106.

23. Huggins ML. Solutions of long chain compounds. J Chem Phys. 1941;9(5):440.

24. Flory PJ. Thermodynamics of high polymer solutions. J Chem Phys. 1941;9(8):660-1.

25. H. Tompa, Polymer Solutions. Academic Press, New York, 1956.

26. Altena FW, Smolders CA. Calculation of liquid-liquid phase separation in a ternary system of a polymer in a mixture of a solvent and a nonsolvent. Macromolecules. 1982;15(6):1491-7.

27. Yilmaz L, McHugh AJ. Analysis of Nonsolvent -Solvent -Polymer Phase Diagrams and Their Relevance to Membrane Formation Modeling. J ApplPolym Sci. 1986;31(4):997-1018.

28. Nedoma AJ, Robertson ML, Wanakule NS, Balsara NP. Measurements of the flory-huggins interaction parameter using a series of critical binary blends. Ind and EngChem Res. 2008;47(10):3551-3.

29. Zeman L, Tkacik G. Thermodynamic analysis of a membrane-forming system water/N-methyl-2-pyrrolidone/polyethersulfone. J Membr Sci. 1988;36(C):119-40.

30. S. Callister, A. Keller, R. M. Hikmet. **On thermoreversible gels: Their classification, relation to phase transitions and vitrification, their morphology and properties**. . October 1990;Macromolecular Symposia:19–54.

31. Radovanovic P, Thiel SW, Hwang S-. Formation of asymmetric polysulfone membranes by immersion precipitation. part I. modelling mass transport during gelation. J Membr Sci. 1992;65(3):213-29.

32. Radovanovic P, Thiel SW, Hwang S-. Formation of asymmetric polysulfone membranes by immersion precipitation. part II. the effects of casting solution and gelation bath compositions on membrane structure and skin formation. J Membr Sci. 1992;65(3):231-46.

33. Burghardt WR, Yilmaz L, McHugh AJ. Glass transition, crystallization and thermoreversible gelation in ternary PPO solutions; relationship to asymmetric membrane formation. Polymer. 1987;28(12):2085-92.

34. Gaides GE, McHugh AJ. Gelation in an amorphous polymer: A discussion of its relation to membrane formation. Polymer. 1989;30(11):2118-23.

35. Mandelkern. Comprehensive polymer science. In: Crystallization and melting .Pergamon, Oxford; 1989. p. Vol. 2,.

36. Zwijnenburg A, Pennings AJ. Longitudinal growth of polymer crystals from flowing solutions III. polyethylene crystals in couette flow. Colloid and Polymer Science Kolloid-Zeitschrift&ZeitschriftfürPolymere. 1976;254(10):868-81.

37. A. Keller, in A. Hiltner (Ed.). Structure property relationships of polymeric solids. New York: Plenum Press; 1983.

38. Cheng L, Dwan A, Gryte CC. Isothermal phase behavior of nylon-6, -66, and -610 polyamides in formic acid-water systems. J PolymSci Part B. 1994;32(7):1183-90.

39. Van De Witte P, Esselbrugge H, Dijkstra PJ, Van Den Berg JWA, Feijen J. Phase transitions during membrane formation of polylactides. I. A morphological study of membranes obtained from the system polylactide-chloroform-methanol. J Membr Sci. 1996;113(2):223-36.

40. Mulder J. Basic Principles of Membrane Technology. Dordrecht: Kluwer; 1996. p. 3344.

41. Barton BF, Reeve JL, Mchugh AJ. Observations on the dynamics of nonsolvent-induced phase inversion. J PolymSci Part B. 1997;35(4):569-85.

42. Smolders CA, Reuvers AJ, Boom RM, Wienk IM. Microstructures in phase-inversion membranes. part 1. formation of macrovoids. J Membr Sci. 1992;73(2-3):259-75.

43. Zhenxin Z, Matsuura T. Discussions on the formation mechanism of surface pores in reverse osmosis, ultrafiltration, and microfiltration membranes prepared by phase inversion process. J Colloid Interface Sci. 1991;147(2):307-15.

44. S. Sourirajan and T. Matsuura. Reverse osmosis/ultrafiltration process principles. In: National Research Council; 1985.

45. Nguyen, T. D., Matsuura, T. and Sourirajan, S. Effect of the casting solution on the pore size and pore size distribution of resulting aromatic polyamide membranes. Chem. Eng. Commun., 57, 351–369.

46. Yeow ML, Liu YT, Li K. Morphological study of poly(vinylidene fluoride) asymmetric membranes: Effects of the solvent, additive, and dope temperature. J ApplPolym Sci. 2004;92(3):1782-9.

47. Mansourizadeh A, Ismail AF. Effect of additives on the structure and performance of polysulfone hollow fiber membranes for CO2 absorption. J Membr Sci. 2010;348(1-2):260-7.

48. Wienk IM, Boom RM, Beerlage MAM, Bulte AMW, Smolders CA, Strathmann H. Recent advances in the formation of phase inversion membranes made from amorphous or semi-crystalline polymers. J Membr Sci. 1996;113(2):361-71.

49. Yeo H-, Lee S-, Han M-. Role of a polymer additive in casting solution in preparation of phase inversion polysulfone membranes. J ChemEng Japan. 2000;33(1):180-4.

50.Cabasso I, Klein E, Smith JK. Polysulfone hollow fibers. I. Spinning and properties. J ApplPolym Sci. 1976;20(9):2377-94.

51. Matsuyama H, Maki T, Teramoto M, Kobayashi K. Effect of PVP additive on porous polysulfone membrane formation by immersion precipitation method. Sep Sci Technol. 2003;38(14):3449-58.

52. Vásárhelyi K, Ronner JA, Mulder MHV, Smolders CA. Development of wet-dry reversible reverse osmosis membrane with high performance from cellulose acetate and cellulose triactate blend. Desalination. 1987;61(3):211-35.

53. Kesting RE, Menefee A. The role of formamide in the preparation of cellulose acetate membranes by the phase inversion process. Kolloid-Zeitschrift&ZeitschriftfürPolymere. 1969;230(2):341-6.

54. Tomaszewska M. Preparation and properties of flat-sheet membranes from poly(vinylidene fluoride) for membrane distillation. Desalination. 1996;104(1-2):1-11.

55. Bottino A, Capannelli G, Munari S, Turturro A. High performance ultrafiltration membranes cast from LiCl doped solutions. Desalination. 1988;68(2-3):167-77.

56. Wang S, Wang Z, Zhang Y, Wu W, Liu D, Zhang X. Experimental study of the control of pore sizes of porous membranes applying chemicals methods. Desalination. 2005;177(1-3):7-13.

57. Wang D, Li K, Teo WK. Porous PVDF asymmetric hollow fiber membranes prepared with the use of small molecular additives. J Membr Sci. 2000;178(1-2):13-23.

58. Uragami T, Fujimoto M, Sugihara M. Studies on syntheses and permeabilities of special polymer membranes. 27. concentration of poly(styrene sulphonic acid) in various aqueous solutions using poly(vinylidene fluoride) membranes. Polymer. 1981;22(2):240-4.

59. Strathmann H, Scheible P, Baker RW. Rationale for the preparation of loeb- sourirajan-type cellulose acetate membranes. J ApplPolym Sci. 1971;15(4):811-28.60. Kurokawa H, Kuroda O, Takahashi S, Ebara K. Vapor permeate characteristics of membrane distillation. Sep Sci Technol. 1990;25(13-15):1349-59.

61. Khayet M, Velázquez A, Mengual JI. Modelling mass transport through a porous partition: Effect of pore size distribution. J Non EquilibThermodyn. 2004;29(3):279-99.

62. Martínez L, Rodríguez-Maroto JM. On transport resistances in direct contact membrane distillation. J Membr Sci. 2007;295(1-2):28-39.

63. García-Payo MC, Izquierdo-Gil MA, Fernández-Pineda C. Wetting study of hydrophobic membranes via liquid entry pressure measurements with aqueous alcohol solutions. J Colloid Interface Sci. 2000;230(2):420-31.

64. Imdakm AO, Matsuura T. A montecarlo Simulation model for membrane distillation processes: Direct contact (MD). J Membr Sci. 2004;237(1-2):51-9.

65. Zolotarev PP, Ugrozov VV, Volkina IB, Nikulin VM. Treatment of waste water for removing heavy metals by membrane distillation. J Hazard Mater. 1994;37(1):77-82.

66. Mart´inez L, Florido-D´iaz FJ, Hernandez A, Pradanos P. Estimation of vapor transfer coefficient of hydrophobic porous membranes for applications in membrane distillation. Separation and Purification Technology. 2003;33(1):45-55.

67. Schofield RW, Fane AG, Fell CJD. Gas and vapour transport through microporous membranes. II. membrane distillation. J Membr Sci. 1990;53(1-2):173-85.

68. Martínez L. Comparison of membrane distillation performance using different feeds. Desalination. 2004;168(1-3):359-65.

69. Chan MT, Fane AG, Matheickal JT, Sheikholeslami R. Membrane distillation crystallization of concentrated salts - flux and crystal formation. J Membr Sci. 2005;257(1-2):144-55.

70. Bandini S, Sarti GC. Heat and mass transport resistances in vacuum membrane distillation per drop. AIChE J. 1999;45(7):1422-33.

71. Lawson KW, Lloyd DR. Membrane distillation. I. module design and performance evaluation using vacuum membrane distillation. J Membr Sci. 1996;120(1):111-21.

72. Khayet M, Matsuura T. Pervaporation and vacuum membrane distillation processes: Modeling and experiments. AICHE J. 2004;50(8):1697-712.

73. Matsuura T. Synthetic Membranes and Membrane Separation Processes. 1994.

74. Lawson KW, Lloyd DR. Review: Membrane distillation. J MembrSci. 1997;124:1-25.

75. Kim Y, Rana D, Matsuura T, Chung W-. Influence of surface modifying macromolecules on the surface properties of poly(ether sulfone) ultra-filtration membranes. J Membr Sci. 2009;338(1-2):84-91.

76. Shannon MA, Bohn PW, Elimelech M, Georgiadis JG, Marias BJ, Mayes AM. Science and technology for water purification in the coming decades. Nature. 2008;452(7185):301-10.

77. Bandini S, Gostoli C, Sarti GC. Separation efficiency in vacuum membrane distillation. J Membr Sci. 1992;73(2-3):217-29.

78. Gryta M, Barancewicz M. Influence of morphology of PVDF capillary membranes on the performance of direct contact membrane distillation. J Membr Sci. 2010;358(1-2):158-67.

79. Owens DK, Wendt RC. Estimation of the surface free energy of polymers. J ApplPolym Sci. 1969;13(8):1741-7.

80. Kaelble DH, Moacanin J. A surface energy analysis of bioadhesion. Polymer. 1977;18(5):475-82.

81. Yildirim Erbil H. Surface energetics of films of poly(vinyl acetate-butyl acrylate) emulsion copolymers. Polymer. 1996;37(24):5483-91.

82. Vert M, Doi Y, Hellwich K-, Hess M, Hodge P, Kubisa P, et al. Terminology for biorelated polymers and applications (IUPAC recommendations 2012). Pure and Applied Chemistry. 2012;84(2):377-410.

83. Kendall K. Adhesion: Molecules and mechanics. Science. 1994;263(5154):1720-5.

84. Khulbe, K. C., Feng, C. Y., & Matsuura, T. Synthetic polymer membranes: Characterization by atomic force microscopy (chapter 5). In: Springer Laboratory; 2008.

85. Elimelech M, Zhu X, Childress AE, Hong S. Role of membrane surface morphology in colloidal fouling of cellulose acetate and composite aromatic polyamide reverse osmosis membranes. J Membr Sci. 1997;127(1):101-9.

86. Bowen WR, Doneva TA. Atomic force microscopy characterization of ultrafiltration membranes: Correspondence between surface pore dimensions and molecular weight cut-off. Surf Interface Anal. 2000;29(8):544-7.

87. Surface roughness [Internet]. Available from: http://membranes.edu.au/wiki/index.php/Surface_Roughness#cite_note-1.

88. Smolders K, Franken ACM. Terminology for membrane distillation. Desalination. 1989;72(3):249-62.

89. García-Payo MC, Izquierdo-Gil MA, Fernández-Pineda C. Air gap membrane distillation of aqueous alcohol solutions. J Membr Sci. 2000;169(1):61-80.

90. Franken ACM, Nolten JAM, Mulder MHV, Bargeman D, Smolders CA. Wetting criteria for the applicability of membrane distillation. J Membr Sci. 1987;33(3):315-28.

91. Alklaibi AM, Lior N. Membrane-distillation desalination: Status and potential. Desalination. 2005;171(2):111-31.

92. Khayet M, Khulbe KC, Matsuura T. Characterization of membranes for membrane distillation by atomic force microscopy and estimation of their water vapor transfer coefficients in vacuum membrane distillation process. J Membr Sci. 2004;238(1-2):199-211.

93. Introduction of pore size [Internet]. Available from: http://membranes.edu.au/wiki/index.php/Pore_Size.

94. El-Bourawi MS, Ding Z, Ma R, Khayet M. A framework for better understanding membrane distillation separation process. J Membr Sci. 2006;285(1-2):4-29.

95. Khayet M, Mengual JI, Zakrzewska-Trznadel G. Direct contact membrane distillation for nuclear desalination. part I: Review of membranes used in membrane distillation and methods for their characterisation. International Journal of Nuclear Desalination. 2005;1(4):435-49.

96. Lawson KW, Lloyd DR. Membrane distillation. J Membr Sci. 1997;124(1):1-25.

97. Schneider K, Hölz W, Wollbeck R, Ripperger S. Membranes and modules for transmembrane distillation. J Membr Sci. 1988;39(1):25-42.

98. Miyano T, Matsuura T, Sourirajan S. Effect of polymer molecular weight, solvent and casting solution composition on the pore size and the pore size distribution of polyethersulfone (victrex) membrane. ChemEngCommun. 1990;95.

99. Yasuda H, Tsai JT. Pore size of microporous polymer membranes. J ApplPolym Sci. 1974;18(3):805-19.

100. Khayet M, Matsuura T. Preparation and characterization of polyvinylidene fluoride membranes for membrane distillation. Industrial and Engineering Chemistry Research. 2001;40(24):5710-8.

101. Philip Crosbie Carman. Flow of gases through porous media. London Butterworths; 1956.

102. Cabasso I, Robert KO, Klein E, Smith JK. Porosity and pore size determination in polysulfone hollow fibers. J ApplPolym Sci. 1977;21(7):1883-900.

103. Shimizu Y, Akabane H, Tanioka A, Miyasaka K, Ishikawa K. Effects of extension on the gas permeability of hard elastic polypropylene film. J PolymSciPolymPhys Ed. 1979;17(9):1495-506.

104. Banerjee S, Yang R, Courchene CE, Conners TE. Scanning electron microscopy measurements of the surface roughness of paper. Industrial and Engineering Chemistry Research. 2009;48(9):4322-5.

105. Widiatmoko E, Abdullah M, Khairurrijal. A method to measure pore size distribution of porous materials using scanning electron microscopy images. AIP conference proceedings; ; 2010.

106. Khulbe KC, Matsuura T. Characterization of synthetic membranes by raman spectroscopy, electron spin resonance, and atomic force microscopy; a review. Polymer. 2000;41(5):1917-35.

107. Phattaranawik J, Jiraratananon R, Fane AG. Effect of pore size distribution and air flux on mass transport in direct contact membrane distillation. J Membr Sci. 2003;215(1-2):75-85.

108. Epstein N. On tortuosity and the tortuosity factor in flow and diffusion through porous media. Chemical Engineering Science. 1989;44(3):777-9.

109. Srisurichan S, Jiraratananon R, Fane AG. Mass transfer mechanisms and transport resistances in direct contact membrane distillation process. J Membr Sci. 2006;277(1-2):186-94.

110. Laganà F, Barbieri G, Drioli E. Direct contact membrane distillation: Modelling and concentration experiments. J Membr Sci. 2000;166(1):1-11.

111. Qtaishat M, Matsuura T, Kruczek B, Khayet M. Heat and mass transfer analysis in direct contact membrane distillation. Desalination. 2008;219(1-3):272-92.

112. Wang H, Li B, Wang L, Song S, Wang J, Feng Y, et al. Permeate flux curve characteristics analysis of cross-flow vacuum membrane distillation. Industrial and Engineering Chemistry Research. 2012;51(1):487-94.

113. Phattaranawik J, Jiraratananon R. Direct contact membrane distillation: Effect of mass transfer on heat transfer. J Membr Sci. 2001;188(1):137-43.

114. Phattaranawik J, Jiraratananon R, Fane AG. Heat transport and membrane distillation coefficients in direct contact membrane distillation. J Membr Sci. 2003;212(1-2):177-93.

115. Izquierdo-Gil MA, García-Payo MC, Fernández-Pineda C. Air gap membrane distillation of sucrose aqueous solutions. J Membr Sci. 1999;155(2):291-307.

116. Tomaszewska M, Gryta M, Morawski AW. Study on the concentration of acids by membrane distillation. J Membr Sci. 1995;102(C):113-22.

117. Banat F, Al-Rub FA, Bani-Melhem K. Desalination by vacuum membrane distillation: Sensitivity analysis. Separation and Purification Technology. 2003;33(1):75-87.

Chapter 3.

Study on Structure and Vacuum Membrane Distillation Performance of PVDF Composite Membranes: Influence of Molecular Weight

Zuolong Chen, Derek Meng, DipakRana, Takeshi Matsuura, Christopher Q. Lan*
Department of Chemical and Biological Engineering
University of Ottawa, Ottawa, Canada

3.1 **Abstract**

In this study, membranes were fabricated from three polyvinylidene fluoride (PVDF) of different molecular weights by the phase inversion process. The membranes so fabricated were characterized by scanning electron microscopy, gas permeation tests, contact angle (CA) and liquid entry pressure of water (LEPw) measurements, and further subjected to the test of flux for vacuum membrane distillation (VMD) in a scenario that is applicable for cooling processes, where the feed water temperature is maintained at 27^{o}C.

The experimental results showed that the increase in PVDF molecular weight increased the viscosity and thermodynamic instability of the casting solution significantly. Regarding characterization and performance testing, the membrane prepared from the intermediate molecular weight of MG 15 polymer showed the highest VMD flux (325g/m^2·h) at the feed temperature of 27 °C and the lowest LEPw (622 kPa) due to the largest pore size (49.8 nm) observed among all the tested membranes. The highest flux of this particular membrane seems also due to the thinnest finger-like and sponge-like layer. The surface properties such as surface roughness, water contact angle and surface energy, on the other hand, did not necessarily affect the VMD performance.

Key words: Polyvinylidene fluoride, three different PVDF, membrane characterization, vacuum membrane distillation

3.2 **Introduction**

Since the introduction of reverse osmosis membranes in 1960, there has been extensive improvement and integration of membrane separation processes to be used in many fields of engineering. Furthermore distillation membranes have also been explored to be used in a system known as vacuum desiccant cooling(1), where the distillation membranes are instead, used to provide a surface for water to be evaporated in a vacuum environment maintained by the absorption of vapor by a desiccant. The membranes in question are able to sustain large evaporation fluxes at comparatively low temperatures (e.g. 30^{o}C) for application in vacuum membrane distillation (VMD) cooling.

It is possible to prepare membranes from organic as well as inorganic materials. However, in this study, polymeric materials are used. The membranes can be fabricated by using a profuse amount of polymeric materials such as polysulfone (PS), polytetrafluoroethylene (PTFE), polyvinylchloride (PVC) and polyvinylidene fluoride (PVDF). Most notably, PVDF has already been used in ultrafiltration and microfiltration due to its high mechanical strength, chemical resistance, and hydrophobicity. As a result, PVDF membranes are deemed to be suitable for membrane distillation (2).

Many attempts have been made to improve PVDF membranes. In order to optimize and enhance PVDF membrane performance, researchers have paid much attention to membrane fabrication conditions such as; casting solutions, coagulation bath composition and temperature due to their effects on the characteristics of PVDF membranes. However, there has been limited information regarding the effect of the change in the viscosity and thermodynamic properties of the PVDF solution, which are caused by different molecular weights, on the structure and performance of PVDF based membranes.

Therefore the objective of this study is to investigate the effect of the molecular weight of PVDF on the morphology and VMD performance of PVDF based membranes. Membrane properties and experimental conditions were mainly aimed at meeting requirements in cooling garment research. The casting solutions made from PVDF of three different molecular weights were characterized by viscosity and cloud point measurement. Membranes so prepared were characterized by employing scanning electron microscopy (SEM), membrane surface properties, gas permeation test, membrane porosity measurement, liquid entry pressure of water (LEPw) and VMD testing.

3.3 Experimental Methods

3.3.1 Materials

PVDF of three different molecular weights were used in this sturdy: Kynar® 740 Pellet, (Mw=410kD; melt viscosity 18.5±2.5 k Poise; melting temperature, Tm 160.1ºC) (3), Kynar® MG 15 Powder, (Mw= 1548 kD, melt viscosity 37 k Poise, density 1.77-1.79 g/cm^3, melting point 165-172°C) and Kynar®HSV900 (Mw= 92840 kD, powder, melt viscosity 49.3 k Poise; Tm 165.1ºC). The Kynar® HSV 900 PVDF was supplied as a resin powder from Arkema Inc. (Philadelphia, PA, USA). Kynar® HSV900 is a homopolymer that has the highest viscosity due to its high molecular weight among the Kynar® polymers (4). The Kynar®740 PVDF has the lowest molecular weight and Kynar® MG 15 has the intermediate value. It is noted that the melt viscosity (kPs@100 s^{-1}) was measured using the ASTM D3835 at 232°C. Anhydrous N, N-dimethylacetamide (DMAC) supplied by Sigma-Aldrich with the purity of 99.9% was used as the solvent. Deionized water was used as the additive to the casting solution as well as the coagulation media. The polyester non-woven fabric (Hollytex, grade 3396) was used as the backing material. The air permeability is 0.009 cubic feet per minute per square meter

(CFM) of fabric. The tensile strength (lb. /in) is 85 and 52 in the machine direction (MD) and cross direction (CD), respectively. The elongation (%) is 75 and 85 in the MD and CD, respectively.

3.3.2 **Preparation of Casting Solutions**

The casting solutions were made with $1.25\ wt.\%$ water, $15\ wt.\%$ polymer material (5), and $83.75\ wt.\%$ N, N-dimethlyacetamide. The casting solutions were homogenized by a shaker at an rpm of 180 and a temperature of 50°C. This process was run for a period of 48 h to ensure that each solution was homogenized.

3.3.3 **Membrane Casting Method**

The homogenized polymer solutions were cast on a backing material made of a nonwoven polyester backing material. Through the use of a brass casting bar, membranes were cast to a thickness of 0.25mm (6). After waiting for15 seconds, the backing material with the cast film on top, was immersed into a coagulation bath of deionized water at 23°C and kept there for 4 h. Afterwards the partially solidified film was transferred to another deionized water (23°C) bath for 20 h. The membranes were further dried under ambient conditions.

3.3.4 **Characterization of Polymer Solution**

3.3.4.1 ***Cloud Point Measurement***

The cloud point measurement was done by titrating a polymer solution into an aqueous DMAC solution. The polymer solution was composed of 66.66wt. % DMAC and 33.33 wt. % of PVDF membrane casting solution. The titrant was composed of 33.33 wt.% water and 66.66 wt.% DMAC. Titration was carried out at 25°C by continuously dropping the titrant into the polymer solution. At the first sign of turbidity, titration was stopped, and the solution was shaken for 10 minutes until the solution turned transparent again. If, after 10 minutes, the

solution remained cloudy, it was assumed that the cloud point was reached, and titration was discontinued. For each casting solution, this measurement was done three times, and the average value was calculated. A ternary phase diagram was constructed from cloud point titration data.

3.3.4.2 *Viscosity Measurement*

The viscosity of the casting solutions was measured by using a rotational rheometer (Brookfield, Synchro-Lectric Viscometer, model LVF). A number of testing valves were filled with different polymer solutions. A spindle was connected with the torsion spring and dipped into the solutions. The rotation factor was observed until the reading reached a constant value. The viscosity of the polymer solutions were calculated using rotation factor, spindle factor and rotation speed. This was done three times per different polymer solution, and the average value per solution was taken.

3.3.5 **Membrane Characterization**

3.3.5.1 *Scanning Electron Microscopy (SEM)*

A scanning electron microscope (Tescan,VegaII XMU) was used to study the membrane morphology. For this purpose, samples of the membrane were prepared by immersion into liquid nitrogen to embrittle. Afterwards, the sample was broken and placed on the metal holder. Anatech Hummer VII was used to coat the sample with conductive metal under a vacuum.

For cross-sectional views of membrane samples, the membrane tested was peeled off from the support material because the support material was too tough to break in liquid nitrogen.

3.3.5.2 *Gas Permeation Test*

The mean pore size of the membranes was determined by the gas permeation test using the experimental setup shown in Figure 3-1. Gas flow rate was measured by a bubble-soap flow meter at five different trans-membrane pressure differences. Five measurements were made at each pressure and the average value was reported.

The pore size was obtained by the method described by Khayet et al (5) by using permeance calculated by equation [1] (7).

$$B = \frac{4}{3}\left(\frac{2}{\pi MRT}\right)^{0.5}\frac{r_p\varepsilon}{L_p} + \frac{P_m}{8\mu RT}\frac{r_P^2\varepsilon}{L_p} = I_o + S_oP_m \qquad (1)$$

Where B is the gas permeance $(mol/m^2s \cdot Pa)$, M is the molecular weight of the gas (kg/mol), R is the gas constant $(J/mol \cdot K)$, T is the absolute temperature (K), r_p is the pore size (m), μ is the viscosity of the gas $(Pa \cdot s)$, ε is the membrane porosity, L_p is the effective pore length (m), and P_m is the mean pressure within the membrane pore (Pa) set to the average of the feed and permeate gas pressures.

According to the equation slope S_o and intercept I_o can be obtained by the linear plot of B versusP_m, the pore size r_p is calculated by equation [2].

$$r_p = \frac{16}{3}\left(\frac{S_o}{I_o}\right)\left(\frac{8RT}{\pi M}\right)^{0.5}\mu \qquad (2)$$

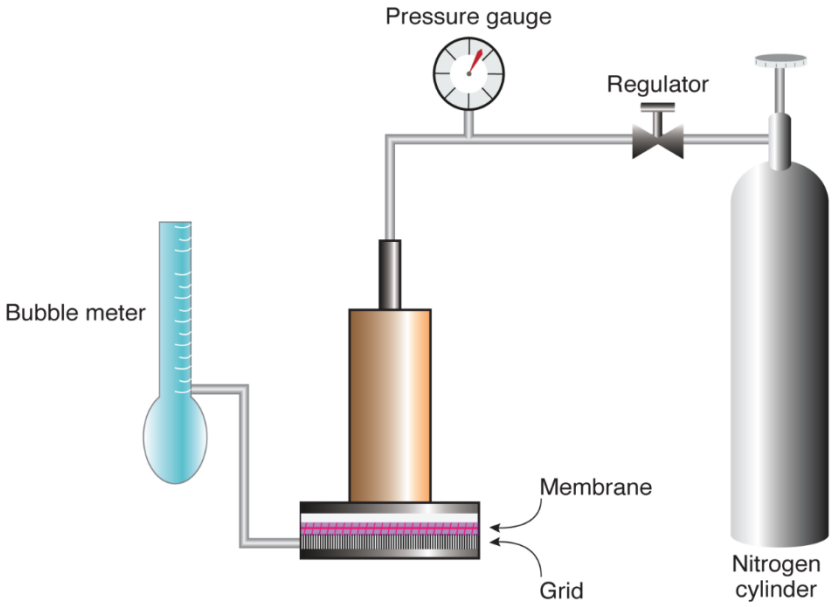

Figure 3-1 Gas permeation test equipment.

3.3.5.3 ***Membrane porosity measurement***

The membrane porosity was measured by the wet and dry method. First, the membrane was immersed in a liquid for 12 h. After blotting the membrane surface, the wet membrane was weighed. Then, the wet membrane was dried in an oven at 50˚C for 24h to thoroughly evaporate the liquid in membrane pores. After that, the dry membrane sample was weighed.

The porosity of the membrane was calculated by using equation [3]:

$$P = \frac{(W_W - W_D)}{Ah\rho} \times 100\% \qquad (3)$$

Where P is the membrane porosity (%), W_W and W_D are the weight of the wet and dry membrane (g), respectively; A is the membrane area (cm^2); h is the membrane thickness (cm) and ρ is the density of the liquid (g/cm^3).

Ethylene glycol and isopropyl alcohol were chosen as the liquid, because their surface tensions are much lower than water. Consequently, membrane pores could be easily filled with the liquid.

3.3.5.4 *Measurement of Liquid Entry Pressure of Water (LEPw)*

LEPw was measured by using the method developed by Smolders and Franken (8). The membrane cell was a stainless steel filter holder with a reservoir of 200 mL and an effective membrane area of 13.1 cm^2(9). The experimental setup used is shown in Figure 3-2.

The dried membrane sample was placed on a sintered metal plate. The liquid reservoir was filled with distilled water. Compressed nitrogen gas was fed into the reservoir starting at 5psi. The pressure was increased steadily at an interval of 3-5psi, until water droplets continuously flowed out of the testing cell. When this occurred, the pressure was no longer increased. The pressure shown on the gauge was the LEPw value. For each membrane, five measurements were made and the average value was calculated per membrane.

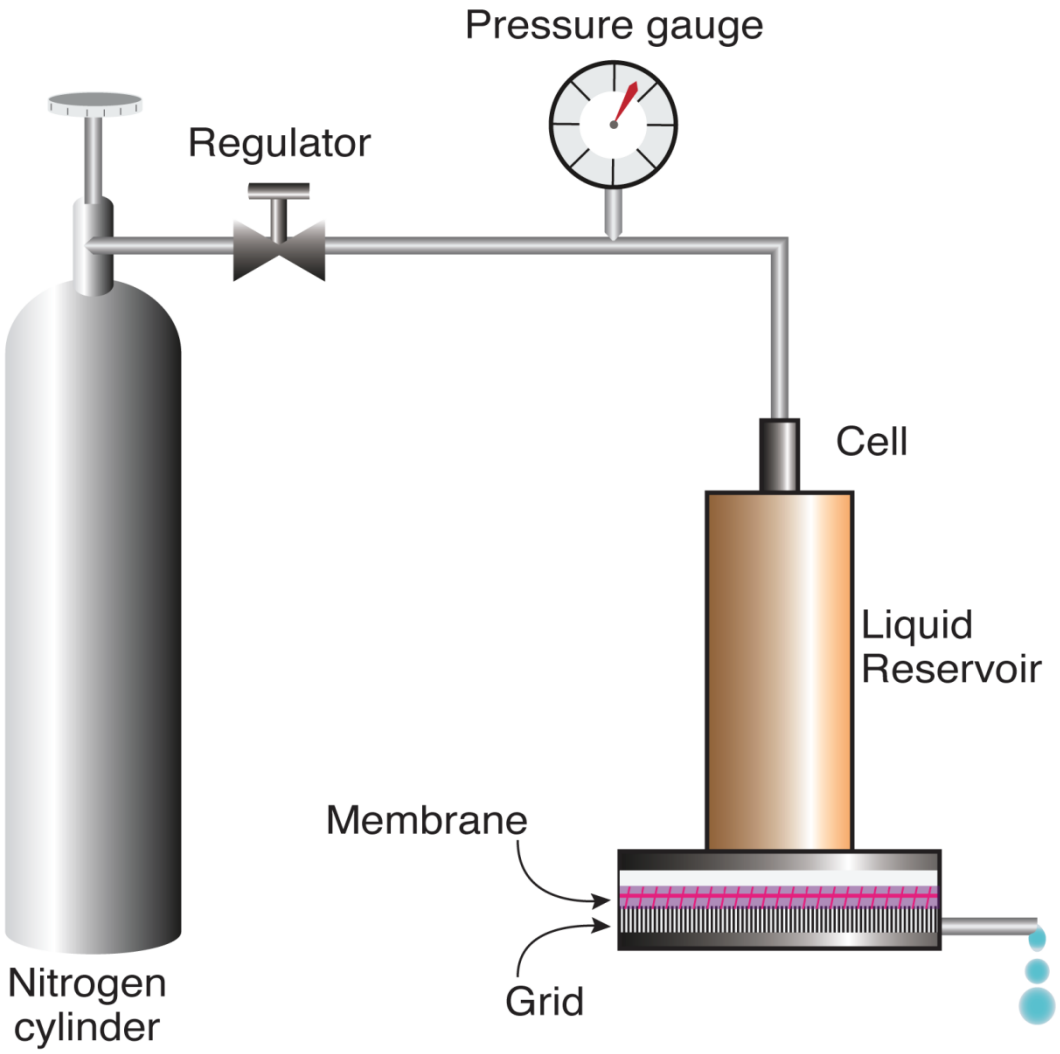

Figure 3-2 Setup for LEPw measurement.

3.3.5.5 ***Membrane surface property***

3.3.5.5.1 Water contact angle

Membrane hydrophobicity was characterized by measuring water contact angle using a VCA Optima Surface Analysis System (AST Products, Inc. Billerica, MA). For each type of blended composite membrane, two samples were casted for the purpose of measurement, one of which was cut in parallel and the other was cut perpendicular to the longer edge of the membrane sheet. The dimensions of those samples were 5mmx80mm. The membrane sample

was then placed on a glass plate and a small amount of distilled water (1 μL) was dropped by employing a micro syringe (Hamilton Company, Reno, NV). The contact angle was measured within a 10 s period. In order to maintain high accuracy, ten measurements were done on each sample and the average water contact value was calculated.

3.3.5.5.2 Surface free energy calculation

The surface free energy γ (also called as surface tension) is calculated by using the Lifshitz-van der Waals (LW) method. In order to calculate the surface free energy, the Young equation, Lifshitz-van der Waals (apolar), Lewis acid and Lewis base interactions are considered as in the following equation:

$$(1+\cos\theta)\gamma_L = 2\left(\gamma_S^{LW}\gamma_L^{LW}\right)^{\frac{1}{2}} + 2(\gamma_S^{+}\gamma_L^{-})^{\frac{1}{2}} + 2(\gamma_S^{-}\gamma_L^{+})^{\frac{1}{2}} \qquad (4)$$

This equation has been widely used, in which γ is the surface free energy. The subscripts S and L indicate the solid/vapor and liquid/vapor interface, respectively. The superscripts LW, +, - mean the Lifshitz-van der Waals component (apolar), Lewis acid component and Lewis base component of the surface free energy, respectively. The three components of the surface free energy of the solid membrane, γ_S^{LW}, γ_S^{+} and γ_S^{-}, are obtained by measuring the contact angles of three liquids, namely water, ethylene glycol and diiodomethane. Obtaining the overall surface tension (γ_L) from experiments and knowing the surface tension components of the above three liquids (γ_L^{LW}, γ_L^{+} and γ_L^{-}) from the literature, three simultaneous equations can be solved for the unknowns: γ_S^{LW}, γ_S^{+} and γ_S^{-}. The total surface energy of membrane γ_S is calculated by:

$$\gamma_s = \gamma_s^{LW} + \gamma_S^{AB} = \gamma_s^{LW} + 2(\gamma_S^{+}\gamma_S^{-})^{\frac{1}{2}} \qquad (5)$$

The results are shown in Fig. 3-14.

3.3.5.6 *Vacuum Membrane Distillation (VMD)*

Vacuum membrane distillation was conducted using an experimental setup which is shown in Figure 3-3 following the method described by Suk et al (10).

Inside the permeation cell, the feed chamber was filled with de-ionized water. In VMD configuration, a pump is utilized to create a vacuum ($3.78\ kPa\ absolute$) on the permeate side of the membrane to force the water vapor to permeate through the membrane. The temperature of the feed chamber was maintained at 27°C through the use of a heating tape (which was wrapped around the outside of the feed chamber). In addition, a magnetic stirrer was used to stir the feed liquid to prevent extreme temperature polarization. Three cold traps were cooled using liquid nitrogen. Permeated vapor was first collected in cold trap 1 for one hour until the system reached the steady state. Once this was reached, the permeate stream was allowed to enter cold trap 2. The condensation was collected for a predetermined time.

The membrane flux was calculated by equation [6].

$$Flus = \frac{m}{tA} \qquad (6)$$

m is the weight of the water (kg) collected in cold trap 2 during the time period$t$ ($in\ seconds$), through the effective membrane area$A$ (m^2).

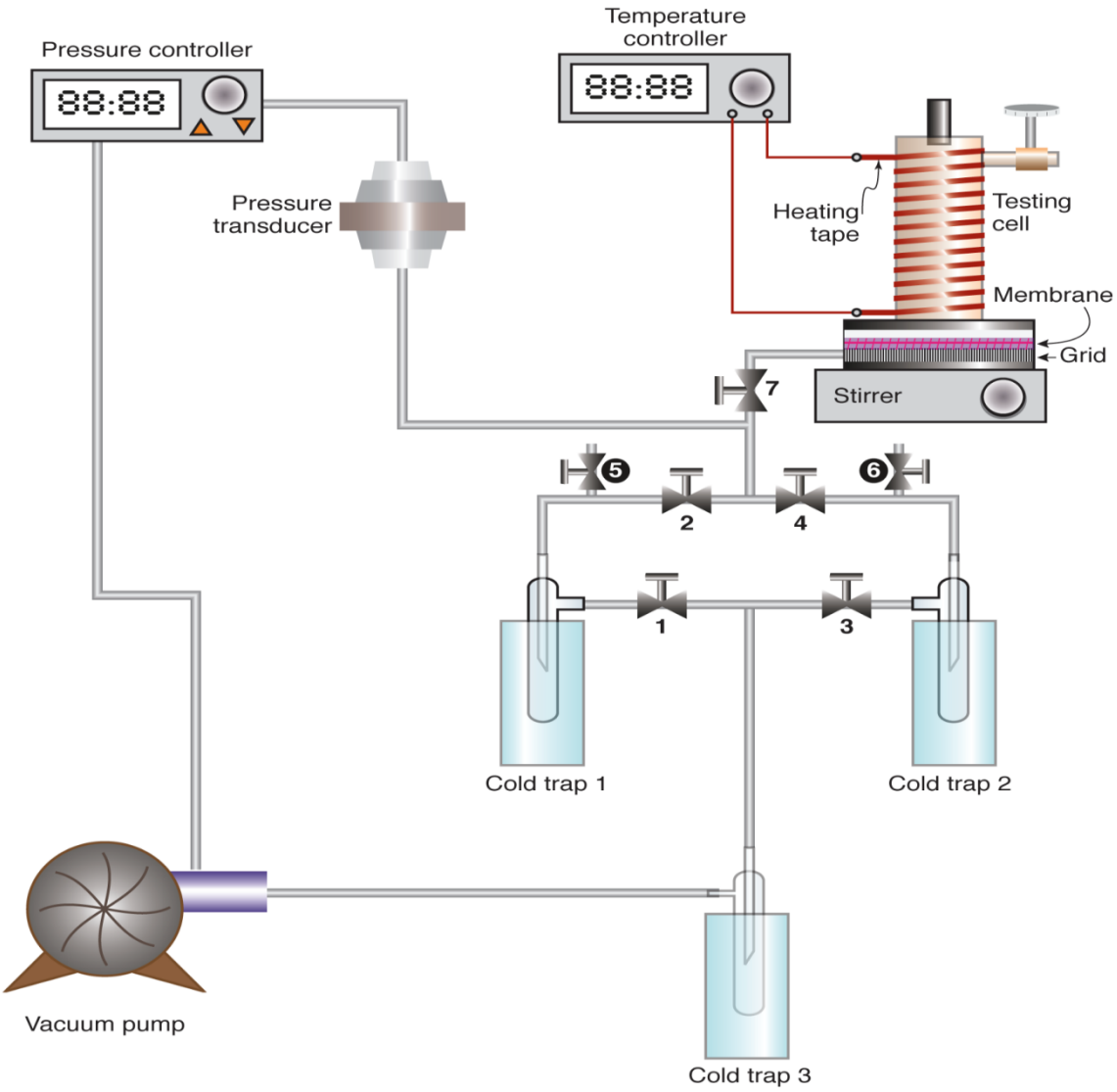

Figure 3-3 Vacuum membrane distillation set up.

3.4 Results and discussion

3.4.1 Polymer solution characterization

3.4.1.1 *Polymer solution viscosity*

Due to the fact that solvent/nonsolvent exchange rate, the velocity of phase separation, and the gelation dynamic are determined by the viscosity of membrane casting solutions. Thus the viscosity of polymer solution can play an important role in the membrane formation process. It has been proved that higher viscosity caused by higher molecular weight brings about higher hindrance and decreases the solvent/nonsolvent exchange rate during the phase inversion process, thus affecting the precipitation kinetics and the formation of membrane morphology(6). The viscosity values of the casting solutions made by three molecular weights PVDF polymers were measured and shown in Figure 3-4.

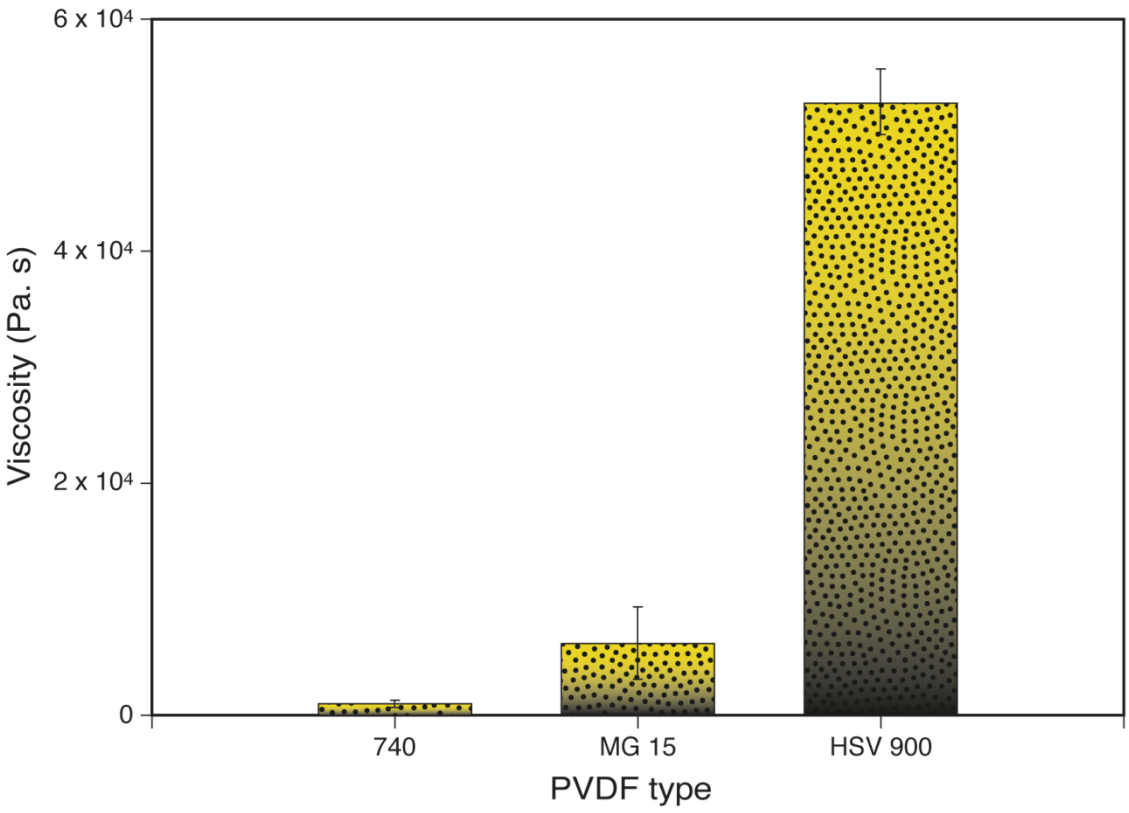

Figure 3-4 Viscosity of casting solutions with three types of PVDF

The viscosity of casting solutions shows a drastic growth in Figure3-5. It is 500 Pa·s and 6000 Pa·s for membrane casting solutions made from the Kynar®740 PVDF and the MG 15 PVDF respectively, while for the HSV 900 PVDF, it reached 53,000 Pa·s. It is noted that the solution viscosity (not the casting solutions used in this study) of the three polymers given by Kynar Company's official information is 100, 1700, and 8000 for Kynar®740, Kynar® MG 15, and Kynar® HSV 900, respectively. The solution viscosity (nominal cps) was measured by spindle viscometer by using 20 RPM #2 spindle at 20°C (4).

3.4.1.2 *Cloud points*

A polymer/solvent/nonsolvent ternary phase diagram is used to show the thermodynamic instability of the casting solutions. The thermodynamic instability is a key factor that determines membrane formation in the phase inversion process. As shown in Figure 3-5, the cloud point of higher PVDF molecular weight is located closer to the solvent/polymer axis, meaning that the solution made of higher PVDF molecular weight is thermodynamically more unstable. Instantaneous liquid-liquid demixing progress is favoured by the instability of polymer solutions. Consequently, higher molecular weight PVDF may result in a condition that favours instantaneous liquid-liquid demixing. Thus finger-like macro-void structure would be more likely to be formed (11).

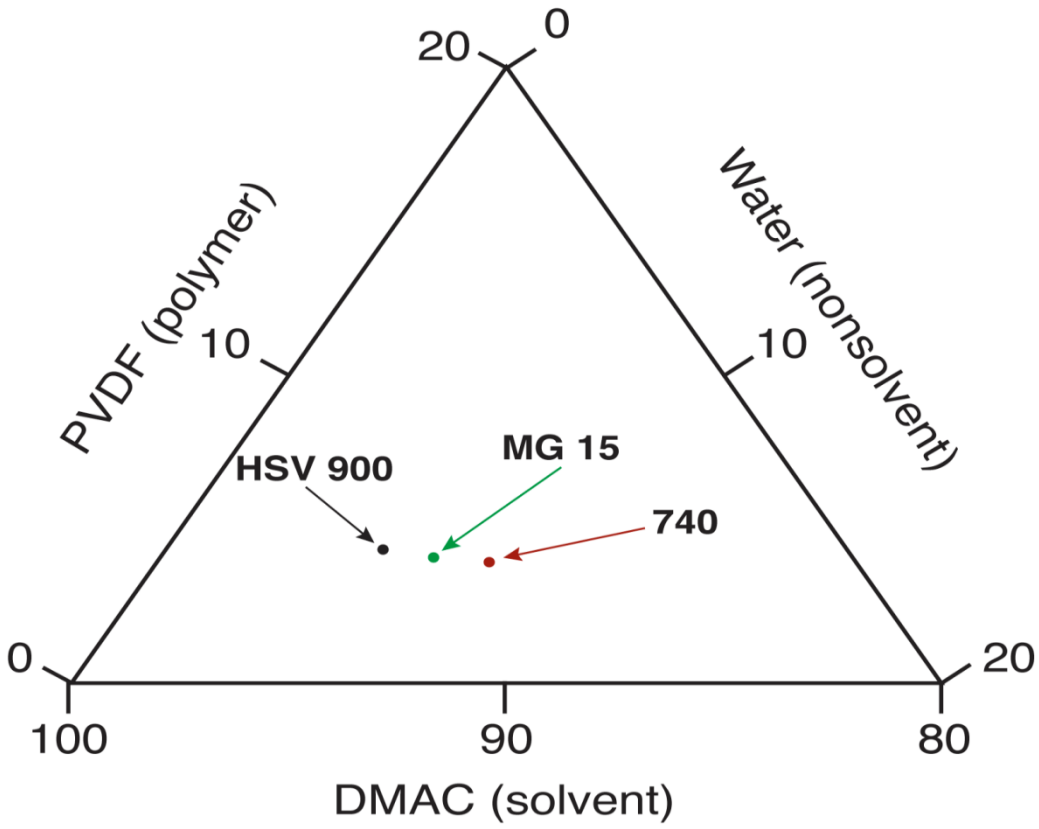

Figure 3-5 Cloud points of polymer solutions prepared by three types of PVDF

3.4.2 **Membrane characterization**

3.4.2.1 ***Scanning electron microscopy (SEM)***

Figure 3-6 shows the cross-sectional SEM images of the membranes prepared by using different PVDF polymers. The coated layers were peeled off in this experiment. The phase inversion process can result in two parts in membrane morphology: the upper part with finger–like macro-voids and the lower part with a dense sponge-like structure. Figure 3-6 shows both the above mentioned structures together with a thin top skin layer that is hardly visible. In Figs. 3-6 a, b and c, it is observed that the thickness of the upper finger-like layer diminished as the PVDF molecular weight increased from 740 to MG 15, and slightly increased from MG 15 to HSV 900 PVDF. The macro-void structure also turned to be

smaller and shallower as molecular weight increases. In the upper layer of the HSV 900 membrane, the amount of macro-voids is almost the same as the other membranes, even though some of the channels did not grow in depth and width. The sponge layer is significantly thicker in the HSV 900 membrane than others and the thinnest in the MG 15 membrane. The thickness of the entire cross-section showed the minimum in the MG 15 membrane and the maximum in the HSV 900 membrane.

The thermodynamic (cloud point) and the kinetic (viscosity) effect on the phase separation could be used to explain the above observation. From the thermodynamic view point, enhanced thermodynamic instability with an increase in the PVDF molecular weight, observed as the shift of the cloud point to the PVDF-DMAC axis on the ternary phase diagram, significantly promotes the instantaneous demixing in the phase separation process, resulting in thinning of the top skin layer, and the formation of more finger–like structures and less sponge-like structures (12, 13). From the kinetic view point, on the other hand, the increase in viscosity with an increase in the PVDF molecular weight decreases the solvent/nonsolvent exchange rate by increasing kinetic hindrance in the phase inversion process, which promotes the delayed demixing, resulting in the thickening of the top skin layer, and formation of less finger-like structures and more sponge-like structures (14). Therefore, the thickest finger-like structure and the thinnest sponge-like structure are expected to be formed in the intermediate range of molecular weight as a result of the superimposition of the thermodynamic and the kinetic effect, if the thermodynamic effect controls the phase inversion process earlier than the kinetic effect.

The cross-sectional images of Fig. 3-6 show that both the finger-like layer and sponge-like layer of the MG 15 membrane are obviously thinner than other two membranes, even though the MG 15 PVDF polymer has the intermediate viscosity and thermodynamic instability. The formation of the thinnest finger-like layer is against the expectation. This means that the

thermodynamic effect was not necessarily dominating the formation of the sponge-like layer. Also, Kynar® MG 15 membrane shows a porous structure with well-formed macro-void structure, and the channels there are shorter than the Kynar® 740 membrane but longer than the Kynar® HSV 900 membrane. This means that the instantaneous liquid-liquid demixing was not dramatically inhibited by the diffusive (kinetic) hindrance (caused by high viscosity). On the other hand, the thinnest sponge-like layer observed in Kynar® MG 15 membrane was as expected.

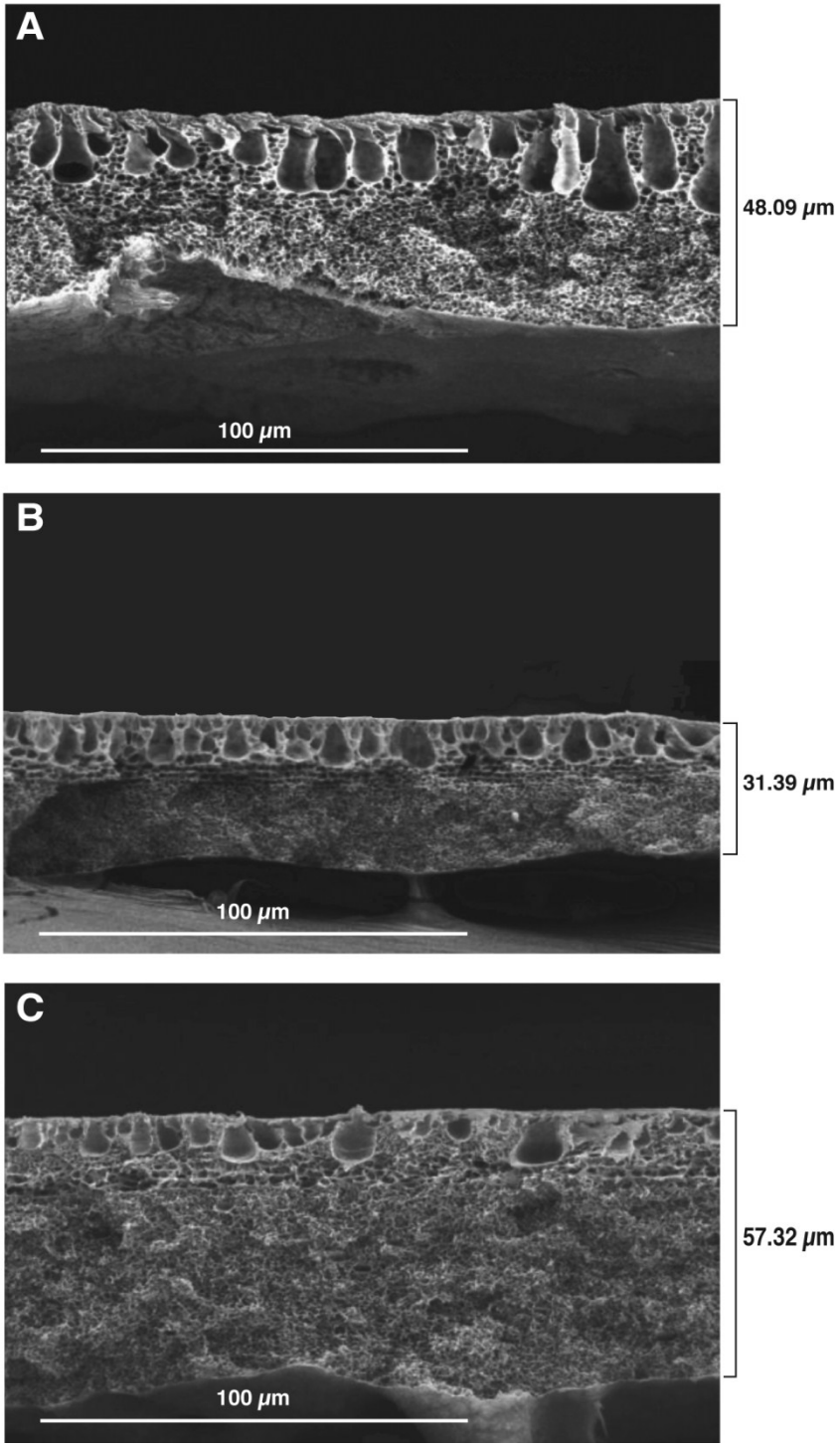

Figure 3-6 Cross-sectional images of three PVDF membranes: (a) Kynar 740, (b) MG 15, and (c) HSV 900.

In order to study the membrane surface roughness by using SEM top view images, Image J software (15, 16) was used to digitize SEM images to 8-bit grayscale images. By plotting the

pixel brightness data for each image, 256-level histograms of those SEM images were converted. These histograms show the grayscale levels on the x-axis and pixel frequency on the y-axis. Also, in order to study the surface morphology, three-dimensional graphs of the pixel intensities in a grayscale were generated and used to simulate the surface conditions of membrane samples. In histograms, the lighter areas (have lower grayscale) are considered to present smooth polymer mass while the darker areas (have higher grayscale) are considered to be void space/pores. The darker the pixel brightness, the deeper the void space was. Thus the standard deviations of pixel brightness values can be used as a measure of surface uniformity (15). Higher standard deviation represents higher surface roughness; and the standard deviation is named as the surface roughness index here to quantify the surface roughness of composite membranes. A histogram picture of Kynar®740 is shown in Fig. 3-7 as an example.

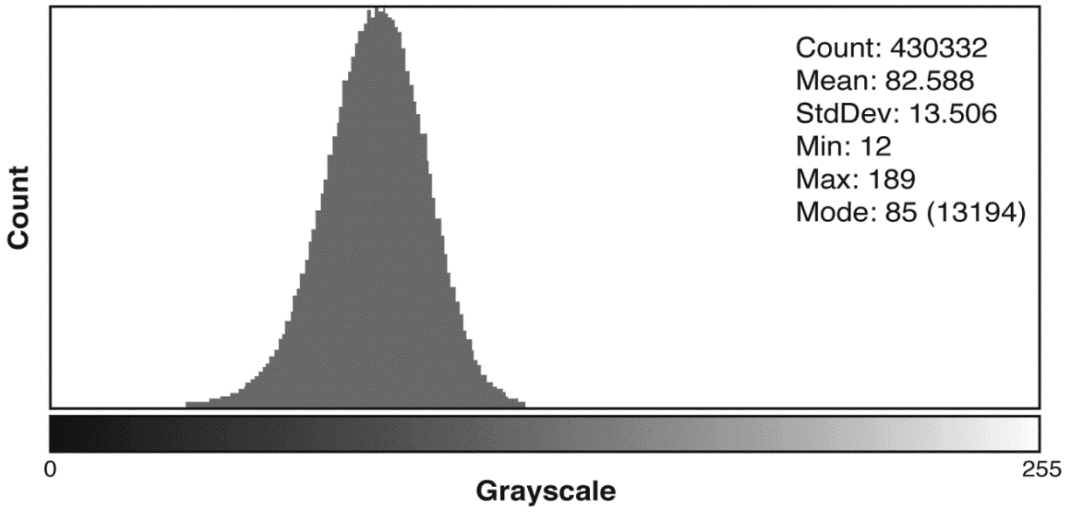

Figure 3-7 A representative histogram of a Kyner 740 membrane.

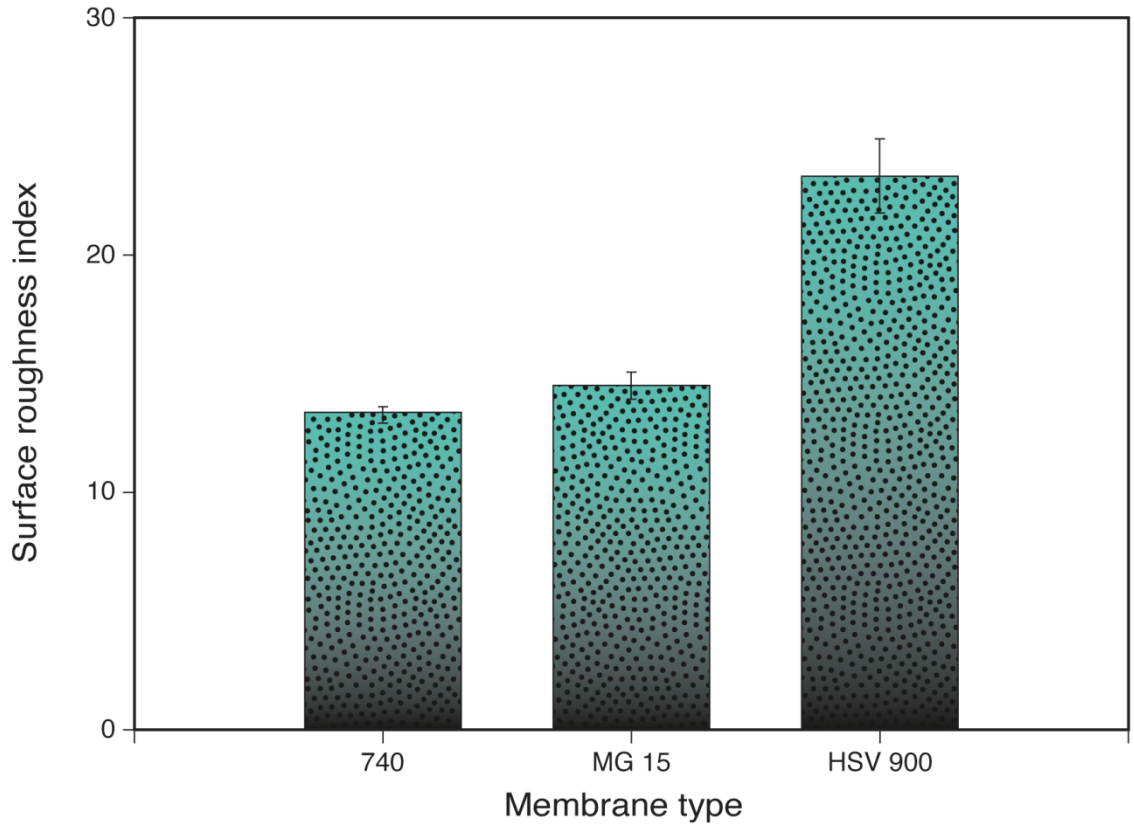

Figure 3-8 Surface roughness index with three types of PVDF.

It is shown in Fig. 3-8 that higher molecular weight leads to higher surface roughness. More specifically, for the Kynar® 740 membrane, the surface roughness index is 13.27, which is very close to the surface roughness index of the Kynar® MG 15 membrane (14.58). For the Kynar® HSV 900 membrane, the index is 23.41, which may be caused by the higher shrinkage of membrane surface casted from high molecular weight PVDF.

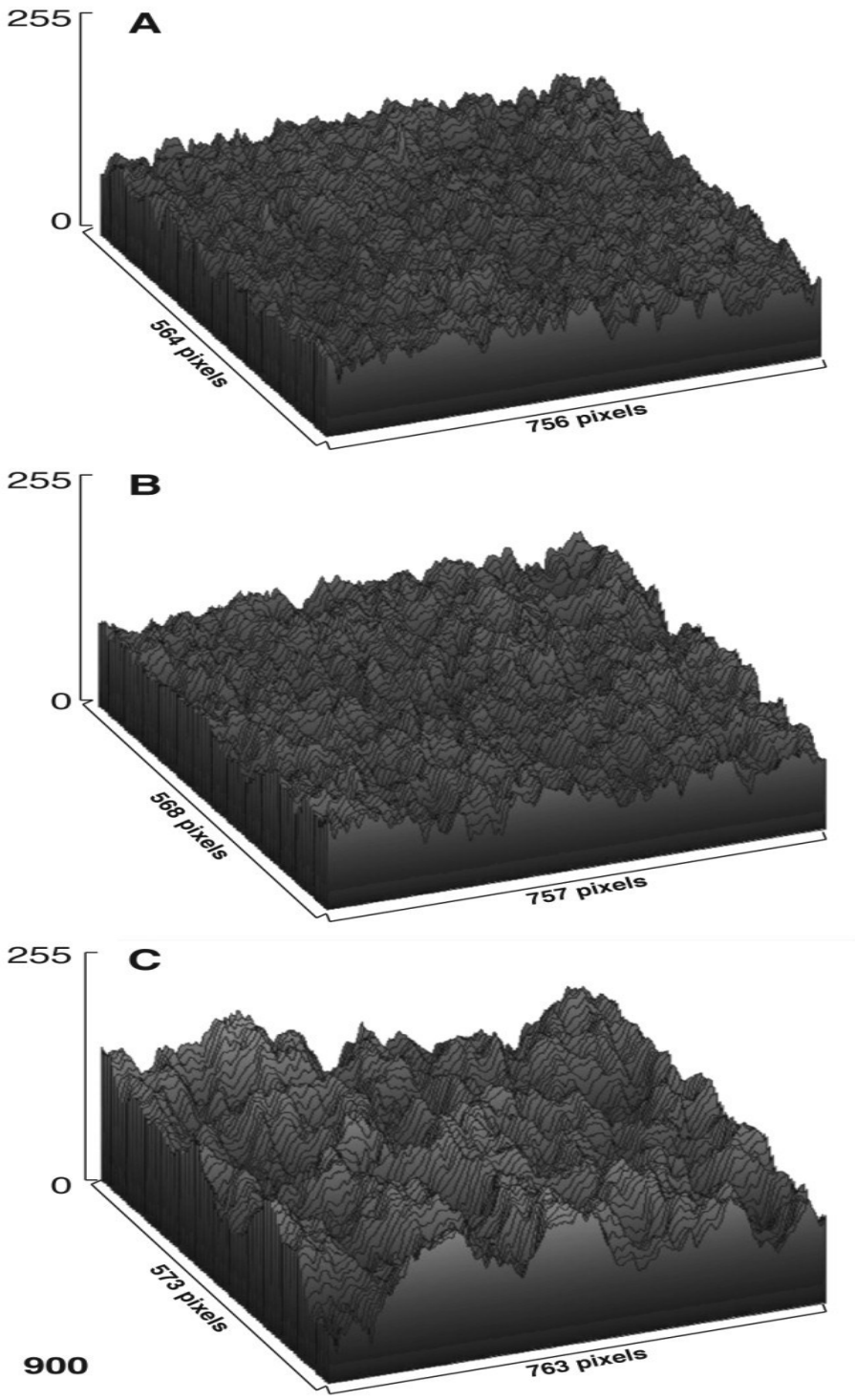

Figure 3-9 Three dimension graphs of the intensities of pixels in a grayscale: (a) Kynar 740, (b) MG 15, and (c) HSV 900.

The 3D images of three membrane surfaces were shown in Figure 3-9. It is obvious that for Kynar®HSV 900 membrane, the surface is rougher thanKynar®740 and Kynar® MG 15 membranes. The distance of the peak and bottom is larger than it is in other 3D images.

3.4.2.2 *Gas permeation test*

In regard to the gas permeation test, it should be mentioned that the intrinsic inaccuracy in the measurement of the intercept and slope made the result unreliable. Thus the data here only proves a comparison of pore sizes of the skin layers of three types of membranes. Figure 3-10 shows the pore sizes measured by using gas permeation test.

Kesting(17) suggested two possible pore formation mechanisms in polymeric membranes. Pores in membrane structures are the void spaces that are filled with solvent in membrane solutions. While during the liquid-liquid exchange in the pore formation process, the solvent would quickly diffuse to water bath, which then formed the void space as pores. This space can be generated either from the space that is surrounded by a large amount of spherical polymer molecules (called network pores, see Figure 3-11a); or from a space generated between aggregates which are formed by the agglomeration of individual polymer molecules (called aggregate pores, see Figure 3-11b).

When the molecular weight of PVDF increased from Kynar®740 to Kynar® MG 15, the aggregate pore formation mechanism is favoured and larger aggregate pores were formed. However, as the molecular weight increases, the effect of polymer entanglement becomes gradually more dominant as observed in the dramatic increase in viscosity. As a result, pore size starts to decrease due to the formation of large amount of polymer entanglements. This hypothesis could be given to explain the change of pore size in three different PVDF membranes.

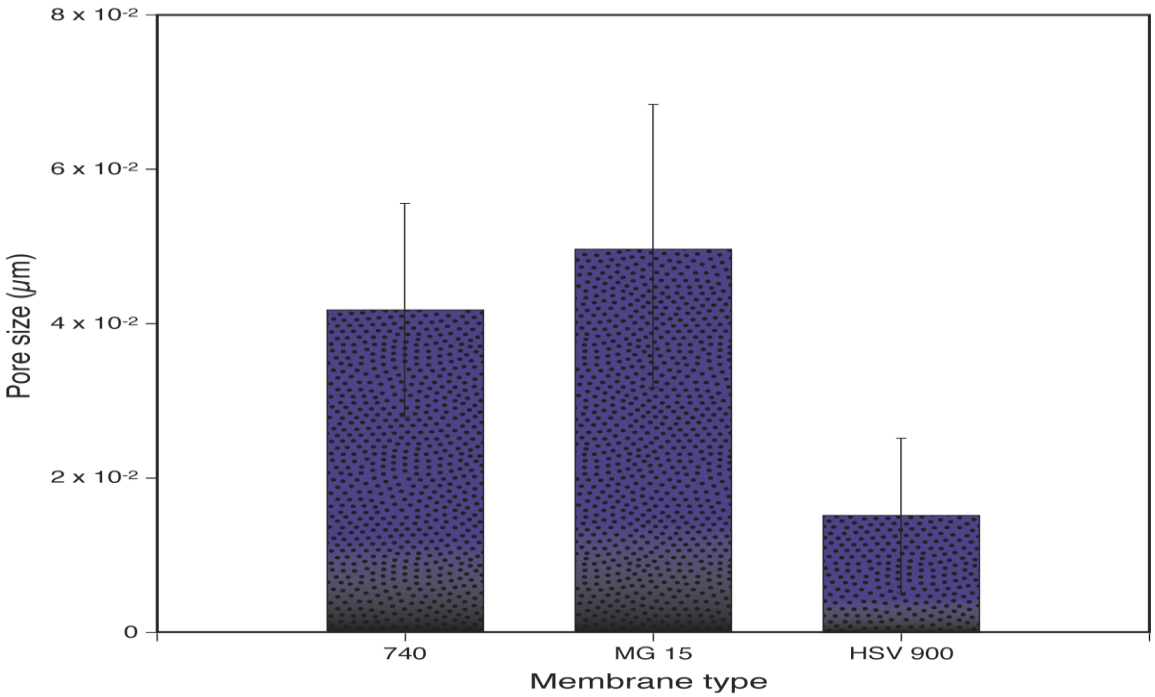

Figure 3-10 Pore size of three PVDF membranes

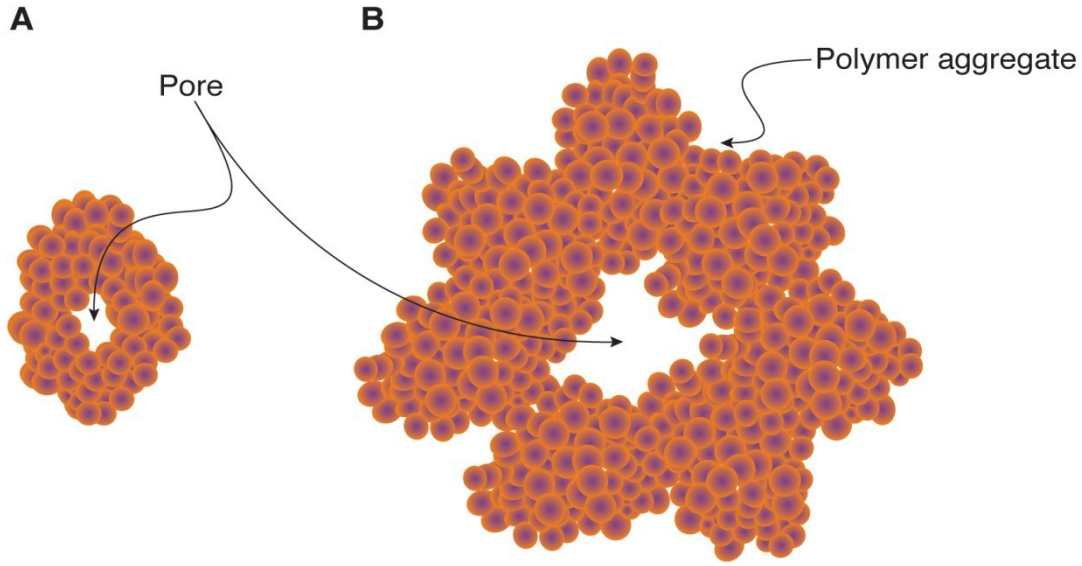

Figure 3-11 Two types of pores.

3.4.2.3 *Membrane Porosity Measurement*

As shown in Figure 3-12, the porosity of membranes was influenced by the molecular weight of PVDF polymers. The high molecular weight in the Kynar® HSV 900 PVDF membrane has the highest porosity (29.42%) while the porosity values of the Kynar®740 membrane (21.81%) and the Kynar® MG 15 membrane (20.67%) did not show a significant difference.

In the literature, it was mentioned that high molecular weight polymer would result in a porous membrane with relatively low porosity (6).But in this study, it was found that the HSV 900 membrane had the highest porosity while the Kynar® MG 15 had the lowest porosity. Both the viscosity and thermodynamic instability data of the MG 15 are in the intermediate range compared with the Kynar® HSV 900 PVDF and the Kynar®740 PVDF. A plausible explanation is that as the Kynar® HSV 900 PVDF solution has a significantly high thermodynamic instability, the porous structure in the Kynar® HSV 900 PVDF membrane would be easily initialized and formed, while as the viscosity of the Kynar® HSV 900 PVDF is dramatically higher than the other two PVDF polymer solutions, the development and growth of porous structures were highly inhibited by the kinetic hindrance caused by high viscosity, thus the porosity of the Kynar® HSV 900 membrane is relatively higher than the other two.

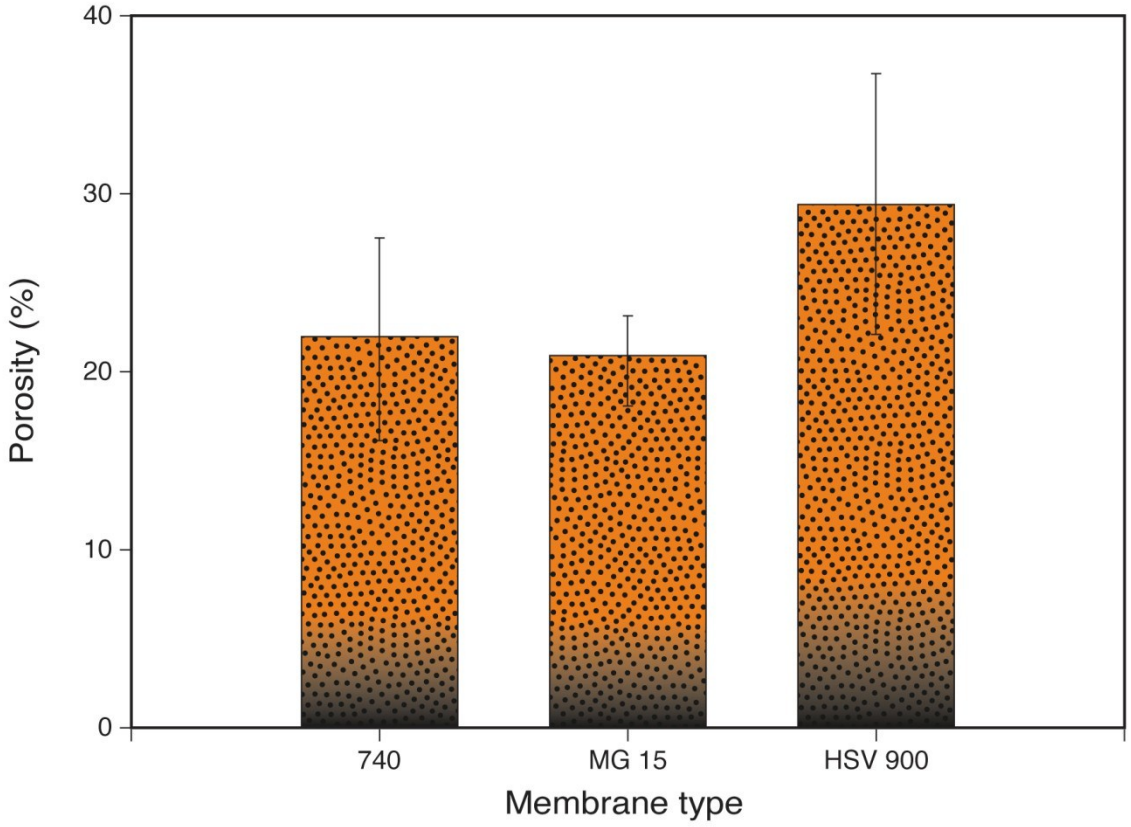

Figure 3-12 Membrane porosity of three PVDF membranes.

3.4.2.4 ***Membrane surface properties***

Figure 3-13 shows the data for the water contact angle. BothKynar®740 and Kynar® MG 15 membranes have almost the same value of 83˚, while that of Kynar® HSV 900 membrane is slightly lower (77.48˚).

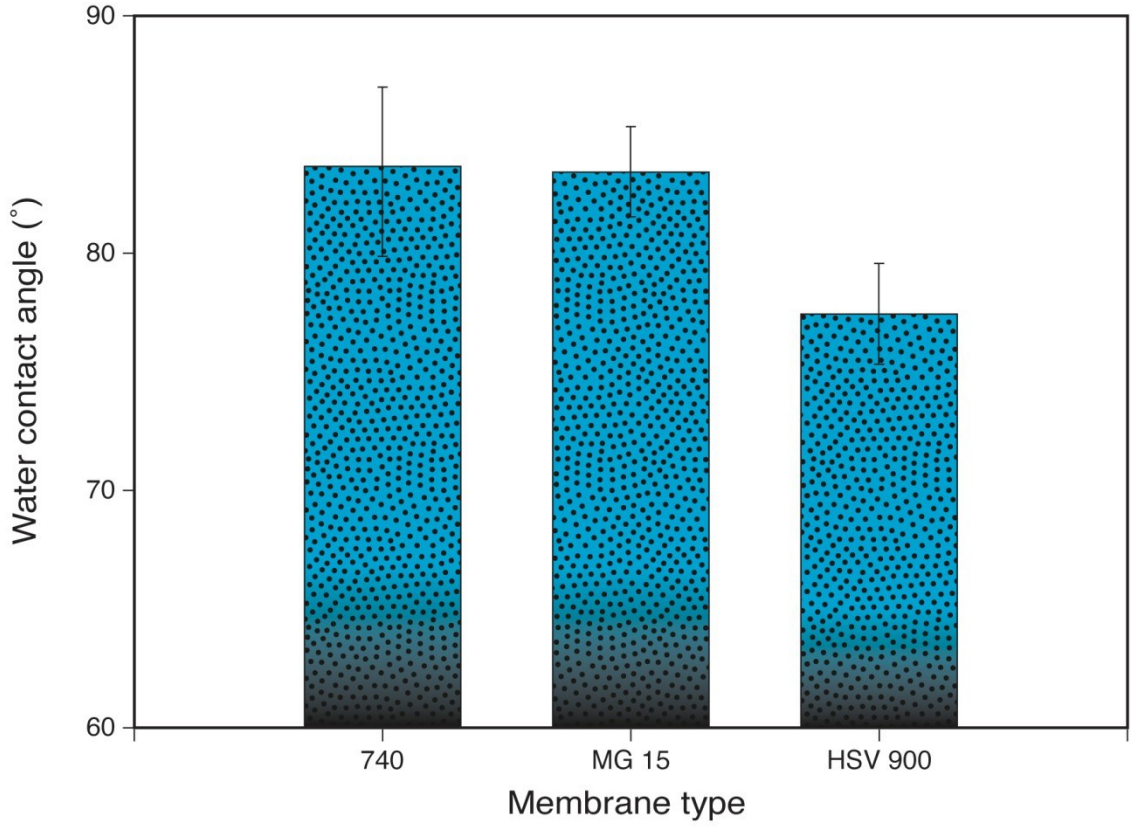

Figure 3-13 Water contact angle of three PVDF membranes.

By employing the test of contact angle of ethylene glycol and diiodomethane, the surface energy data is also obtained. Figure 3-14 illustrates that no significant difference was observed among the surface energy data of three PVDF membranes.

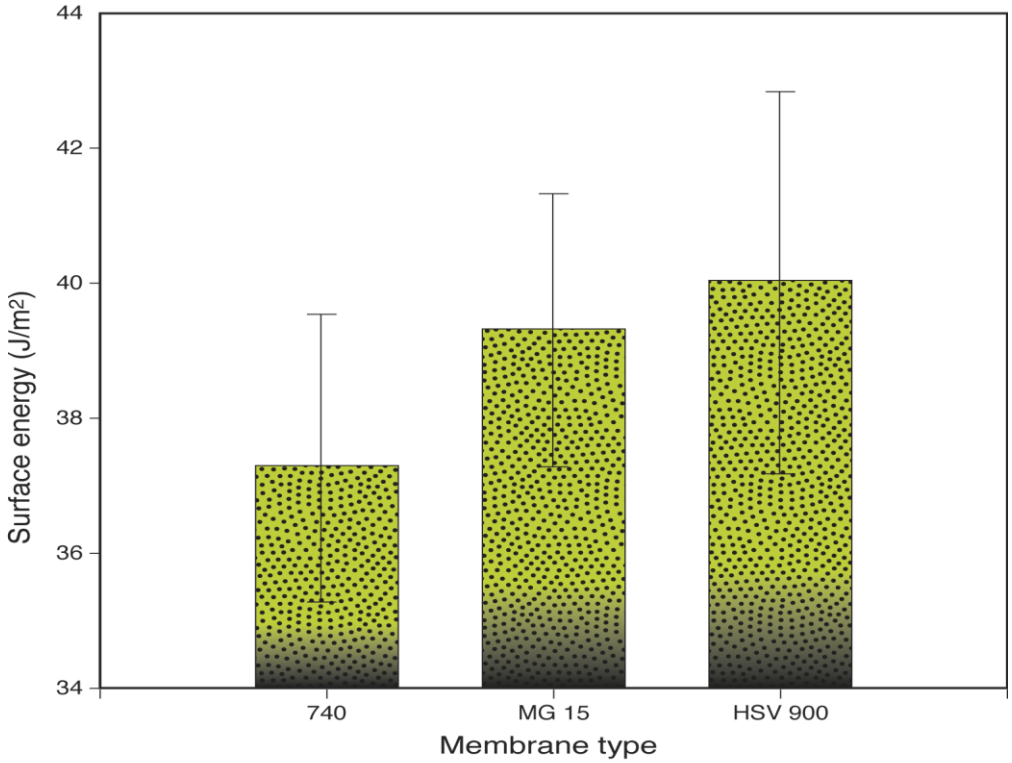

Figure 3-14 Membrane surface energy of three PVDF membranes

The membrane surface properties are determined by the type of polymer, solvent, nonsolvent and additives in casting solutions. In this study, all the casting solutions were prepared by using the same solvent (DMAC) and nonsolvent (water) at the same concentrations, and no additives were added into casting solutions. The PVDF materials used are the same type of polymers with different molecular weights, thus no obvious change brought about by the molecular weight difference was observed on membrane surface properties. The minor difference in membrane surface properties may have been caused by the differences in membrane pore size and surface roughness.

3.4.2.5 *LEPw measurement*

The LEPw values are displayed in Fig. 3-15. From the figure, all three membranes show very high LEPw values. More specifically, the Kynar® MG 15 has the lowest LEPw (622 kPa), while bothKynar®740 and Kynar® HSV 900 membrane show LEPw values higher than 700 kPa. As illustrated in Fig. 3-10, the MG 15 has the largest pore size (49.8 nm), which is consistent with the lowest LEPw value. The high LEPw value of the Kynar® HSV 900 membrane could be explained by its small pore size (14.9 nm) and thicker membrane cross sectional thickness. The LEPw values obtained for these membranes were larger than the commercial PTEF membrane we tested. It should also be noted that Hwang et al. reported 158.58kPa for the PTFE membrane they tested (18).

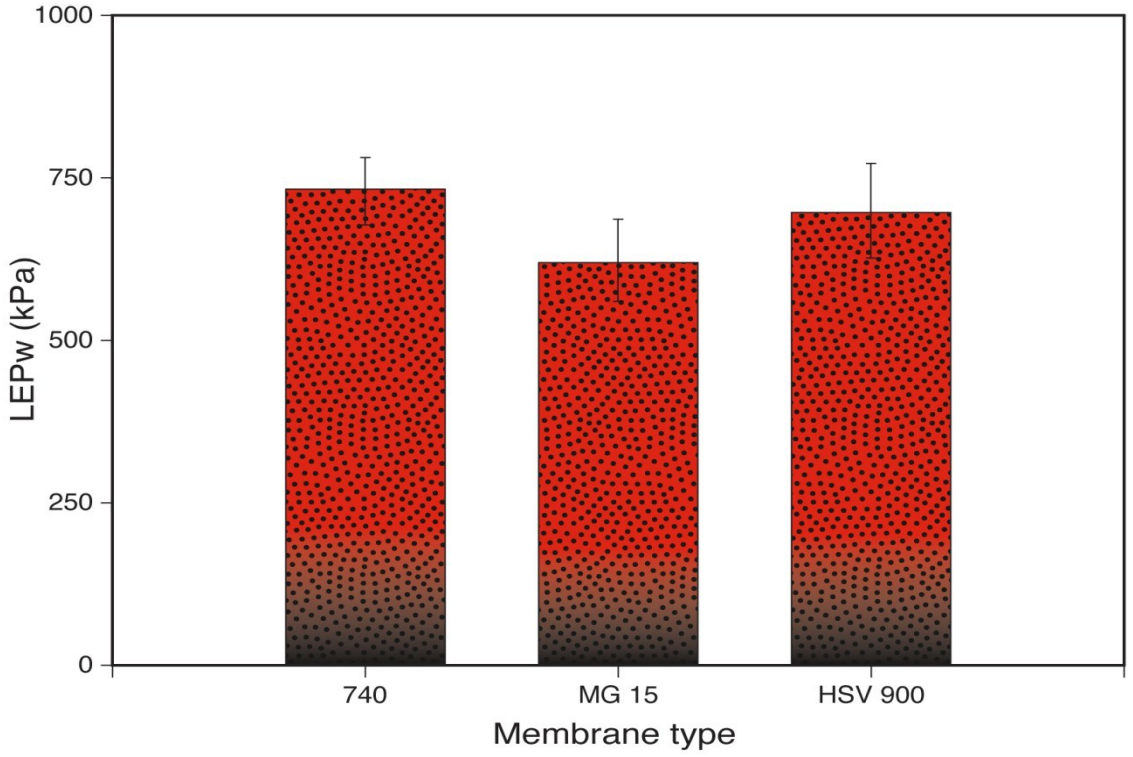

Figure 3-15 LEPw value of three PVDF membranes.

3.4.3 **Vacuum Membrane Distillation Flux measurement**

The flux data for VMD are shown in Fig. 3-16 for the PVDF membranes under study together with the error bars. With its largest pore size among all three types of membranes, thinnest cross section layer thickness and well-formed finger-like channels, the Kynar® MG 15 membrane shows the highest Flux value (325 g/m^{2}h), even though its porosity is not the highest one. Regardless of its relatively small pore size, the second highest flux value occurs in the the Kynar® HSV 900 membrane (311g/m^{2}h). This may be due to its highest porosity which offers a larger space for water vapor to go through the membrane. For the Kynar®740 membrane, even though it has the medium porosity, pore size and cross sectional thickness, its flux is relatively lower than the HSV 900 membrane and the MG 15 membrane. Indicating the Kynar®740 membrane may cause higher resistance for water vapor to transport through the membrane.

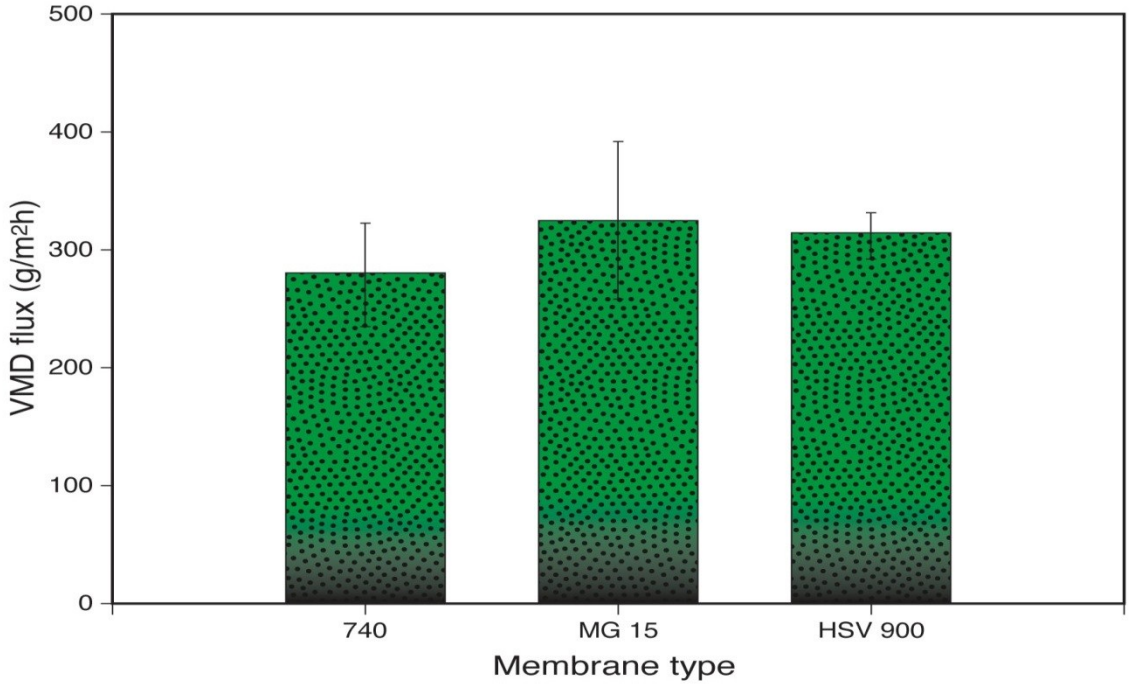

Figure 3-16 VMD flux of three PVDF membranes

3.5 **Conclusion**

In this study, three types of PVDF materials with different molecular weights were used to prepare polymeric membranes. Then the membranes were subjected to characterization and performance testing. It was observed that the molecular weight affected both membrane properties and performances due to the change in the viscosity of the polymer solution and, its thermodynamic instability. The following trends were observed in the experimental results.

1) The cross-sectional SEM images showed the thinnest finger-like and sponge-like layers at the intermediate molecular weight of Kynar® MG 15 PVDF.
2) Surface roughness increased with an increase in molecular weight.
3) The pore size of the top skin layer showed a maximum at the intermediate molecular weight of Kynar®MG15.
4) The membrane porosity increased with an increase in molecular weight.
5) The water contact angle decreased with an increase in molecular weight.
6) The surface energy increased with an increase in molecular weight.
7) LEPw showed a minimum at the intermediate molecular weight of Kynar® MG 15.
8) The VMD flux showed a maximum in the intermediate molecular weight of Kynar® MG 15.

From the observation given in 1), 3), 7) and 8), it can be concluded that the highest flux shown by MG 15 is due to the largest pore size and the thinnest finger–like and sponge-like layers, both of which cause the least resistance for the vapour transport through the

membrane. The smallest LEPw is also due to the largest pore size of Kynar® MG 15 membrane.

On the other hand, the surface roughness, the membrane (bulk) porosity, contact angle and surface energy are not necessarily associated with the VMD performance of the membrane.

It can also be concluded that the membrane performances and properties are determined by the interplay of various factors such as polymer molecular weight, viscosity and thermodynamic instability. Thus, future works are called for to cover a wider range of molecular weights, viscosities and thermodynamic instability values. Also, the effect of backing materials, casting solution additives and other factors should be combined with molecular weight studies to have better insight of the membrane formation process, which will ultimately lead to improved membrane design.

3.6 **Acknowledgements**

We would like to thank the Arkema Inc. (Philadelphia, PA, USA) for the gift of polyvinylidene fluoride (Kynar) polymers and the National Research Council, Ottawa, Canada for generously offering the backing material.

References

1. Yang Y. Man-portable personal cooling garment based on vacuum desiccant cooling. - Applied Thermal Engineering. 2012:- 18.

2. Wu B, Li K, Teo WK. Preparation and characterization of poly(vinylidene fluoride) hollow fiber membranes for vacuum membrane distillation. J ApplPolym Sci. 2007;106(3):1482-95.

3. Dang, H.T., Amelot, C., Rana, D., Narbaitz, R.M. , Matsuura, T. Performance of a newly developed hydrophilic additive blended with different ultrafiltration base polymers. - Journal of Applied Polymer Science. 15 May 2010(- 4):- 2205.

4. Kynar® and kynar flex® :Polyvinylidene fluoride (PvdF) resins for batteries [Internet].; 2012. Available from: http://www.arkema-inc.com/kynar/literature/pdf/666.pdf.

5. Khayet M, Matsuura T. Preparation and characterization of polyvinylidene fluoride membranes for membrane distillation. Industrial and Engineering Chemistry Research. 2001;40(24):5710-8.

6. Zhou C, Hou Z, Lu X, Liu Z, Bian X, Shi L, et al. Effect of polyethersulfone molecular weight on structure and performance of ultrafiltration membranes. Industrial and Engineering Chemistry Research. 2010;49(20):9988-97.

7. Philip Crosbie Carman. Flow of gases through porous media. London Butterworths; 1956.

8. Smolders K, Franken ACM. Terminology for membrane distillation. Desalination. 1989;72(3):249-62.

9. García-Payo MC, Izquierdo-Gil MA, Fernández-Pineda C. Wetting study of hydrophobic membranes via liquid entry pressure measurements with aqueous alcohol solutions. J Colloid Interface Sci. 2000;230(2):420-31.

10. Kaelble DH, Moacanin J. A surface energy analysis of bioadhesion. Polymer. 1977;18(5):475-82.

11. Han M-, Nam S-. Thermodynamic and rheological variation in polysulfone solution by PVP and its effect in the preparation of phase inversion membrane. J Membr Sci. 2002;202(1-2):55-61.

12. Bakeri G, Matsuura T, Ismail AF. The effect of phase inversion promoters on the structure and performance of polyetherimide hollow fiber membrane using in gas-liquid contacting process. J Membr Sci. 2011;383(1-2):159-69.

13. Wienk IM, Boom RM, Beerlage MAM, Bulte AMW, Smolders CA, Strathmann H. Recent advances in the formation of phase inversion membranes made from amorphous or semi-crystalline polymers. J Membr Sci. 1996;113(2):361-71.

14. Smolders CA, Reuvers AJ, Boom RM, Wienk IM. Microstructures in phase-inversion membranes. part 1. formation of macrovoids. J Membr Sci. 1992;73(2-3):259-75.

15. Banerjee S, Yang R, Courchene CE, Conners TE. Scanning electron microscopy measurements of the surface roughness of paper. Industrial and Engineering Chemistry Research. 2009;48(9):4322-5.

16. Image J [Internet]; 2004 Available from: http://rsb.info.nih.gov/ij/.

17. R Kesting. The nature of pores in integrally-skinned phase inversion membranes. paper presented at the 3rd North American Chemical Congress, Toronto. June 7, 1988.

18. Hwang HJ, He K, Gray S, Zhang J, Moon IS. Direct contact membrane distillation (DCMD): Experimental study on the commercial PTFE membrane and modeling. J Membr Sci. 2011;371(1-2):90-8.

Chapter 4.
Study on Structure and Vacuum Membrane Distillation Performance of PVDF Composite Membranes: Influence of Blending

Zuolong Chen, DipakRana, Takeshi Matsuura, Christopher Q. Lan*
Department of Chemical and Biological Engineering
University of Ottawa, Ottawa, Canada

4.1 **Abstract**

In this study membranes were fabricated from the blend of high (H) and low (L) molecular weights polyvinylidene fluoride by the phase inversion process. The membranes so fabricated were characterized by scanning electron microscopy, gas permeation tests, contact angle (CA) and liquid entry pressure of water (LEPw) measurement, and further subjected to vacuum membrane distillation (VMD) in a scenario that was applicable for cooling processes, where the feed water temperature was maintained at 27^{o}C.It was found that the H:L mixing ratio did not affect the membrane surface hydrophobicity (as reflected by the CA) significantly. The water vapor flux of VMD was found to be the highest at the intermediate range of H:L ratio, i.e., 4:6, at which the thickness of the sponge-like layer showed a minimum, the pore size showed a maximum, the finger-like macro-voids formed a more orderly single-layer structure, and the LEPw showed a minimum.

Key words: Polyvinylidene fluoride, low and high molecular weight, blended membrane, membrane characterization, vacuum membrane distillation

4.2 **Introduction**

Since reverse osmosis membrane for seawater desalination was developed in 1960s, a significant amount of progresses have been made in membrane separation processes to be utilized in environmental, chemical, biological, physical and other areas and a large number of membranes have been synthesized and tested for various applications. In addition to applications in separation processes, distillation membranes have also been explored for the use in different cooling processes. Of particular relevance, a novel cooling concept, vacuum desiccant cooling (VDC), was demonstrated in our previous studies to be an effective technology for niche applications such as personal cooling garment (1), in which distillation membranes are used to provide the surface for water evaporation at a vacuum that is generated by a vacuum pump but maintained by the adsorption of vapor by desiccant. The membranes for application in VDC or other cooling processes are required to be able to sustain large evaporation fluxes at relatively low temperatures, e.g., 30^{o}C or less for application with VDC for personal cooling.

Although synthetic membranes can be made from both organic and inorganic materials, polymeric materials are most commonly used. A copious amount of polymeric materials can be used to fabricate membranes, including polysulfone (PS), poly(ether sulfone) (PES), polyacrylonitrile (PAN), polyamide, polyimide, polyethylene (PE), polypropylene (PP), polytetrafluoroethylene (PTFE), polyvinylidene fluoride (PVDF), polyvinylchloride (PVC) and others. Among those different materials, PVDF (2) has been mainly applied in ultrafiltration and microfiltration for a long time due to its high mechanical strength, outstanding chemical resistance and high hydrophobicity, which made PVDF membrane also suitable for membrane distillation (3).

Aiming at optimization and enhancement of PVDF membrane performances, researchers have paid attention especially to membrane fabrication conditions, i.e. membrane casting solutions (additives, water content, polymer content, solution viscosity, etc.) and casting conditions (casting temperature, coagulation bath composition and temperature, drying methods, etc.) since they affect the characteristics of PVDF membranes significantly. However, even though a large amount of studies have been done to investigate the effects of casting solutions on PVDF membrane performances, the effect of molecular weight of PVDF has not yet been systematically studied.

The objective of this work is to investigate the effect of the molecular weight of PVDF on the morphology and the VMD performance of PVDF membranes. This work is also useful for the membrane designing project in a Man-portable personal cooling garment research, in which the first generation of this cooling garment applied desiccant cooling technology (1) and VMD technology was employed in the second generation. Consequently, membrane properties and experimental conditions were designed to meet the requirements in the cooling garment research. Aiming at this goal, membranes are fabricated from PVDF materials of different molecular weights and their blends, and they are characterized by gas permeation experiments, vacuum membrane distillation tests, liquid entry pressure of water (LEPw) test and scanning electron microscopy (SEM).

4.3 **Experimental methods**

4.3.1 **Materials**

Polyvinylidene fluoride (PVDF) of two different molecular weights: Kynar® 740 Pellet, (average molecular weight 410kD; melt viscosity 18.5±2.5 kpoise; melting temperature, Tm 160.1ºC) (4) and Kynar® HSV900 (Mw= 92840 kD, Powder, melt viscosity 49.3 kpoise; Tm

165.1ºC) were supplied as resin powder from Arkema Inc. (Philadelphia, PA, USA). According to the description on the product datasheet (5), Kynar® HSV900 is a homopolymer that has the highest viscosity because it has the highest molecular weight among the Kynar® polymers. And the 740 PVDF has the lowest molecular weight. It is noted that the melt viscosity was measured using the ASTM D3835 at 232°C. Anhydrous N, N-dimethylacetamide (DMAC) supplied by Sigma-Aldrich with the purity of 99.9% was used as the solvent. Deionised water was used as the additive to the casting solution as well as the coagulation media. The polyester non-woven fabrics (Hollytex, grade 3396) were used as the backing material. The air permeability is 0.009 cubic feet per minute per square meter (CFM) of the fabric. The tensile strength (lb/in) is 85 and 52 in the machine direction (MD) and cross direction (CD), respectively. The elongation (%) is 75 and 85 in the MD and CD, respectively. A commercial PTFE (Teflon) unlaminated membrane was used as a comparison. It was purchased from Sterlitech Company and the LEPw of this membrane was 413.6kPa.

4.3.2 **Preparation of casting solutions**

All casting solutions contained 1.25 wt.% water, 15 wt.% polymers and 83.75 wt.% dimethylacetamide. The additive and the solution composition were employed based on the previous work done by Khayet and Matsuura (6). According to their work, the liquid entry pressure showed the maximum value when the water content was less than 1.5 wt.%.For the polymer, PVDF Kynar®900 (high molecular weight, H), PVDF Kynar® 740 (low molecular weight, L) and their blends of different mixing ratios were used. The polymer solution is coded as H: L according to the mixing ratio and the membrane made of the solution H: L is also coded as H: L. The casting solutions were homogenized by a shaker at the rpm of 180 and at

the temperature of 50°C. The homogenization was continued for 48 hours to ensure that all the solutions were well homogenized.

4.3.3 **Membrane casting method**

The polymer solution was cast on a nonwoven polyester backing material, which was generously supplied by the National Research Council of Canada, by using a brass casting bar to a thickness of 0.25 mm(7). Then the cast film together with the backing material was immersed into a coagulation bath (deionized water at 23°C) for 4 h, followed by transferring the solidified film to another deionized water bath, where it was kept for 20 h. The membrane was further dried under ambient conditions. The temperature was kept at 23°C during the casting process.

4.3.4 **Characterization of polymer solution**

4.3.4.1 ***Cloud point measurement***

The casting solution was diluted by DMAC to the dilution weight ratio of casting solution: DMAC=1:3. The titrant was prepared by diluting water by DMAC to the dilution weight ratio of 1:3. The titration was carried out at 23^{o}C by continuously dropping the titrant into the polymer solution from a burette until the clear polymer solution turned cloudy. Then the solution was shaken for 10 minutes to observe if the turbid solution would become clear again. If it did not, titration was stopped assuming that the cloud point was reached. Otherwise, titration was restarted (8). For each casting solution, three measurements were made and the average value was obtained.

4.3.4.2 ***Viscosity measurement***

The viscosity of the casting solutions was measured by using a rotational rheometer (Brookfield, Synchro-Lectric Viscometer model: LVF). Several testing vales were filled with

different solutions. Then a spindle was connected with the torsion spring and dipped into the solution. The motor was turned on and the rotation factor was monitored on the dial until it reached a constant value. The viscosity of the casting solutions was calculated according to the rotation factor, spindle factor and rotation speed. For each solution, three measurements were made and the average value was recorded.

4.3.5 **Membrane characterization**

4.3.5.1 ***Scanning electron microscopy (SEM)***

In order to study membrane morphology, cross-sectional SEM images of membrane samples were taken by using a SEM system (Tescan, Vega II XMU). The membrane was immersed into liquid nitrogen to embrittle, and then the sample was broken. After being positioned on a metal holder, the sample was sputtered with conductive metal coating under vacuum. The coating machine used was Anatech Hummer VII.

For cross-sectional views of membrane samples, the membrane tested was peeled off from the support material because the support material was too tough to break in liquid nitrogen.

4.3.5.2 ***Gas permeation test***

The mean pore size of the membranes was determined by the gas permeation test using the experimental setup shown in Figure 4-1. Pressurized nitrogen gas was supplied from a nitrogen cylinder to the permeation cell. A bubble-soap flow meter was employed to measure the gas permeation rate through the dried membrane sample at different transmembrane pressure differences. For each membrane, five measurements were made at five different pressures, and the average value was recorded for each pressure. The pore size was obtained

by the method described by Khayet and Matsuura (6).According to the method, the permeance is given as (9)

$$B = \frac{4}{3}\left(\frac{2}{\pi MRT}\right)^{0.5}\frac{r_p\varepsilon}{L_p} + \frac{P_m}{8\mu RT}\frac{r_P^2\varepsilon}{L_p} = I_o + S_oP_m \qquad (1)$$

where B is the gas permeance (mol/m^2·s·Pa), M is the molecular weight of the gas (kg/mol), R is the gas constant(J/mol·K), T is the absolute temperature(K), r_p is the pore size (m), μ is the viscosity of the gas (Pa s), ε is the membrane porosity, L_p is the effective pore length (m), and P_m is the mean pressure within the membrane pore (Pa), which is set equal to the average of the feed and permeate gas pressures. From the linear plot of B versus P_m, slope S_o and intercept I_o are obtained. The pore size, r_p is calculated by

$$r_p = \frac{16}{3}\left(\frac{S_o}{I_o}\right)\left(\frac{8RT}{\pi M}\right)^{0.5}\mu \qquad (2)$$

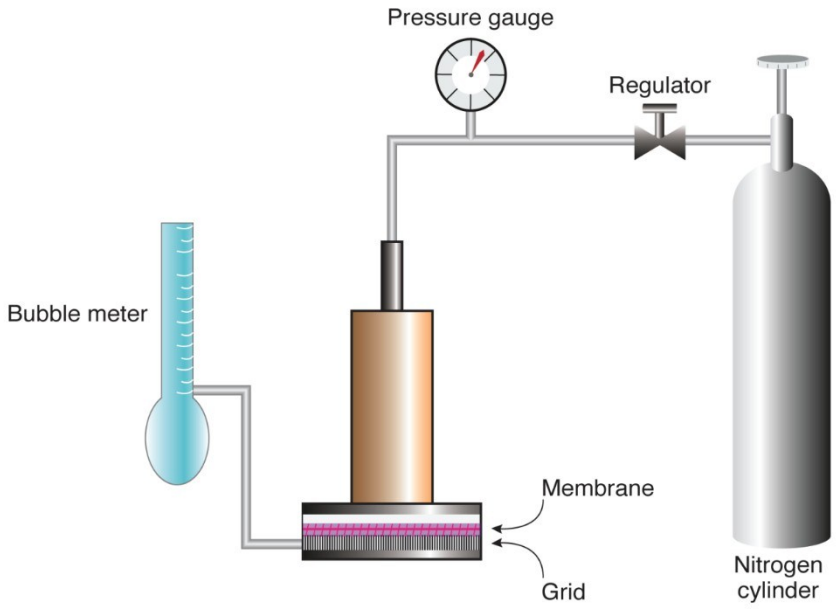

Figure 4-1 Gas permeation test equipment.

4.3.5.3 *Membrane porosity measurement*

The membrane porosity was measured by the wet and dry method. First, the membrane was immersed in liquid for 12 h. After blotting the membrane surface, the wet membrane was weighed as W_W. Then, the wet membrane was dried in an oven at 50˚C for 24hto thoroughly evaporate the liquid in membrane pores. After that, the dry membrane sample was weighed again. The weight of dry membrane was recorded as W_D.

The porosity of membrane could be calculated by using the equation:

$$P = \frac{(W_W - W_D)}{Ah\rho} \times 100\% \qquad (3)$$

Where P is the membrane porosity (%), W_W and W_D are the weight of the wet and dry membrane (g), respectively; A is the membrane area (cm^2); h is the membrane thickness (cm) and ρ is the density of the liquid (g/cm^3).

Ethylene glycol and isopropyl alcohol were chosen in this research as the liquid used to wet membrane samples, because their surface tensions are much lower than water. Consequently, membrane pores could be easily filled with the liquid.

4.3.5.4 *Liquid entry pressure of water (LEPw) measurement*

LEPw was measured according to the method of Smolders and Franken (10). The experimental setup used is shown in Figure 4-2. The membrane cell was a stainless steel filter holder with a reservoir of 2 x 10^{-4} $m^{-3}$and an effective membrane area of 0.00131m^2 (11).A dry membrane sample was placed on a sintered metal plate and the liquid reservoir was filled with water. Compressed gas (nitrogen) was supplied to the reservoir from the nitrogen cylinder, and the pressure was increased stepwise by using a precision pressure regulator at

an interval of 20.684- 34.473 kPa until water drops started to flow continuously from the testing cell outlet. At this point, the LEPw value was read from the pressure gauge. For each membrane sample, five measurements were made and the average value was recorded.

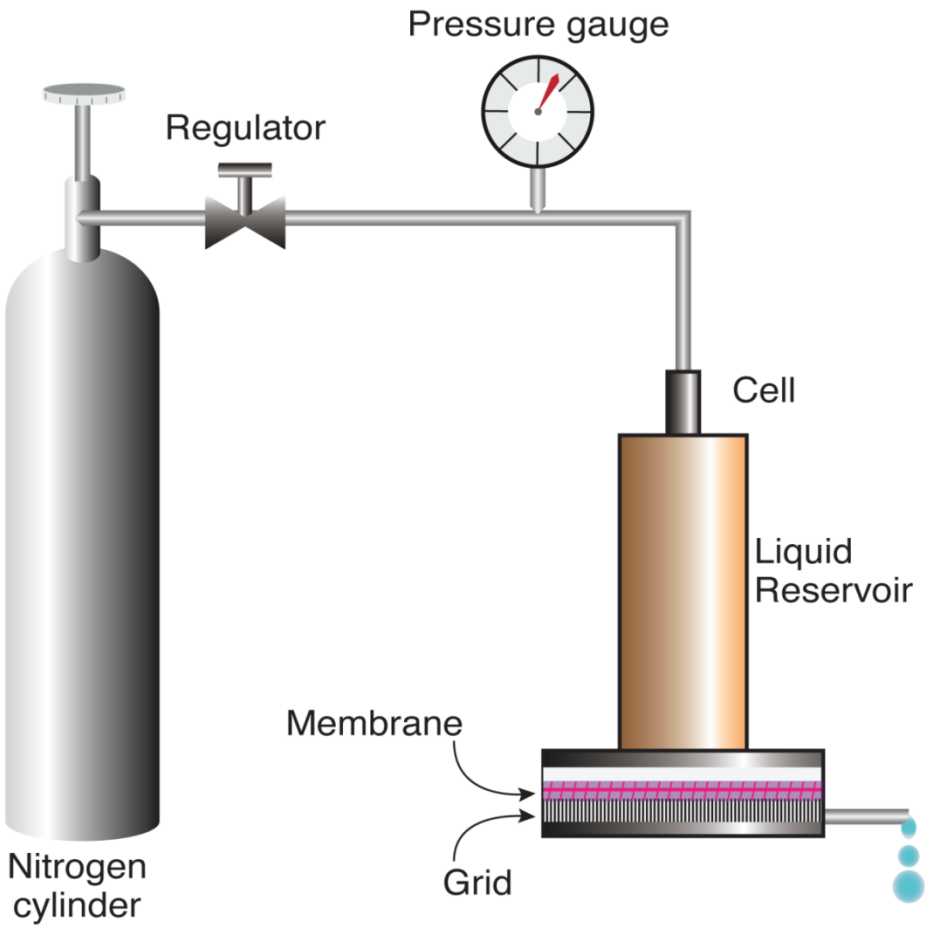

Figure 4-2 Setup for LEPw measurement.

4.3.5.5 *Membrane surface property*

4.3.5.5.1 Water contact angle

Membrane surface property is a very important membrane property that determines the liquid wettability, adhesion and repellency properties of polymeric membranes (12). Membrane hydrophobicity was characterized by measuring water contact angle using a VCA Optima Surface Analysis System (AST Products, Inc. Billerica, MA). For each type of blended

composite membrane, two samples were casted for the purpose of measurement, one of which was cut in parallel and the other was cut perpendicular to the longer edge of the membrane sheet. The dimensions of those samples were 5mmx80mm. The membrane sample was then placed on a glass plate and a small amount of distilled water (1 μL) was dropped by employing a micro syringe (Hamilton Company, Reno, NV). The contact angle was measured within a 10 s period. In order to maintain high accuracy, ten measurements were done on each sample and the average water contact value was calculated.

4.3.5.5.2 Surface free energy calculation

The surface free energy γ (also called as surface tension) is calculated by using the Lifshitz-van der Waals (LW) method. In order to calculate the surface free energy, the Young equation, Lifshitz-van der Waals (apolar), Lewis acid and Lewis base interactions are considered as in the following equation:

$$(1+\cos\theta)\gamma_L = 2\left(\gamma_S^{LW}\gamma_L^{LW}\right)^{\frac{1}{2}} + 2(\gamma_S^{+}\gamma_L^{-})^{\frac{1}{2}} + 2(\gamma_S^{-}\gamma_L^{+})^{\frac{1}{2}} \qquad (4)$$

This equation has been widely used, in which γ is the surface free energy. S and L indicate the solid/vapor and liquid/vapor boundary, respectively. LW, +, - mean the Lifshitz-van der Waals component (apolar), Lewis acid component and Lewis base component of the surface free energy, respectively (13). Knowing the overall surface tension (γ_L) from experiments and obtaining the surface tension components of the above three liquids (γ_L^{LW}, γ_L^{+} and γ_L^{-}) from the literature, three simultaneous equations can be solved for the unknownsγ_S^{LW}, γ_S^{+} and γ_S^{-}. The total surface energy of membrane γ_S is calculated by:

$$\gamma_s = \gamma_s^{LW} + \gamma_S^{AB} = \gamma_s^{LW} + 2(\gamma_S^{+}\gamma_S^{-})^{\frac{1}{2}} \qquad (5)$$

4.3.5.6 *Vacuum membrane distillation (VMD)*

Vacuum membrane distillation (VMD) was conducted by using a laboratory setup shown in Figure 4-3 according to the method described by Suk et al. (14). The feed chamber of the permeation cell was filled with deionized water and vacuum (3.78 kPa absolute) was applied on the permeate side so that water vapor permeated through the membrane. The effective area of the membrane was 0.0011 m^2. The feed chamber was slightly heated by the heating tape to maintain the temperature at 27°C. The feed liquid was stirred by a magnetic stirrer to prevent severe temperature polarization. The permeated vapor was first collected in the cold trap 1, cooled with liquid nitrogen, during the first 1 h until the system reached the steady state. Then, the permeate stream was switched to the cold trap 2, also cooled with liquid nitrogen, to collect the condensate for a predetermined period.

The VMD flux was calculated by

$$Flux = \frac{m}{tA} \quad (6)$$

Where m (kg) is the weight of water collected during the time period t (s) through the effective membrane area A (m^2). VMD experiments were performed at a rather low feed temperature of 27°C, since potable cooling garment is kept near body temperature.

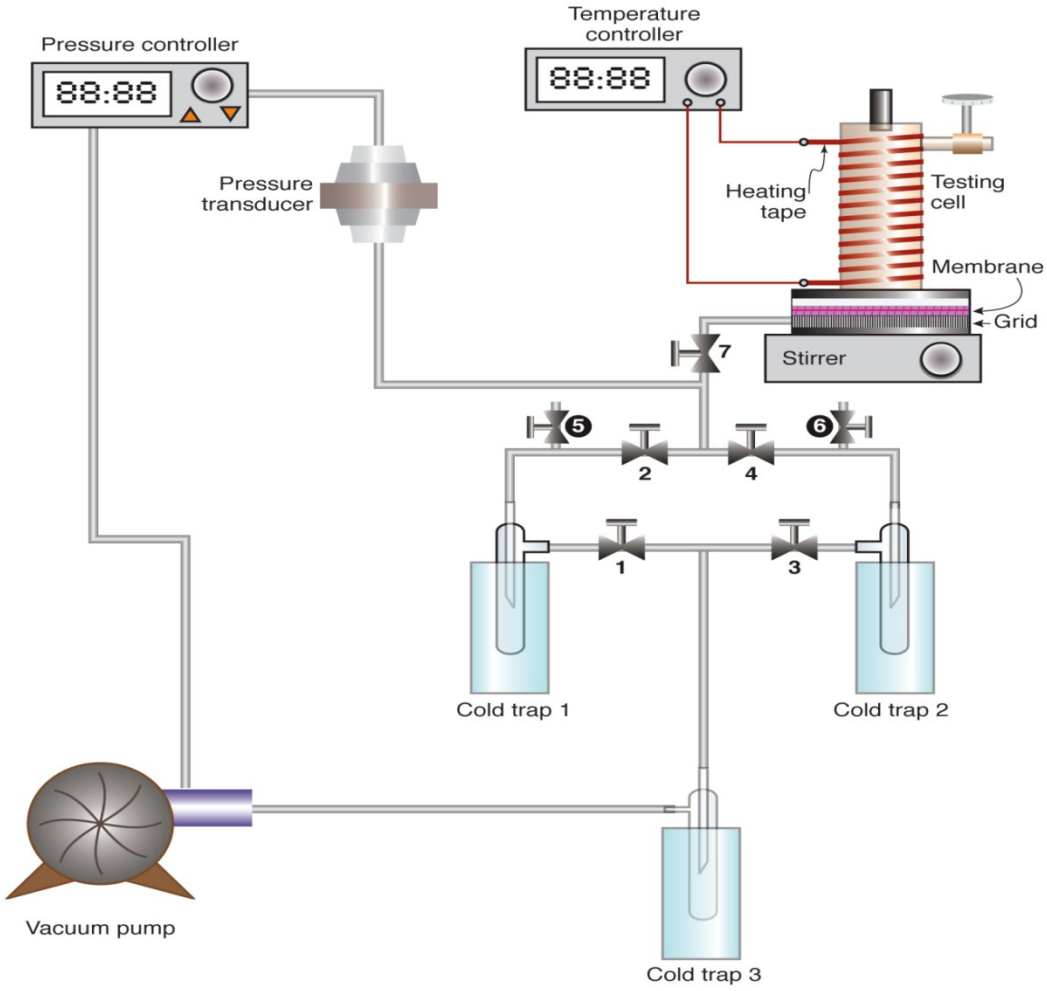

Figure 4-3 Vacuum membrane distillation set up.

4.4 Results and discussion

4.4.1 Polymer solution characterization

4.4.1.1 *Polymer solution viscosity*

The viscosity of polymer solution is an important factor in membrane forming process. It can affect the solvent/nonsolvent exchange, the velocity of phase separation, and the gelation dynamics (7).More specifically, higher viscosity can slow down the solvent/nonsolvent exchange rate during the phase inversion process, thus affecting the precipitation kinetics and

the formation of membrane morphology (7). Hence the viscosity of the casting solutions was measured and Figure 4-4 shows the experimental results. From the figure 4-4, the viscosity increases from the mixing ratio 0:10 to 10:0, i.e. with an increase in the content of high molecular weight PVDF. In particular, the viscosity increase is dramatic when the mixing ratio is above 5:5.

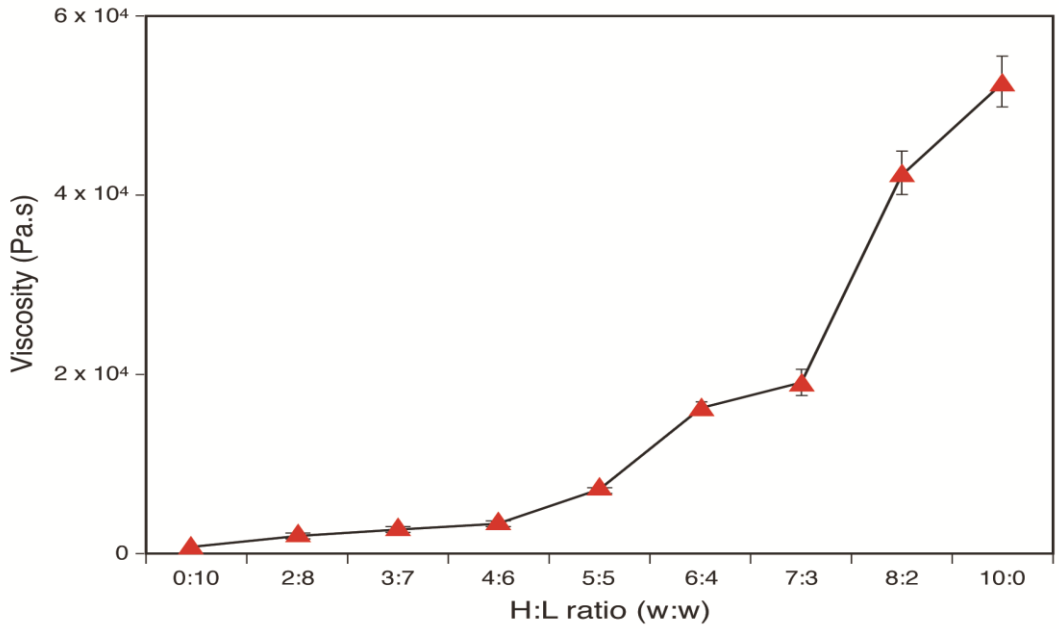

Figure 4-4 Viscosity as a function of H/L mixing ratio.

4.4.1.2 ***Cloud points***

The location of the cloud point on the polymer/solvent/nonsolvent ternary phase diagram shows the thermodynamic stability of the casting solution in the phase inversion process (8). Figure 4-5 shows the cloud points of the polymer solutions for different H: L ratios. It could be indicated that as the mixing ratio increased from 0:10 to 10:0, the cloud point moved towards the solvent/polymer axis progressively, meaning that the thermodynamic instability of polymer solutions grew progressively as the content of high molecular weight PVDF increased in blend PVDF system. As the instantaneous liquid-liquid demixing progress is favoured by the instability of polymer solutions. Consequently, the increase of H:L ratio may

result in a condition that favours instantaneous liquid-liquid demixing. Thus finger-like macrovoid structure would be more likely to be formed.

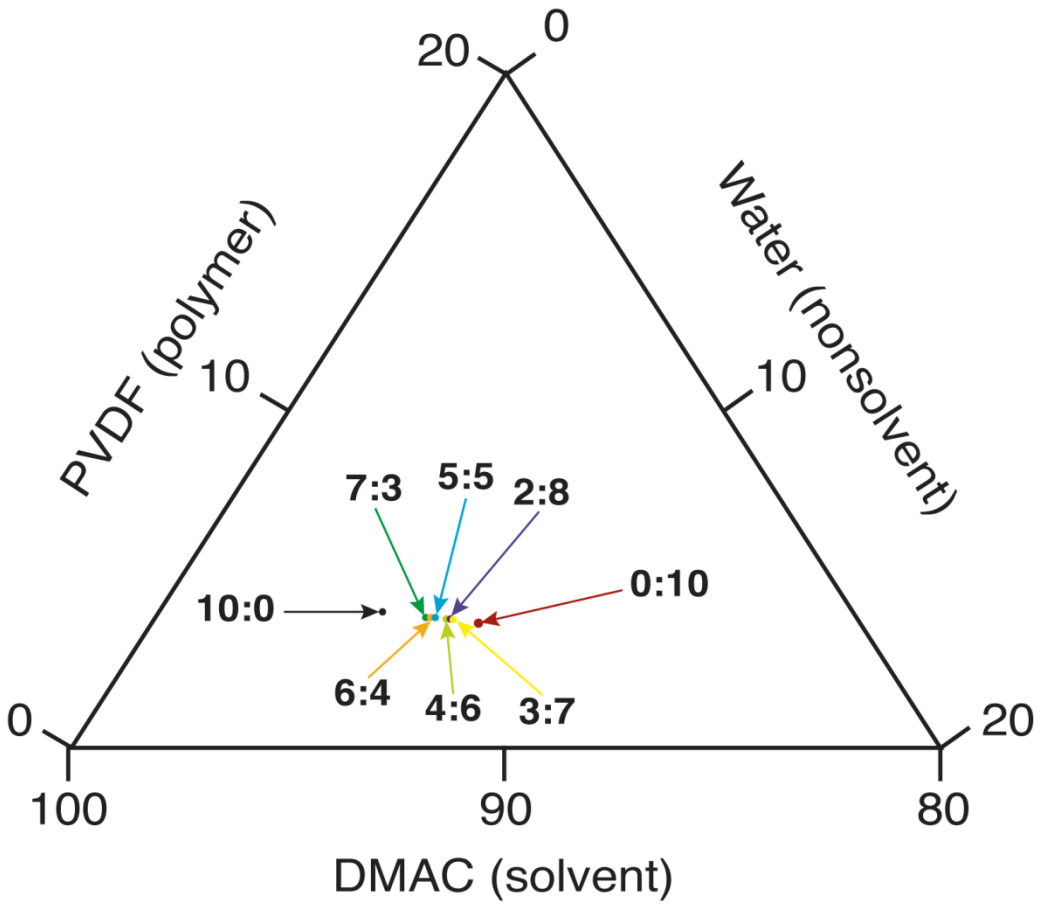

Figure 4-5 Cloud points of polymer solutions with different H:L mixing ratios.

4.4.2 **Membrane characterization**

4.4.2.1 ***Scanning electron microscopy (SEM)***

Figure 4-6 shows the cross-sectional SEM images of the membranes with different H: L mixing ratios. The figure 4-6 shows that the image consists of two parts; the upper part with finger –like macrovoids and the lower part with a sponge-like structure. In Figure 4-6a, b, c and d (H: L ratios 0:10, 2:8, 4:6, and 6:4), it is observed that both the upper and the lower layer thicknesses decrease and, as a result, the thickness of the entire cross-section decreases

as the H: L ratio increases. From Figure 4-6d to Figure 4-6f, on the other hand, the trend is reversed. In particular, when we focus on the thickness of the lower sponge-like layer, it decreases from Figure4-6a to Figure 4-6d and increases from Figure 4-6d to Figure 4-6f. In other words, a minimum in the thickness of the lower sponge-like layer appears at the middle range of the H: L mixing ratio.

The formation of the porous membrane structure could be attributed to the demixing that happened in immersion precipitation process. Demixing is defined as the separation of the homogeneous polymer solution, which results in two phases: the polymer-rich phase that forms the continuous solid phase of the membrane structure and the polymer-poor phase which forms the pores in membrane structure. Due to this process, an asymmetric membrane with a dense thin top layer and a porous sublayer can be created (7). The difference in membrane structures in blend composite membranes can be attributed to the interplay of the thermodynamic (cloud point) and the kinetic (viscosity) effect on the phase separation. From the thermodynamic view point, enhanced thermodynamic instability with an increase in the H: L mixing ratio, observed as the shift of the cloud point to the PVDF-DMAC axis on the ternary phase diagram, promotes the instantaneous demixing in the phase separation process, resulting in thinning of the top skin layer, and formation of more finger–like structure and less sponge-like structure (15). From the kinetic view point, on the other hand, the increase in viscosity with an increase in the H:L mixing ratio decreases the solvent/nonsolvent exchange rate in the phase inversion process, which promotes the delayed demixing, resulting in the thickening of the top skin layer, and formation of less finger-like structure and more sponge-like structure(16). Therefore, the thickest finger-like structure and the thinnest sponge-like structure are expected to be formed as a result of the superimposition of the thermodynamic and the kinetic effect.

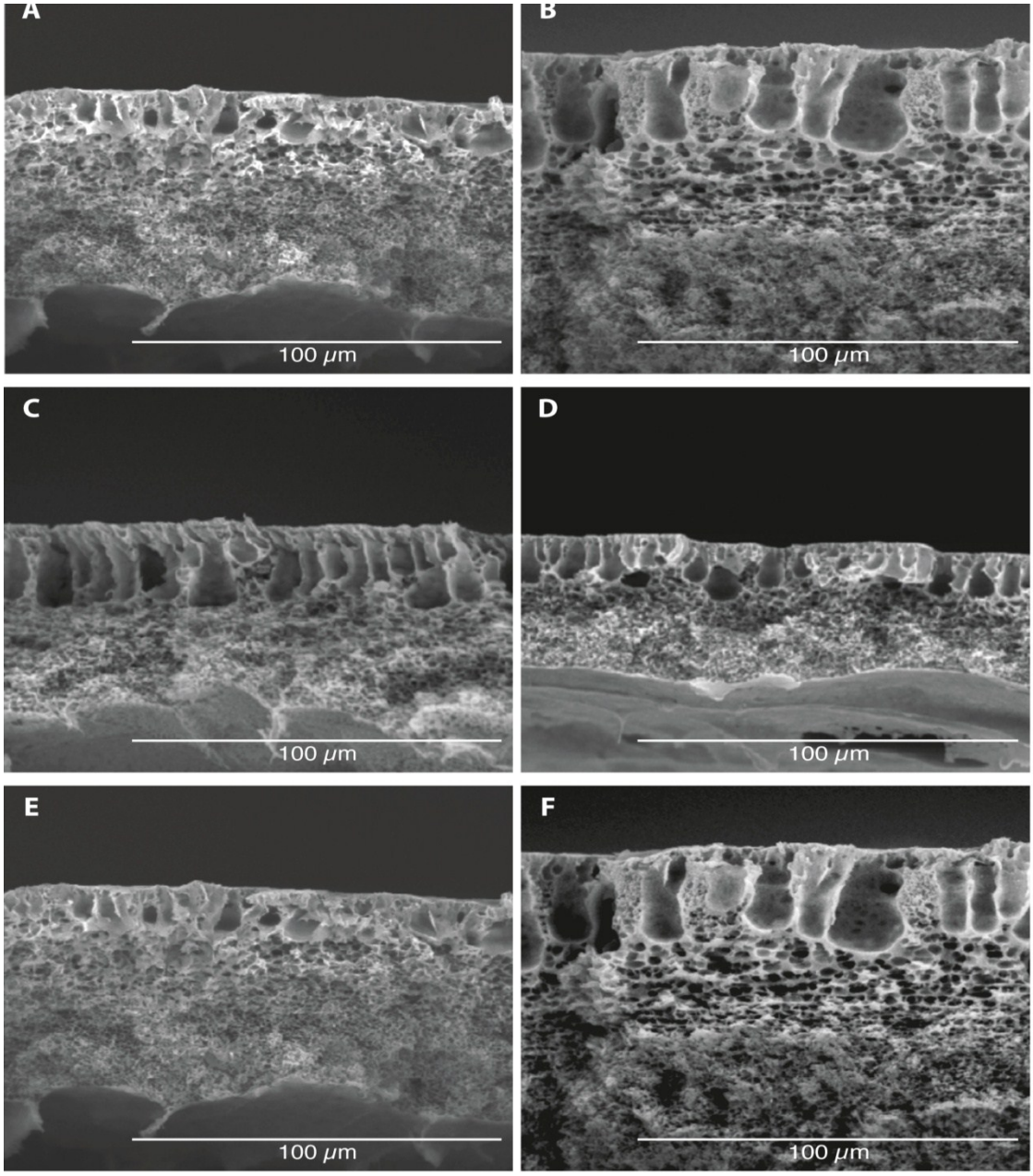

Figure 4-6 Cross-sectional images of the membranes: a) H:L = 0:10, b) H:L =2:8, c) H:L=4:6, d) H:L=6:4, e) H:L=8:2,and f) H:L=10:0.

Membrane surface roughness is also studied in this research by employing SEM top view pictures. SEM images were digitized to 8-bit grayscale images by employing Image J software (17, 18). Then 256-level histograms of those SEM images were converted from plotting the pixel brightness data for each image. These histograms show the grayscale levels on x-axis and pixel frequency on y-axis. Also, in order to study the surface morphology,

three-dimensional graphs of the intensities of pixels in a grayscale were generated and used to simulate the surface conditions of membrane samples. In histograms, the lighter areas (have lower grayscale) in this case was considered to present to smooth polymer mass while the darker areas (have higher grayscale) are considered to be void space/pores. Darker pixel brightness presents deeper void space. Thus the standard deviations of pixel brightness values could be used as a measure of surface uniformity (18). Higher standard deviation represents higher surface roughness; and the standard deviation was named as the SEM roughness index here to quantify the surface roughness of composite membranes.

A representative histogram picture of SEM images taken in this study is shown in Figure 4-7.

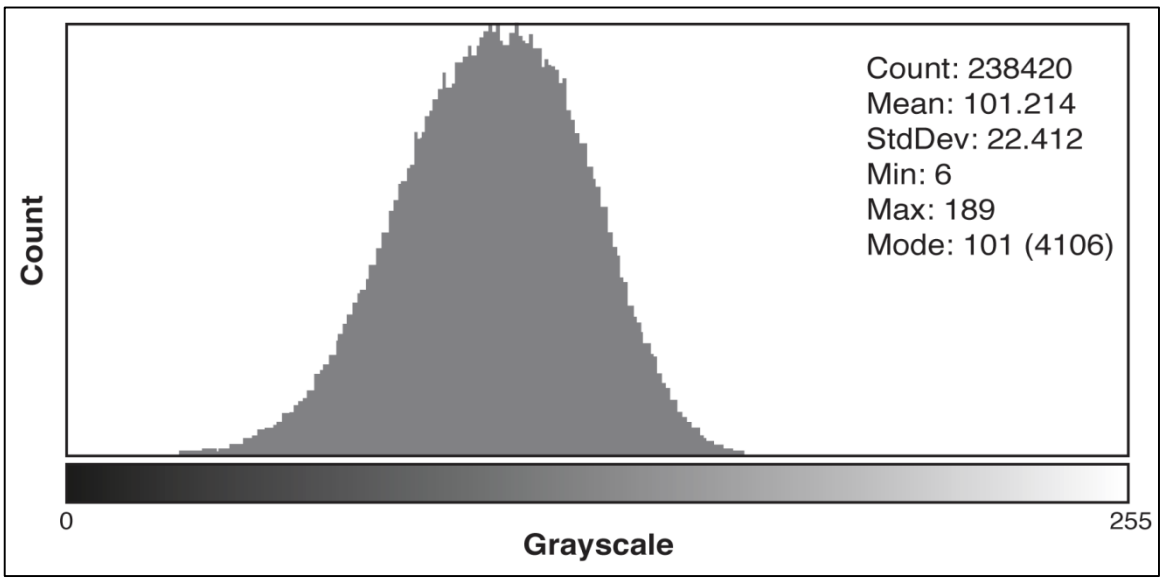

Figure 4-7 A histogram picture of a SEM image H:L=4:6.

Table 4-1 Surface roughness index value in histograms and H:L mixing ratio

Membrane sample H:L	Surface roughness index
2:8	33.16
4:6	25.51

6:4	31.44
8:2	30.78

For each composition, two samples were used to take SEM pictures. For each sample, 10 histograms were generated from random areas and the mean surface roughness index values were calculated (Table 4-1).

It can be concluded that, for the membrane sample casted by using blend solution with the mixing ratio of 4:6, its SEM image has the lowest standard deviation of the grayscale value (25.51) - which indicates that the surface roughness index of this sample is the lowest. While for other three histograms of other SEM images, their standard deviation values are very close to each other, i.e., for the samples casted by using polymer solutions with the mixing ratios of 2:8, 6:4 and 8:2, the surface roughness index values are 33.16, 31.44 and 30.78, respectively. It shows that the difference between these standard deviation values is not very significant. Even though the 2:8 sample has obviously the highest value.

The three dimension graphs of the intensities of pixels in a grayscale were generated, as presented in Figure 4-8.

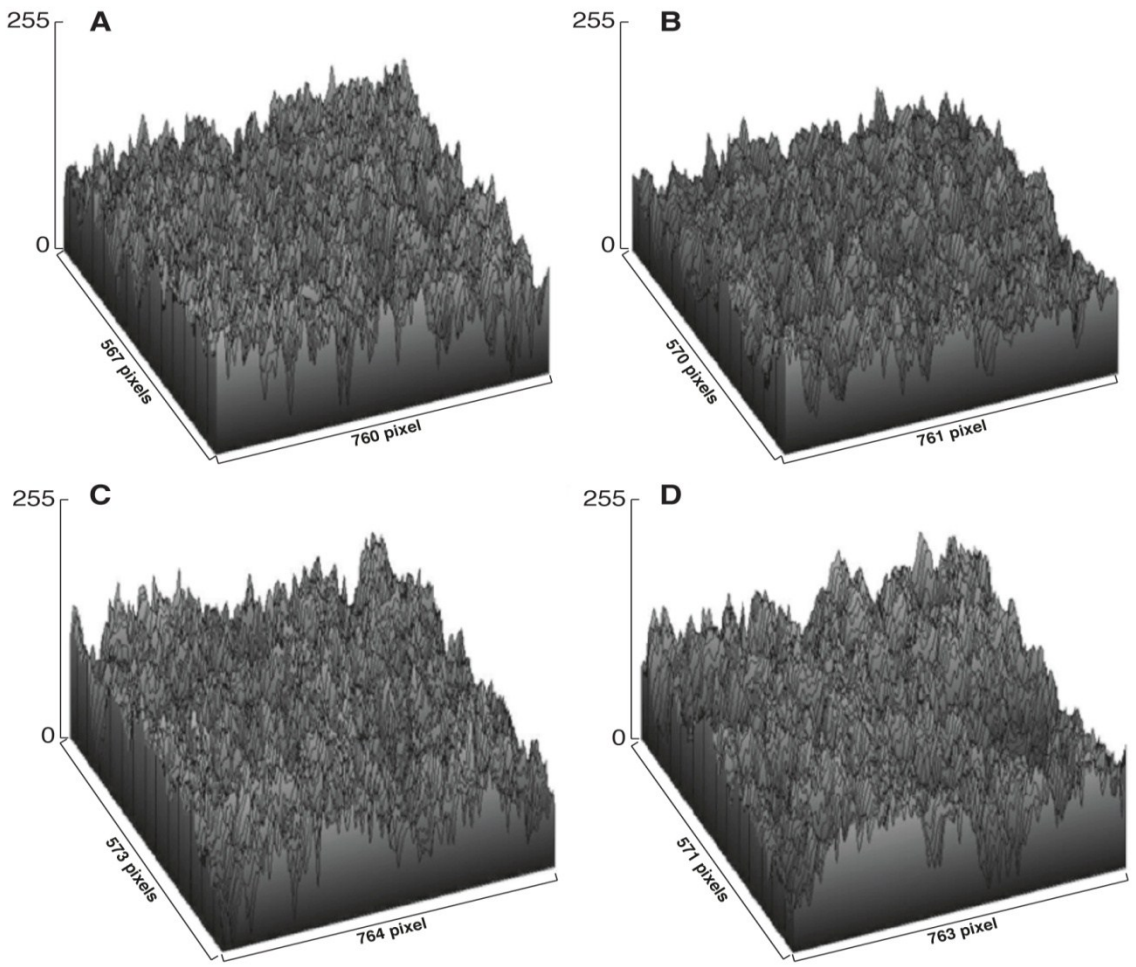

Figure 4-8 Three dimension graphs of the intensities of pixels in a grayscale. a) H:L=2:8, b)H:L=4:6, c) H:L=6:4, and d)H:L=8:2.

It can be seen from the three dimension graphs that 4:6 sample has obviously the lowest peak greyscale value and the gap between the peak and bottom is smaller than the three dimension graphs of other samples. Also, the surface of the 4:6 sample is more even and smooth than other samples as well. Thus it could be concluded that the membrane casted by using the polymer solution with a mixing ratio of H:L= 4:6 has the smoothest surface. The surface roughness of this membrane is lower than other samples.

4.4.2.2 *Gas permeation test*

The pore size was determined by the nitrogen gas permeation method. Figure 4-9 shows the results of the experiments. It should be noted that for the membrane made of low molecular

weight Kynar® 740 only (H: L mixing ratio 0:10), the nitrogen gas flux was very low, suggesting the presence of the smallest pore among all the tested membranes. Moreover inaccuracy in the measurement of intercept and slope made the result unreliable. Hence, the data are shown only for the H:L mixing ratio 2:8 and above. In Figure 4-9, the maximum in the pore radius (0.0327 μm) was observed at the H:L mixing ratio of 4:6. Note that at around this ratio, the minimum in the thickness of the sponge-like layer also appeared.

A plausible explanation can be provided by the two mechanisms proposed by Kesting (19) for the formation of membrane pores. In which it was mentioned that the pore could be formed from a solvent-filled space in a film casting solution which is surrounded by a large amount of spherical polymer molecules (called network pores, see Figure 4-10 a); while another mechanism is that the pore can be formed from a space generated between aggregates which are formed by the agglomeration of individual polymer molecules (called aggregate pores, see Figure 4-10 b). The latter pore is obviously larger than the former pore.

Most likely, the formation of aggregate pores becomes more dominant as the content of high molecular weight PVDF increases in the polymer blend, which leads to an increase in the pore size. However, as the molecular weight increases, the effect of polymer entanglement becomes gradually more dominant as observed in the dramatic increase in viscosity. As a consequence, the voids between the polymer aggregates are filled with the polymer segments and the pore size starts to decrease. Probably, these two opposing effects has resulted in a maximum in the pore size as the H;L ratio is increased.

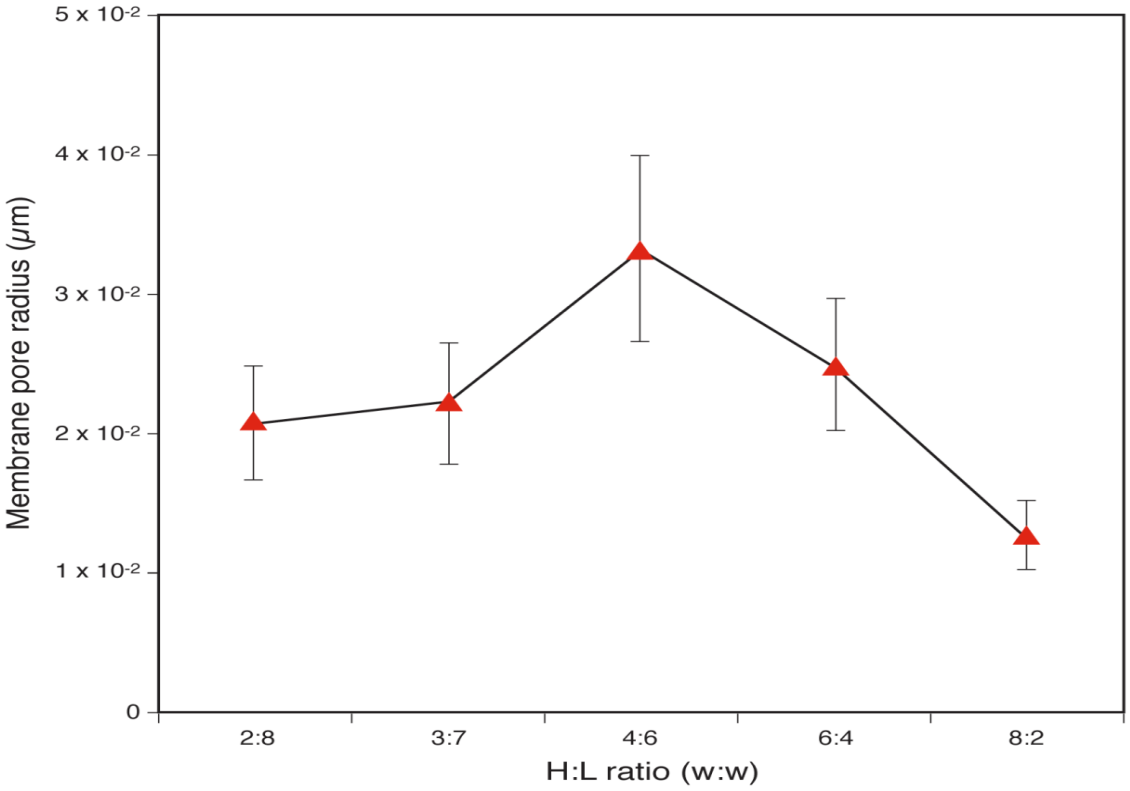

Figure 4-9 Pore radius of membranes with different H:L ratios.

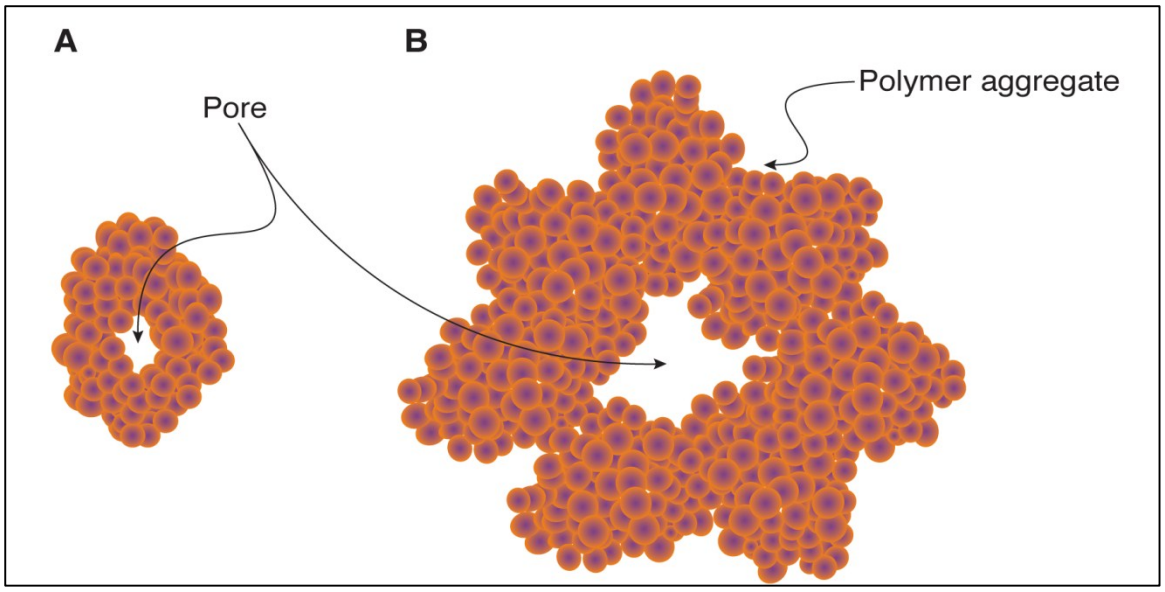

Figure 4-10 Formation of a) network pores and b) aggregate pore.

4.4.2.3 *Membrane Porosity Measurement*

Figure 4-11 illustrates the effect of H:L ration on the porosity. The porosity of the PVDF-coated membrane shows a maximum (27.65 %) at the H:L ratio of 6:4. While at the mixing ratio of 4:6, the porosity shows the second highest value (25.32%).

These results coincide with the trend observed by the SEM observation, i.e. thick finger-like void layer and thin sponge-like void layer, which appeared in the middle range of H:L ratio. As well, it coincides with the position of the maximum of pore radius, and the minimum of LEPw, both of which were also observed in the middle range of H:L ratio.

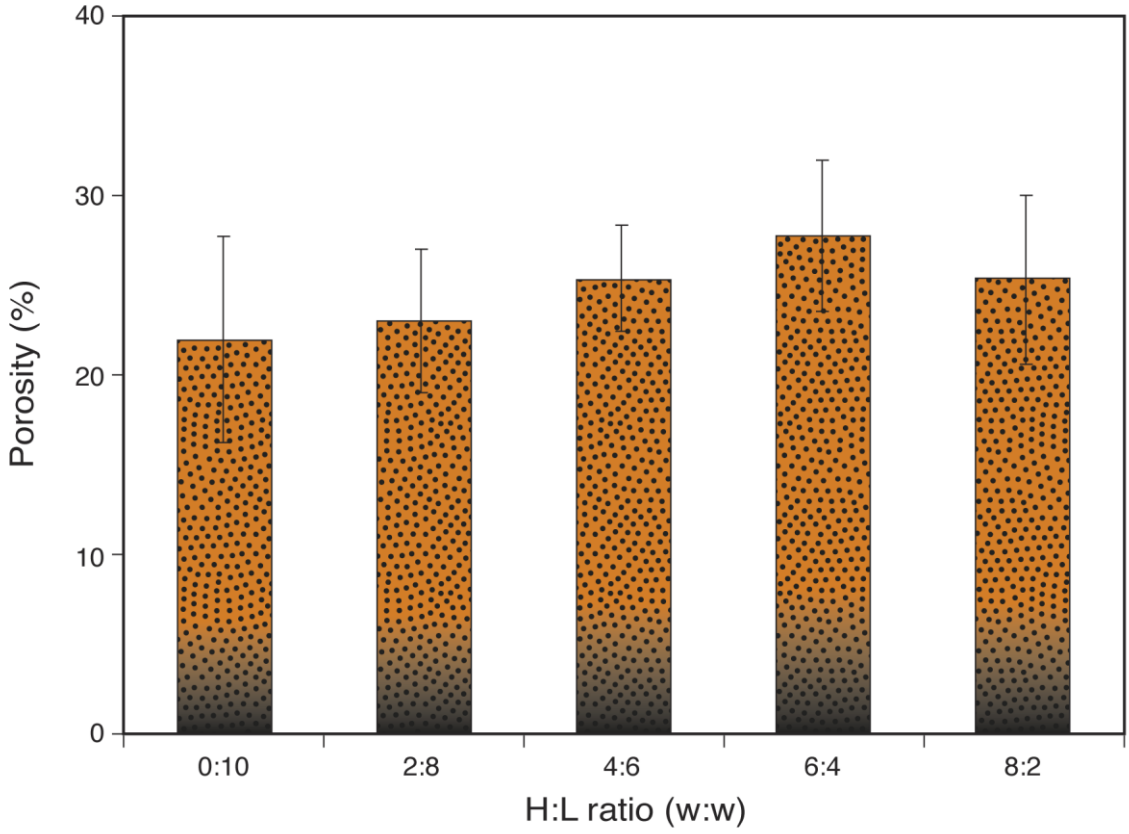

Figure 4-11 Membrane porosity with different H:L mixing ratios.

4.4.2.4 *LEPw measurement*

The experimental data for LEPw is shown in Figure 4-12 for different H:L mixing ratios. The minimum values in LEPw of water appeared at the H:L ratios of 3:7 (422.5kPa) and 4:6 (471.8 kPa), which approximately coincide with the H:L value of 4:6 where the maximum pore size was observed (see Figure 4-9). It is quite natural considering the Laplace equation

$$\Delta p = \frac{2\sigma}{r_p} \qquad (7)$$

Where Δp is the pressure required for water to enter the pore of radius r_p and σ is the surface tension of water. The LEPw values obtained for these membranes were larger than the commercial PTEF membrane we tested. It should also be noted that Hwang et al. reported 158.6kPa for the PTFE membrane they tested (20).

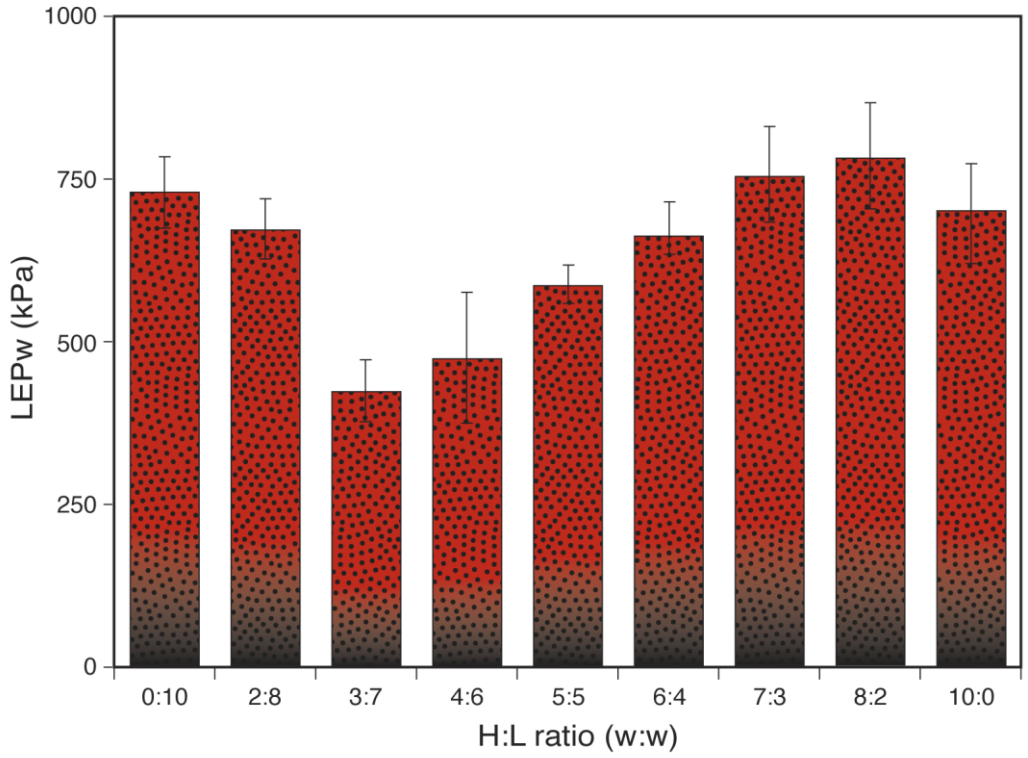

Figure 4-12 LEPw value of membranes with different H:L mixing ratios.

4.4.2.5 ***Membrane surface properties***

4.4.2.5.1 Water contact angle

The water contact angles are shown in Figure4-13 for all the tested membranes. For each sample, 10 measurements were taken and the mean values of water contact angles were calculated. Membrane sample with the mixing ratio of 6:4 has the highest water contact angle, reaching 88°, which is close to the values reported earlier, 86–88° (21). The lowest water contact angle (70°) was obtained when the H:L ratio was 7:3.

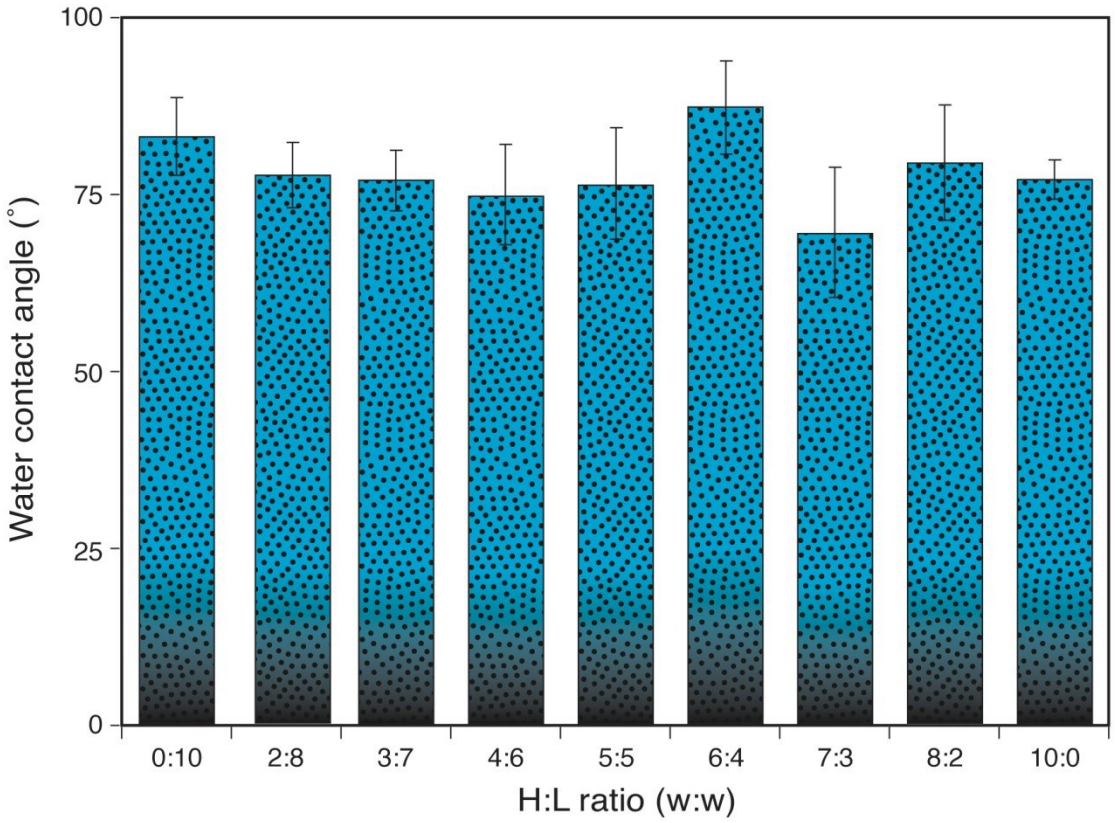

Figure 4-13 Water contact value of blended composite membranes.

4.4.2.5.2 Surface energy

After measuring water contact angle, those of ethylene glycol and diiodomethane were also measured to calculate the surface free energy of the membrane samples. Surface free energies were then calculated by using equation 4. The experimental contact angle data and the surface free energies are summarized in Table 4-2.

Table 4-2 Membrane contact angle measured by using three liquids and calculated surface energy.

Mixing ratio High:Low	contact angle water(°)	contact angle ethylene glycol(°)	contact angle diiodomethane(°)	Surface free energy,γ_S (mJ/m^2)
0:10	83.65	44.77	52.17	37.29
2:8	78.54	41.69	50.04	39.56
3:7	77.14	42.8	42.87	42.35
4:6	74.91	41.41	39.63	35.31
5:5	76.88	41.21	44.39	42.06
6:4	88.35	44.33	55.15	34.37
7:3	70.62	45.11	48.74	39.82
8:2	80.21	49.78	52.65	37.08
10:0	77.48	48.29	45.95	40.06

It can be concluded from the table that the surface free energy is not significantly influenced by the H:L ratio. The largest surface free energy (42.35 mJ/m^2) was obtained when H:L ratio was 3:7, while the lowest surface free energy (34.37mJ/m^2) was obtained for the ratio of 6:4, which is in excellent agreement with the values (36.2mJ/m^2-42mJ/m^2) reported previously (22, 23). There was no definite trend in the relationship between surface energy and the H:L ratio. In membrane distillation process, the hydrophobicity of membrane is of vital

importance. Generally, membranes for VMD process should be highly porous and hydrophobic. Also good thermal stability and chemical resistance to the feed solution are very important. Polymers that have low value of the surface energy such as PP, PTFE and PVDF are normally used to fulfill aforesaid requirements. In this way, the feed liquid cannot penetrate into the pores easily to ensure that the VMD process has enough pores for vapour to go through membranes.

In blend polymer systems, because of the intrinsic immiscibility of polymer blends, polymer mixtures would demix during the rapid membrane formation process. Due to this fact, immiscible blends usually have combined properties of polymers in blend systems, but they also show segregated structures that are determined by the predominant polymer's properties. Some literatures have already shown that the domain structures are influenced by changing the mixing ratios of polymers in blend systems (24). The process that polymers migrate in blend polymer systems is called migration.

Aiming at explaining this phenomenon, two possible theories have been discussed by some authors. The surface free energy theory explains that the migration is mainly determined by the polymers' surface free energy differences. More specifically, the component that has lower surface free energy will migrate to the surface of blend polymers. In this way, the surface free energy of blend polymer systems could be minimized (25). While in this experiment, as shown in Table 4-2, the surface free energy of the membranes casted by using pure low molecular weight PVDF and high molecular PVDF are 37mJ/m^2 and 40mJ/m^2 respectively. There surface free energy difference is very small, thus an assumption could be made here that the migration shouldn't be determined by the difference of surface free energy.

Another theory attributes the determination of migration to polymers' molecular weight. It is believed that the conformational entropy of a polymer chain at the film surface is smaller

than that in the bulk (26, 27). The difference of conformational entropy is also the entropic penalty of a chain at the surface. The entropic penalty decreases with the decrease in polymer molecular weight. Thus polymers that have high molecular weight would have larger entropy penalty. Consequently, polymers that have high molecular weight would be depleted on the surface of blend polymeric structure and polymers that have low molecular weight would be enriched in this area. Therefore, when there is no significant difference in surface energetic properties between polymers, molecular weight could be the key factor that determines the migration process (28). In this research, the migration theory could be one possibility for the difference of membrane morphologies in membranes casted by using various mixing ratios. And the difference in polymer molecular weight determines the migration.

4.4.3 **VMD flux**

The flux data for VMD are shown in Figure 4-14 for the membranes of different H:L mixing ratios together with the error bars. From the figure 4-14 the highest flux (692 g/h m^2) is observed at the H:L mixing ratio of 4:6. This also seems natural since at this particular mixing ratio the pore size is the largest, according to the gas permeation test. Furthermore, the thickness of the sponge-like structure, which is the main source of the resistance against the vapor flow, is the smallest according to the cross-sectional SEM image (Figure4-6). In addition, the 4:6 membranes had a single-layer finger-like structure, which is likely to be more favorable for vapor transportation in comparison to membranes with multi-layer finger-like structure. The surface hydro-philicity/-phobicity has apparently no effect on the vapor flux since the H:L mixing ratio showed no significant effect on the contact angle (79 $\pm 9^o$ with no trend observed when H:L ratio is changed). It is hence concluded that the VMD flux was primarily affected by the morphology at the surface as well as in the bulk of the membrane underneath the surface.

It should be noted that in this research, only the effect of polymer mixing ratio on membrane properties and performance is studies. In order to optimize polymeric membranes for better VMD and other membrane distillation performances, future researches are worth doing- including the study on membrane backing materials, polymer solution additives and casting conditions, etc.

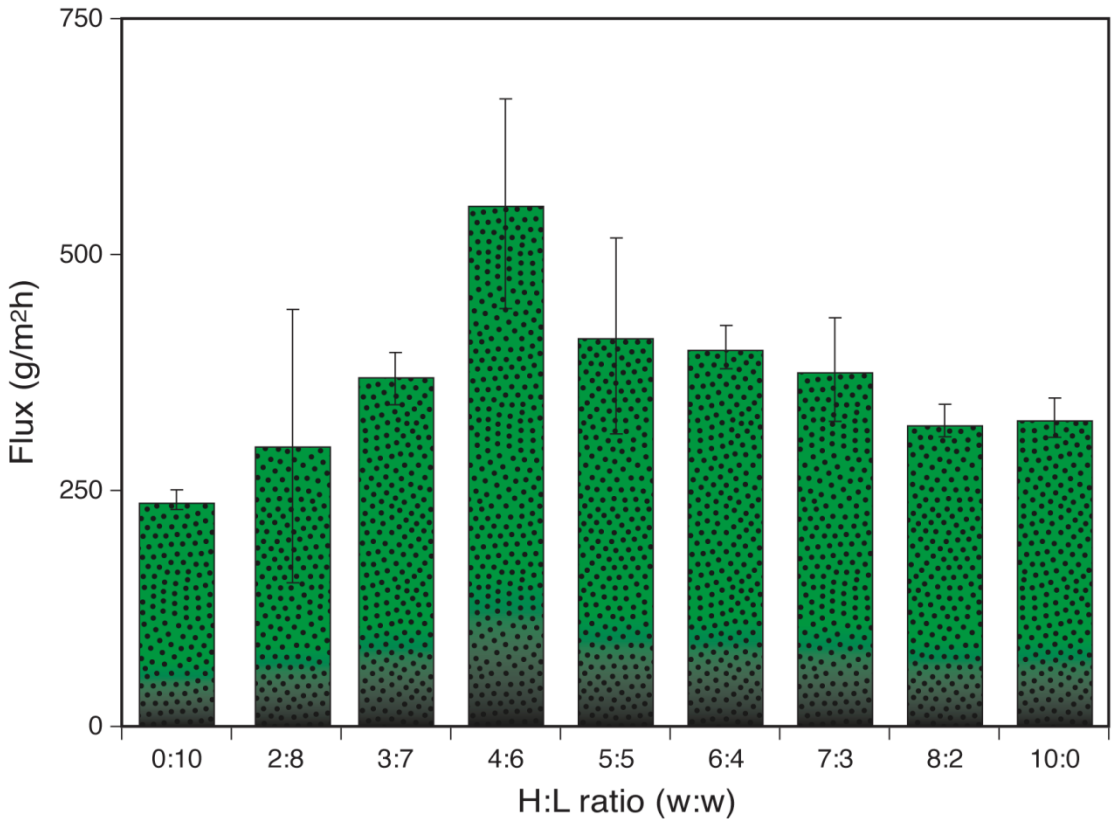

Figure 4-14 VMD flux for membranes of different H:L ratios.

4.5 **Conclusion**

The results of this study indicate that the ratio of high (H) and low (L) molecular weights PVDF (H:L) in the blend membrane has a significant effect on the morphology and VMD performance of the membrane. The VMD flux showed a maximum at the H:L ratio of 4:6, at

which the average flux reached 528 g/h·m^2, suggesting that it is the most appropriate H:L ratio for the VMD and the aforesaid VDC personal cooling garment application. SEM images of the blend membranes revealed asymmetric structures with finger-like macro-voids and sponge-like layer. The thickness of the sponge-like layer showed minimal at the H: L ratio of 4:6 and 6:4.The change in the layer thickness can be explained by the interplay of the thermodynamic and kinetic effects on the phase inversion process, as evidenced by the cloud point and viscosity measurement. The pore size measured by gas permeation test showed a maximum at the H:L ratio of 4:6. This can be explained by the presence of both network and aggregate pores. The porosity measured showed the highest values in the middle range of H:L mixing ratios. The contact angle did not depend on the H: L ratio. The LEPw showed minimum at the H:L ratio of 4:6 and 3:7(the results were 471.8 kPa and 422.5 kPa, respectively) corresponding to the maximum in the pore size. The LEPw is dependent in this case on the pore size of membrane since the hydrophobicity of membrane surface was not affected by the H:L ratio.

4.6 **Acknowledgements**

We would like to thank the Arkema Inc. (Philadelphia, PA, USA) for the gift of polyvinylidene fluoride (Kynar®) polymers and the National Research Council, Ottawa, Canada for generously offering the backing material.

References

1. Yang Y. Man-portable personal cooling garment based on vacuum desiccant cooling. - Applied Thermal Engineering. 2012:- 18.

2. Liu F, Hashim NA, Liu Y, Abed MRM, Li K. Progress in the production and modification of PVDF membranes. J Membr Sci. 2011;375(1-2):1-27.

3. Wu B, Li K, Teo WK. Preparation and characterization of poly(vinylidene fluoride) hollow fiber membranes for vacuum membrane distillation. J ApplPolym Sci. 2007;106(3):1482-95.

4. Dang, H.T., Amelot, C., Rana, D., Narbaitz, R.M. , Matsuura, T. Performance of a newly developed hydrophilic additive blended with different ultrafiltration base polymers. - Journal of Applied Polymer Science. 15 May 2010(- 4):- 2205.

5. Kynar® and kynar flex® :Polyvinylidene fluoride (PvdF) resins for batteries [Internet].; 2012. Available from: http://www.arkema-inc.com/kynar/literature/pdf/666.pdf.

6. Khayet M, Matsuura T. Preparation and characterization of polyvinylidene fluoride membranes for membrane distillation. Industrial and Engineering Chemistry Research. 2001;40(24):5710-8.

7. Zhou C, Hou Z, Lu X, Liu Z, Bian X, Shi L, et al. Effect of polyethersulfone molecular weight on structure and performance of ultrafiltration membranes. Industrial and Engineering Chemistry Research. 2010;49(20):9988-97.

8. Wijmans JG, Kant J, Mulder MHV, Smolders CA. Phase separation phenomena in solutions of polysulfone in mixtures of a solvent and a nonsolvent: Relationship with membrane formation. Polymer. 1985;26(10):1539-45.

9. Philip Crosbie Carman. Flow of gases through porous media. London Butterworths; 1956.

10. Smolders K, Franken ACM. Terminology for membrane distillation. Desalination. 1989;72(3):249-62.

11. García-Payo, M.C., Izquierdo-Gil, M.A., Fernández-Pineda, C. Wetting study of hydrophobic membranes via liquid entry pressure measurements with aqueous alcohol solutions. - Journal of Colloid and Interface Science. 15 October 2000(- 2):- 420.

12. Kaelble DH, Moacanin J. A surface energy analysis of bioadhesion. Polymer. 1977;18(5):475-82.

13. Yildirim Erbil H. Surface energetics of films of poly(vinyl acetate-butyl acrylate) emulsion copolymers. Polymer. 1996;37(24):5483-91.

14. Suk DE, Matsuura T, Park HB, Lee YM. Development of novel surface modified phase inversion membranes having hydrophobic surface-modifying macromolecule (nSMM) for vacuum membrane distillations. Desalination. 2010;261(3):300-12.

15. Bakeri G, Matsuura T, Ismail AF. The effect of phase inversion promoters on the structure and performance of polyetherimide hollow fiber membrane using in gas-liquid contacting process. J Membr Sci. 2011;383(1-2):159-69.

16. Smolders CA, Reuvers AJ, Boom RM, Wienk IM. Microstructures in phase-inversion membranes. part 1. formation of macrovoids. J MembrSci. 1992;73(2-3):259-75.

17. Image J [Internet]. 2004;Availablefrom: http://rsb.info.nih.gov/ij/.

18. Banerjee S, Yang R, Courchene CE, Conners TE. Scanning electron microscopy measurements of the surface roughness of paper. Industrial and Engineering Chemistry Research. 2009;48(9):4322-5.

19. R Kesting. The nature of pores in integrally-skinned phase inversion membranes. paper presented at the 3rd North American Chemical Congress, Toronto. June 7, 1988.

20. Hwang HJ, He K, Gray S, Zhang J, Moon IS. Direct contact membrane distillation (DCMD): Experimental study on the commercial PTFE membrane and modeling. J Membr Sci. 2011;371(1-2):90-8.

21. Teoh MM, Chung T-. Membrane distillation with hydrophobic macrovoid-free PVDF-PTFE hollow fiber membranes. Separation and Purification Technology. 2009;66(2):229-36.

22. Altena FW, Smolders CA. Calculation of liquid-liquid phase separation in a ternary system of a polymer in a mixture of a solvent and a nonsolvent. Macromolecules. 1982;15(6):1491-7.

23. Y. Kitazaki and H. Hata. Setchakukyoshi. In: ; 1972. p. 8, 131.

24. Davies MC, Shakesheff KM, Shard AG, Domb A, Roberts CJ, Tendler SJB, et al. Surface analysis of biodegradable polymer blends of poly(sebacic anhydride) and poly(DL-lactic acid). Macromolecules. 1996;29(6):2205-12.

25. Jones RAL, Kramer EJ, Rafailovich MH, Sokolov J, Schwarz SA. Surface enrichment in an isotopic polymer blend. Phys Rev Lett. 1989;62(3):280-3.

26. Agarwal US, Dutta A, Mashelkar RA. Migration of macromolecules under flow: The physical origin and engineering implications. Chemical Engineering Science. 1994;49(11):1693-717.

27. Khayet M, VázquezÁlvarez M, Khulbe KC, Matsuura T. Preferential surface segregation of homopolymer and copolymer blend films. Surf Sci. 2007;601(4):885-95.

28. Kumar SK, Russell TP. Behavior of isotopic, binary polymer blends in the vicinity of neutral surfaces: The effects of chain-length disparity. Macromolecules. 1991;24(13):3816-20.

Chapter 5. Conclusion

In this study, it was found that the molecular weight can affect membrane properties and performances through changing polymer solutions' viscosities, thermodynamic instabilities, kinetic hindrances and pore formation mechanisms. And the impact of polymer molecular weight is complicated. The result shows that the formation of membrane porous structures and pores can be determined by complicated interplays of the kinetic hindrance, thermodynamic diffusion rate, polymer aggregates and polymer entanglements. More specifically, as the viscosity increased dramatically from the Kynar®740 PVDF solution to the Kynar®HSV 900 PVDF solution, while the thermodynamic instability showed a remarkable rise as well. Consequently, from the Kynar®740 PVDF to the Kynar® MG 15 PVDF, the pore size rose from 41.5 to 49.8 and flux increased from 277 to 325 $g/m^2 \cdot h$. Also, the LEPw value showed a decrease from 731 to 622 kPa as well.

The results of this study also indicate that the mixing ratio of high (H, Kynar®HSV 900), and low (L, Kynar®740) molecular weights PVDF (H:L) in the blend membrane has a significant effect on membrane properties and performance. The VMD flux showed a maximum at the H:L ratio of 4:6, at which the average flux reached 528 $g/h \cdot m^2$ (much higher than pure PVDF membrane), suggesting that it is the most appropriate H:L ratio for the VMD and the aforesaid VDC personal cooling garment application. The change in the membrane morphology is also significant, and it can be explained by the interplay of thermodynamic and kinetic effects on phase inversion process, as evidenced by the cloud point and viscosity measurements. The pore size measured by the gas permeation test showed a maximum at the H:L ratio of 4:6. This can be explained by the presence of both network and aggregate pores.

The interplay of the aforesaid effects is complicated but of great significance. Moreover, the additives and other factors may bring huge impact to membrane properties and performances as well. Thus future work needs to be done to cover a wider range of molecular weights, viscosities and thermodynamic instability values. Also, the effect of backing materials, additives and other factors should be studied together with molecular weight and blended polymer studies to fabricate better membranes to fulfil various demands. Regretfully, due to the restrain of the resources, it was impossible for us to precisely measure the molecular weights of the PVDF polymers used in this study, thus for the sake of doing systematic researches, it would be much appreciated and meaningful if these data could be measured in future studies.